AFOSR 69-2197 TR

AD 693325

FINAL SCIENTIFIC REPORT ON COMBUSTION CHEMISTRY OF HIGH ENERGY PYROPHORIC FUELS

OR 10,119 26 May 1969

Reproduced From
Best Available Copy

Research sponsored by
Air Force Office of Scientific Research,
Office of Aerospace Research
United States Air Force
under Contract No. AF49-638-1566

Prepared by: Charles A. Andrade
Charles A. Andrade,
Principal Investigator

This document has been approved for public release and sale; its distribution is unlimited.

MARTIN MARIETTA CORPORATION
ORLANDO, FLORIDA

Qualified requestors may obtain additional copies from the Defense Documentation Center; all others should apply to the Clearinghouse for Federal Scientific and Technical Information.

Reproduction, translation, publication, use and disposal in whole or in part, by or for the United States Government, is permitted.

ABSTRACT

Research reported herein is directed toward further understanding of the fundamental processes in supersonic combustion. Part One describes a branching chain mechanism constructed for oxy-diborane mixtures diluted in argon. Included in this postulated mechanism is the production of hydroxyl as an ignition intermediate. A spectrograph was used to view the oxy diborane system through the end plate of a single pulse shock tube. Hydroxyl and several boron intermediates were identified, qualitatively verifying both mechanism and equilibrium calculations. Ignition induction measurements were performed up to 950°K behind the reflected shock wave. These measurements extend previously known data by two orders of magnitude in the induction time. Part Two of this report describes the CAL Nonequilibrium Normal Shock Wave Program which was extended for use with highly exothermic branching chain reactions, checked out with known hydrogen oxygen kinetics, and reformulated to include transport and radiative energy transfer mechanisms.

FOREWORD

The investigation reported herein was carried out between 1 June 1965 and 31 May 1969 under the sponsorship of the Air Force Office of Scientific Research Contract AFOSR 49(638)-1566. Technical supervisor for this program is Dr. B. T. Wolfson, Project Scientist, Propulsion Division, Directorate of Engineering Sciences, Air Force Office of Scientific Research.

During various phases of the work the principal investigator was assisted by Donald L. Olsen, Chemist, and Henry Knowls, Computer Programmer. Encouragement and tutalage were given by Professors Symon H. Bauer of Cornell University, Ithaca, New York, and James J. Gallagher of Rollins College, Winter Park, Florida.

CONTENTS

Abstract iii

Foreword v

Introduction and Summary xi

PART I: SHOCK TUBE INVESTIGATIONS OF THE DIBORANE/ OXYGEN SYSTEM

I. The Shock Tube Considered 3

A. Design 3
B. Experimental Procedure 5
1. Instrumentation 5
2. Laboratory Techniques 6
a. Events in the Shock Tube 6
b. Non-Idealities 9
3. Performance 10
a. Transducers and Shock Velocity 10
b. Ignition Induction Check Runs 10
c. Optics 12
d. Shock Tube Calibration 12
e. Sources of Error, Data Scatter, and Uncertainties 15

II. Technical Approach 17

A. Selection of Fuels 17
B. Hypothesized B_2H_6/O_2 Mechanisms 19

III. Shock Induced Ignition of Diborane 25

A. Ignition Induction Measurements 27
B. Detonation Limits 33
C. Spectroscopic Emission Studies 34

PART TWO: MATHEMATICAL INVESTIGATIONS

I. Background 43

II. Reaction Profile Model 45

III. Mathematical Formulation 47

A. Equations of Motion 47
B. Chemical Equilibria and Relaxation Processes 49
C. Equation of State 53
D. Kinetics 54
E. Sample Calculations 54

IV. Extended Model 59

A. Equations Coded. 60
B. Vibration - Dissociation Coupling Model. 63
C. Collisional Transport Properties 63
D. Radiative Energy Transfer. 72

Appendices

A. Optical Absorbimetry of the B_2H_6/O_2 System 83
B. Shock Wave Analysis 87
C. List of Symbols 95

References 99

ILLUSTRATIONS

1 Asymptotic Incident Shock Mach Number, $p_4/p_1 \rightarrow \infty$ 4

2 Shock Tube Parameters versus Test Temperature 4

3 Martin Marietta Aero-Combustion Laboratory 6

4 One Inch Chemical Shock Tube 7

5 Chemical Shock Tube Wave Diagram 8

6 Carbon Monoxide Flame Experiments 11

7 Optical Emission Sensor 13

8 Air/Air Shock Tube Performance 14

9 Helium/Argon Performance Calibration 16

10 Heat of Combustion of B_2H_6/O_2 Compared to H_2/O_2 18

11 Instrumentation Schematic. 25

12 Wave Diagram - Flame Schematic 26

13 Oscillogram Traces, Ignition Induction Measurements of 1:3:96 = B_2H_6:O_2:Ar, p_4=800 mmHg 27

14 Shock Waves in Pure Argon, Initial Temperature = 298°K 29

15 Shock Waves in Ar (96 Percent) + O_2 (3 Percent) + B_2H_6 (1 Percent); Initial Temperature = 298°K; Pressure = 500 mmHg. . . . 30

16 Diborane - Ignition Induction 31

17 Helium/Argon Performance - Calibration 32

18 Comparison of Martin Marietta and Monsanto Detonation Limits. . . 33

19 Computed Equilibrium Compositions in the Reflected Shock Wave Region Ar, H_2O, BO_2, O_2, H_2, BO, and B_2O_3 35

20 Computed Equilibrium Compositions in the Reflected Shock Wave Region OH, HBO_2, O, and H 36

21 Sequence of Three Experimental Runs in the Detonation Mode, p_{41}=11.47 37

22 Densitometer Record of Diborane Combustion Spectrum; Temperature > 945°K 38

23 Hydrogen/Oxygen Ignition Induction 55

24 Envelope of [OH] Concentration versus Time 57

25 Rate of Production of OH, $Q_{OH,j}$ versus Time of Several Reactions in the Hydrogen/Oxygen Chain 58

26 Check Calculation of Thermal Conductivity for Various Binary Systems 70

27 Characteristic Radiation Source Lamp 84

28 Schematic of High Voltage Capacitor Bank and Lovotron Switch to be Used for Energizing the Characteristic Radiation Source. . . . 85

29 Absorptivity Measurement Instrumentation 85

INTRODUCTION AND SUMMARY

Combustion studies reported herein follow the shock tube approach toward determination of oxidation mechanisms and reaction kinetics, applying established techniques to the study of pyrophoric fuels. These studies are set within the framework of a long range AFOSR project directed toward understanding and use of the mutual effects of chemical reactions on collisional transport properties and radiative energy transfer in flow systems of high power density heat release. Results of the Martin Marietta studies include:

1. A branching chain mechanism was constructed for stoichiometric oxygen/diborane (O_2/B_2H_6) systems under high dilution in argon, consistent with thermochemical, kinetic, and structural data. Included in fourteen (forward) steps of the postulated mechanism are thermal decomposition of diborane and production of hydroxyl (OH) as a chain carrier, followed by the plausibly observable oxides and hydrides of boron.

2. A single-pulse chemical shock tube was used to study the high temperature homogeneous reactions of the stoichiometric O_2/B_2H_6 system. Ignition induction measurements were obtained for the pyrophoric O_2/B_2H_6 system in the temperature range from 575 to 945°K and for the O_2/CO system at 2000°K. These measurements extend the previously known data by two orders of magnitudes, into the microsecond regime. A spectroscopic emission study of O_2/B_2H_6 served to identify BO_2 and BO lines in the spectrum, taken in the detonative mode at temperatures exceeding 945°K.

3. Equilibrium normal shock wave calculations were performed, supplementing these emission studies, in an effort to establish a temperature region for measurement of intermediate species rate constants via molecular or atomic absorption spectrophotometry.

4. An OH ultraviolet absorption experiment was designed following the techniques of References 1 and 2.

5. Working in cooperation with Cornell University's Chemistry Department, the Aero Combustion Laboratory at the Martin Marietta Orlando Division has extended and verified the use of Cornell Aeronautical Laboratory's Nonequilibrium Normal Shock Wave Program (Reference 3) in the study of exothermic systems which include branching chain mechanisms. In particular, the previously measured appearance and disappearance of intermediate species occurring during the oxidation of hydrogen from about 1370 to 1540°K, and at 1 Atm, (References 3

and 4) was successfully simulated, using the CAL program coded for the Martin Marietta CDC 6400 electronic computer. Martin Marietta calculated ignition induction times are compared to the measurements of Reference 3.

6 The CAL program* is being used optionally and as subroutine to a Martin Marietta developed reaction profile model which incorporates mutual effects of chemical reactions on collisional transport properties and radiative energy transfer. The transport properties subroutine portion of the Martin Marietta program was satisfactorily checked out for various multicomponent mixtures. A fully developed chemical source matrix is required as input to the CAL subroutine, for each reaction mechanism to be studied. A partially known or postulated mechanism may be described parametrically with the input source deck.

Such computer methods are useful to the chemical kineticist in performing diagnostics on a system for which some of the pre-exponential factors, activation energies, and temperature exponents, associated with unknown specific reaction rates, are currently being determined by measurement. The computer program and various sets of spectrometric measurements are used in an iterative determination of mechanism and reaction kinetics consistent with minimum energy and detailed balancing principles. This technique of complementary measurement and numerical experimentation may prove superior to earlier methods used in attempts to elucidate mechanism which, although yielding results consistent with measured data, did not serve to guarantee uniqueness.

The work reported herein shows how steps may be taken to isolate a physically meaningful region for the investigation of exothermic reactions using a shock tube. Briefly, this is accomplished by establishing the onset of detonations for the pressures and compositions, initially set, that determine shock strengths and intermediate compositions to be monitored spectroscopically. Though the present work did not proceed to the next step, viz., measurement of the production rates and concentrations of intermediates, it is noted that techniques in absorption spectrophotometry are established and under continuous development. It is suggested that one such technique, outlined in Appendix A, may be appropriate in extending the present work to the proper field of chemical kinetics.

In the mathematical portion of this investigation it is shown that the choice of molecular model is important to high temperature flow field applications. Inasmuch as the molecular dynamicist, whether he be engineer or kineticist, now requires extensive use of computer programs to follow reaction paths, it is suggested that continued effort in the development and use of programs, such as the one herein outlined, will yield meaningful results.

Part One of this report presents a discussion of shock tube design considerations and preparation of experimental facilities directed to the task of performing shock tube kinetics.

---

*Herein referred to as the CAL subroutine.

Although no rate measurements have been made, the following preliminary tasks were accomplished:

1. Ignition induction times were measured, extending previously known data by two orders of magnitude.

2. Detonation limits were determined experimentallly.

3. An oxidation mechanism was postulated for the considered pyrophoric system.

4. Equilibrium compositions were calculated.

5. Emission spectra were photographed.

6. Intermediate chemical species were identified from the spectra.

7. An OH ultraviolet absorption experiment was designed to measure specific reaction rates.

Part Two treats the general mathematical reaction profile model under development, giving results of calculations obtained with the Martin Marietta modified CAL normal shock wave and transport properties subroutines.

PART ONE

Shock Tube Investigations

of the Diborane/Oxygen System

I. THE SHOCK TUBE CONSIDERED

A. DESIGN

The shock tube was designed based on ideal flow conditions using equations from Reference 5. The shock tube is divided into two sections, a driver section filled with gas of low molecular weight, M_4, at high pressure, p_4, and a driven section filled with an inert diluent at low pressure, p_1. The division takes place at a diaphragm burst station where a solenoid actuated pin ruptures a cellophane diaphragm. The high pressure driver gas interface on low pressure driven gas then acts as a piston creating a shock wave which moves uniformly down the low pressure section to a reflection plane. The interface (contact surface) between the driver and driven gases follows the shock wave and is intercepted by the reflected wave. Chemical reactions among the reagents in the inert gas take place during the time between reflection of the wave and its interception by the contact surface, the observation time. Thus, during the observation time, spectroscopic study of the test sample is carried out in the region behind the reflected shock wave at the far end of the tube. Analysis of the shock system is given in Appendix B.

For purposes of illustration a general shock tube design based on ideal incident shock wave Mach number, obtained at infinite diaphragm burst pressure ratio p_{41} from Equation (32) of Appendix B, is presented in Figure 1. The solid curves represent selected cases of the quadratic expression for the incident shock Mach number variation with the diaphragm burst sound speed ratio for parametric combinations of γ_4 and γ_1, the ratios of specific heats for the driving and driven gases respectively. The circled point marked He/Ar represents the asymptotic shock Mach number attainable when helium gas at very high pressure is used to drive argon at very low pressure, the gases being initially at room temperature. By heating the driver gas, that is, by raising temperature T_4, one may expect to increase the shock Mach number along the same curve. The locus of points represented by the dashed line shows that a decrease in the molecular weight of driver gas or an increase in molecular weight of driven gas increases the shock Mach number. The latter technique is used in tailoring the gases when changes in molecular weight are introduced by mixing test reaction samples with the inert diluent (driven) gas.

The choice of reaction environment for present experiments was obtained from the helium and argon combination, a finite pressure ratio p_4/p_1, and the temperature range shown in Table I; the shock Mach number does not exceed a nominal value of 3.6, which is less than one third of the asymptotic value shown on Figure 1. A graphic representation of most of the tabulated data is shown on Figure 2. Note that the total shock tube length $x_1 + x_2 \cong 21$ feet is nominally the maximum length of the Orlando Division's chemical shock tube.

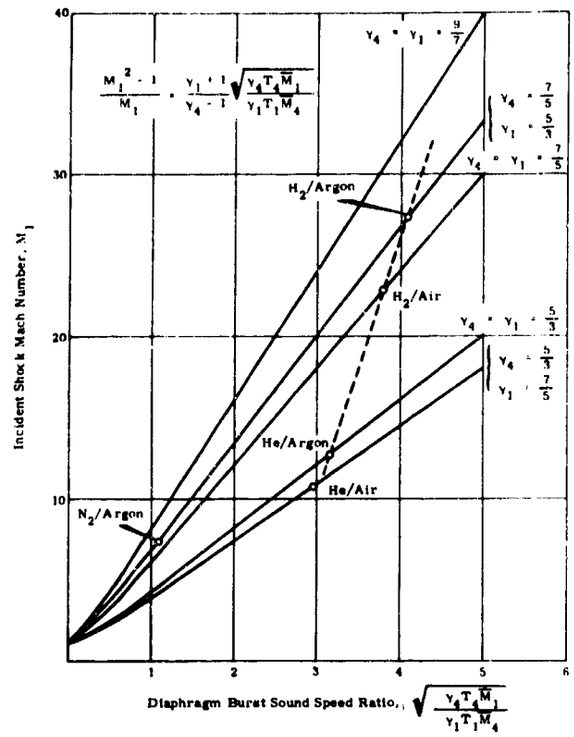

Figure 1. Asymptotic Incident Shock Mach Number, $p_4/p_1 \rightarrow \infty$

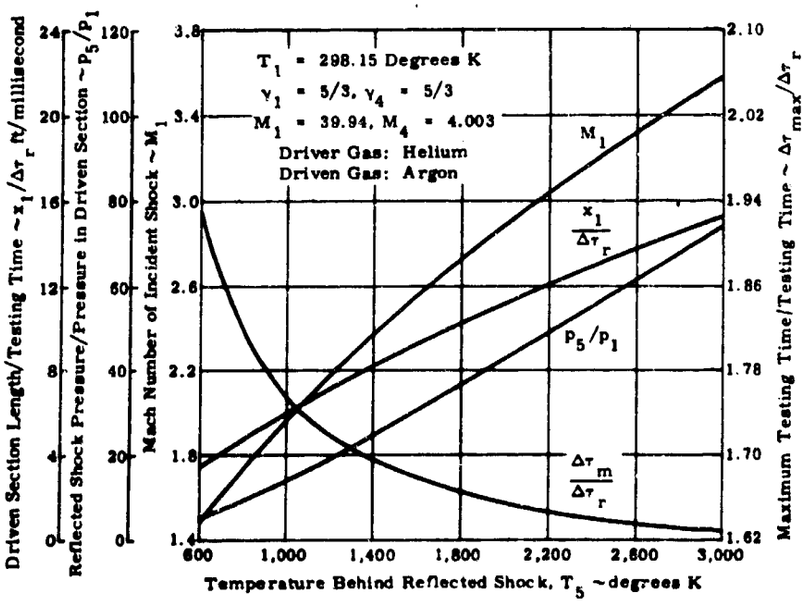

Figure 2. Shock Tube Parameters versus Test Temperature

TABLE I

Shock Tube Parameters at T_1 = 298.15°K for Helium/Argon

T_5(°K)	M_1	W_5 (ft/msec)	W_2 (ft/msec)	u_c (ft/msec)	$\frac{p_2}{p_1}$	$\frac{p_5}{p_1}$	$\frac{x_1}{\Delta\tau_r}$ (ft/msec)
596.3	1.4679	1.5490	1.3924	0.6227	2.4434	5.1801	3.3699
894.4	1.8522	1.9545	1.4285	1.0384	4.0381	10.9658	5.2639
1192.6	2.1765	2.2967	1.5191	1.3590	5.6712	19.4511	7.0498
1490.8	2.4697	2.5986	1.6198	1.6261	7.3189	27.7481	8.6845
1788.9	2.7163	2.8663	1.7206	1.8584	8.9731	36.5470	10.1768
2087.1	2.9504	3.1133	1.8213	2.0670	10.5415	45.6222	11.5691
2385.2	3.1675	3.3427	1.9145	2.2570	12.2915	54.8872	12.8415
2683.4	3.3708	3.5573	2.0057	2.4332	13.9534	64.2902	14.0454
2981.5	3.5627	3.7597	2.0939	2.5976	15.6161	73.7946	15.1757

		T_4 = 200°K, a_4 = 2.7301 ft/msec		T_4 = 298.15°K, a_4 = 3.3333 ft/msec		T_4 = 400°K, a_4 = 3.8609 ft/msec	
T_5(°K)	$\frac{\Delta\tau_m}{\Delta\tau_r}$	$\frac{p_4}{p_1}$	$\frac{x_4}{\Delta\tau_r}$ (ft/msec)	$\frac{p_4}{p_1}$	$\frac{x_4}{\Delta\tau_r}$ (ft/msec)	$\frac{p_4}{p_1}$	$\frac{x_4}{\Delta\tau_r}$ (ft/msec)
596.3	1.9330	3.6277	3.7012	3.3685	4.6540	3.2233	5.4887
894.4	1.7816	7.9542	3.8440	6.9883	4.9437	6.4610	5.9072
1192.6	1.7197	14.0464	3.8644	11.7717	5.0640	10.5824	6.1211
1490.8	1.6864	22.9404	3.3096	17.7732	5.0770	15.5944	6.1968
1788.9	1.6656	32.4907	3.7129	25.0933	5.0280	21.5067	6.1925
2087.1	1.6523	45.4920	3.5980	33.8359	4.9467	28.3970	6.1446
2385.2	1.6414	61.3185	3.4688	44.1609	4.8380	36.3374	6.0593
2683.4	1.6335	81.3204	3.3378	56.2406	4.7230	45.3751	5.9605
2981.5	1.6275	105.1432	3.2054	70.2771	4.5987	55.5668	5.8508

B. EXPERIMENTAL PROCEDURE

Gas dynamical and chemical calibration of shock wave strengths in argon and with argon diluted oxidation of carbon monoxide was conducted, using helium as the driver gas. Approximately ideal shock tube performance was obtained experimentally by causing cellophane and aluminum diaphragms, inserted between the high and low pressure sections of the shock tube, to burst at pressure differences approaching the material yield point. The effect of small differences in laboratory environmental conditions on ideal performance was found negligible from both experimental and theoretical considerations. The experimental ignition induction period was identified for the oxidation of carbon monoxide using Kistler 603 quartz crystal transducers to measure the pressure rise due to combustion. An optical system using an RCA 931A photomultiplier tube was designed and incorporated into the shock tube viewing ports to measure emission outputs during the ignition induction period. Calculations were performed for mixing and handling the oxy-diborane system in the experiments.

1. Instrumentation

The one-inch inside diameter, single pulse chemical shock tube reactor, its associated vacuum equipment, electronics, optical, gas handling and chromatographic systems which have been developed and used during the contract are shown in Figure 3.

Figure 3. Martin Marietta Aero-Combustion Laboratory

Equipment used in this laboratory include the following:

1 P. E. 154D Vapor Phase Chromatograph,

2 Gas mixing and vacuum equipment,

3 Shock tube and 36 liter dump tank, with,

a Photomultiplier mounted on the reaction head,

b Control panel and recording equipment,

4 Gertner monochromator,

5 Optical and mass spectrometers.

2. Laboratory Techniques

The gas handling system is used to mix diborane or carbon monoxide and oxygen in stoichiometric proportions, using argon as the diluent. When mixing pyrophoric fuels with oxygen, the reactants are mixed separately with the diluent to keep the reactants below their explosion limits at room temperature, Reference 6.

a. Events In The Shock Tube

The freshly mixed gases are allowed to stand from one to twelve hours before using, one hour being the minimum time for dilute species to diffuse a distance of 50 cm assuming a diffusion coefficient of 0.3 $cm^2\ sec^{-1}$.

After allowing the mixture to diffuse, the low pressure section of the tube is charged with a mixture sample at initial pressure p_1. Since p_1 may vary from 5 torr to 5 psia depending on the diaphragm rupture and incident shock Mach number requirements, the driven section is evacuated to about 1 micron, using a rough pump when these conditions require that $p_1 \cong 5$ psia. At the high Mach numbers ($p_1 \cong 5$ torr), the 2 inch diffusion pump is used to ensure that

residual air molecules in the driven section are less than 1 percent of the number density of reactant species. An argon flush is used after each run. Pressures in both the high pressure (p_4) and low pressure sections of the tube are measured with a Bourdon gauge calibrated against a standard to within 1 percent. Figure 4 shows an assembly drawing of the shock tube including:

1 Dump tank,

2 Continuously variable high pressure p_4 driver section,

3 Low pressure p_1 driven section (the reactor),

4 Hi vac inlet and bypass valves,

5 Diaphragm station and rupture pin,

6 Reactor head with ball valve shutoff,

7 Pressure transducer, product sampling and optical view ports,

8 Alternate multiple diaphragm assembly.

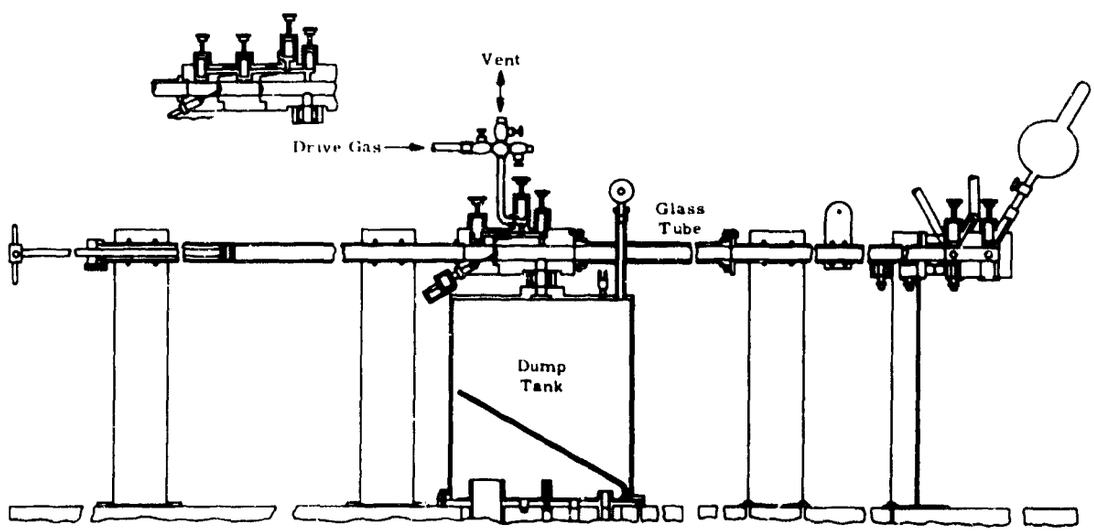

Figure 4. One Inch Chemical Shock Tube

In a typical run sequence, the tube is evacuated to about 1 micron, then helium is charged into the high pressure section to about 1 kilotorr. Samples of the fuel and oxidizer selected for study are separately premixed with an inert diluent, argon. In the non-pyrophoric experiments with CO, the reactants are introduced into the same mixing flask with the diluent. The mixtures are then charged into the tube's reaction section at low values of the total pressure, the reactant's partial pressures being such as to minimize their collision frequency. The reaction section is separated from the high pressure driver by cellophane or aluminum diaphragms. A pin is caused to rupture the diaphragm allowing helium at high pressure to enter the reaction section creating a shock wave ahead of the gas interface. The shock wave excites the gas mixture, elevating its temperature, increasing the reactants' collision probability. The shock wave then reflects from the end plate and proceeds into the excited region, elevating the gas temperature a second time. Thus, homogeneous exothermic reactions are observed in the region of high collision probability between the reflected shock wave and the end plate.

Figure 5 shows a wave diagram, representing the sequence of events along the tube following rupture of the diaphragm. Assuming ideal rupture (instantaneous removal), the diaphragm is replaced by a contact surface, gas interface, which accelerates into the low pressure section. During its short period of acceleration, small disturbances project forward from the contact surface (at the acoustical speed in Region 1). These small disturbances coalesce into a shock wave after which shock wave and contact surface both move forward at uniform velocity.

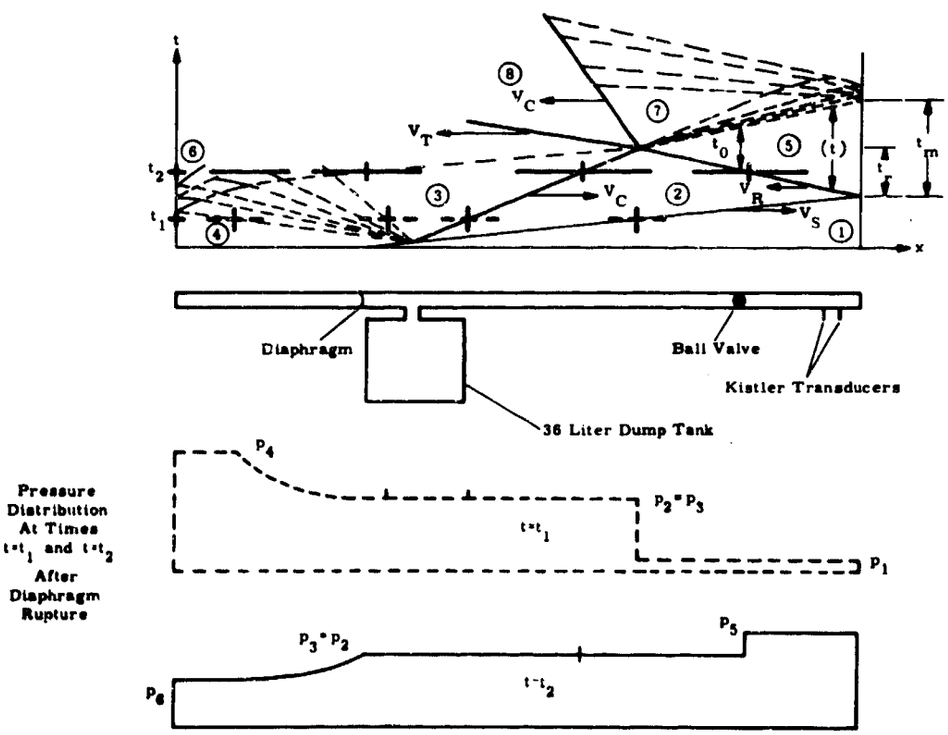

Figure 5. Chemical Shock Tube Wave Diagram

Coincident with formation of the shock wave, a rarefaction (expansion) wave moves from the decelerating contact surface toward the driver section end wall, reflects from the end wall, and is accelerated toward the reaction section, cooling the gas in Region 3. Provided the tube operating conditions are properly selected, the head of the reflected expansion wave terminates on the contact surface-reflected shock wave intersection. In this case the shock wave is partly transmitted into the cold driver gas, Region 3, and partly reflected into Region 5 as an expansion wave which cools the twice processed gas, effectively quenching the reaction. The transmitted shock wave is attenuated by the open dump tank, thereby preventing further heading of the gas sample. The reaction quency rate stated in the literature is 10^{6}°K/sec over an average dwell time of a few hundred microseconds. Because of this effective quench (Reference 7) the tube is called a single pulse chemical shock tube.

b. Non-Idealities

This technique of observing exothermic reactions in the relatively quiescent region downstream of the reflected shock wave (Region 5) is being used extensively (Reference 8 through 14). The principal advantage considered is that measurements are facilitated at high temperatures not available with the incident shock wave technique (measurements made in Region 2) because detonations likely incurred thereby tend to complicate the measurement. However, caution should be exercized when making rate measurements with a single pulse tube. This is because of certain flow non-idealities as follows (Reference 15):

1. Diaphragm rupture causes large initial flow perturbations that could be amplified if there is large exothermicity in Region 2.

2. Boundary layer build-up at the reflection end plate tends to cool large portions of the test samples when these are observed far from the end plate.

3. Slow cooling by means of the centered rarefaction wave may cause systematic errors in the data because the effective reaction test time must be integrated over the cooling time (Reference 16 and 17).

Caution exercized in the present work circumvents many of these nonideal flow problems. The first problem is alleviated in proportion to the amount of diluent used: 96 percent Argon for the stoichiometric oxy-diborane mixture studied. Evidence that detonations did not occur in Region 2 while measuring ignition induction times is given below. Further, according to the criterion given in References 15 and 18, exothermicity below that required for detonations in Region 2, but which could otherwise cause flow perturbations sufficient to accelerate the incident shock wave, is generally avoided by ensuring that the incident shock wave velocity u_1 is greater than the Chapman-Jouguet (CJ) detonation velocity u_{CJ} of the test mixture. The method outlined in Appendix B was used to compute the equilibrium concentrations of species in Regions 2 and 5 under test conditions. The species mole fractions other than the initial reagents and diluent were found to be negligable in Region 2 under those conditions. The flow field is therefore frozen across the incident shock wave, with $\gamma_1 = 1.634$. It

follows that $u_1 > u_{c1}$ when the incident shock Mach number is greater than the square root of the temperature ratio across the shock, i. e., when $M_1 > \sqrt{T_2/T_1}$. This was indeed the case for diborane ignition induction measurements presented below.

The second problem is alleviated according to Mark's criterion, Reference 19, viz. that the effective specific heat ratio be $\gamma_1 > 1.5$ so that the extent of test sample cooling due to boundary later interaction with the bifurcated shock wave is diminished. This is also accomplished by placing the observation port close to the end wall of the tube. In the tube used, the ratio of port-to-end wall distance over the tube diameter is 0.74.

The third problem is alleviated by using the single pulse shock tube modification introduced by Klepeis, Reference 20, viz. the use of a dump tank designed to increase the cooling rate by factors of from 5 to 10, Reference 17.

3. Performance

a. Transducers and Shock Velocity

The shock wave velocity has been measured variously with Martin Marietta designed barium titanate and quartz piezoelectric pressure sensors and by Kistler 701, 606L, and 603 pairs of quartz pressure transducers. The acceleration compensated Kistler 603's give the sharpest response, largest signal-to-noise ratio and most ideal (response to a step input) damping characteristics of all transducers tested; see the lower beam traces of Figure 6 c and d. Transducer spacing was designed to obtain average velocities at various tube stations located between the reflection end plate and the diaphragm. A delay signal is triggered by a barium titanate transducer mounted closest to the origin. This sensor was chosen for the trigger because of its superior sensitivity. The delay signal is swept at a speed chosen so as to display a maximum amount of information on the recording trace. Passage of the shock wave is observed on the traces of Figure 6. The two upper oscilloscope records (a and b) correspond to an initially set pressure ratio $p_4/p_1 = 40$ (ideal incident shock Mach number, $M = 3.075$). Record a is a helium/argon run with Kistler 606L's sensing the shock wave between transducer stations separated 10 inches. Note the short time lapse between the second and third pressure rise. Approximately 1/4 of the lapse corresponds to the time between arrival of the shock wave at the second transducer (the second rise) and the time of reflection of the incident shock wave from the end plate of the tube. Since the reflected shock wave moves at about one-half the speed of the incident shock, the third time lapse (between the 3rd and 4th rise) lasts about twice as long as the first. This is better observed on the three lower records which correspond to an initially set pressure ratio $p_4/p_1 = 20$ ($M = 2.55$).

b. Ignition Induction Check Runs

Notice the flat (but noisy) structure of the third plateau on record 6a. Record 6b corresponds to a 30 percent stoichiometric mixture of O_2 and CO diluted in argon. Similar tests have been reported by K.G.P. Sultzmann (Reference 21). Evidently, the 5 percent

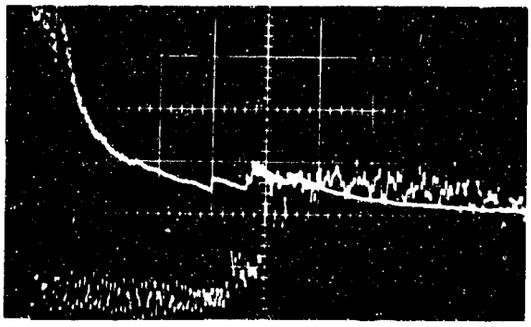

(a) Upper Trace: 1000 μ sec/cm
Lower Trace: 100 μ sec/cm
Helium/Argon tare run
p_1 = 20 mm Hg

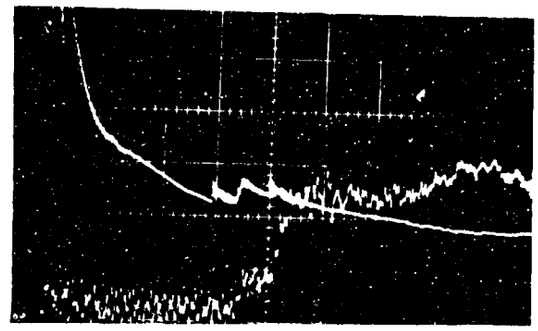

(b) Upper Trace: 1000 μ sec/cm
Lower Trace: 100 μ sec/cm
Helium Argon (30% $CO-O_2$)
p_1 = 20 mm Hg

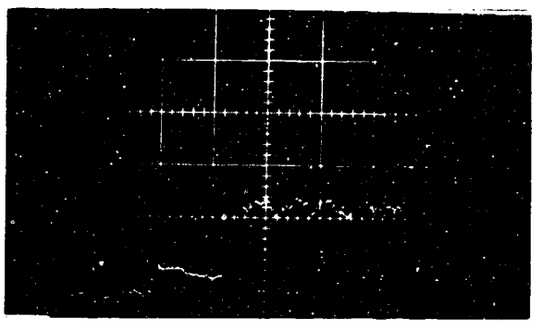

(c) Upper Trace - Photomultiplier Output
Lower Trace - Transducer Output
Sweep rate - 50 μ sec/cm
Helium/Argon tare run
p_1 = 103.4 mm Hg

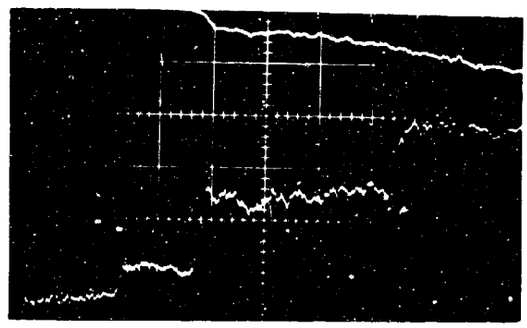

(d) Upper Trace - Photomultiplier Output
Lower Trace - Transducer Output
Sweep rate - 50 μ sec/cm
p_1 = 103.4 mm Hg
Helium/Argon (30% $CO - O_2$)

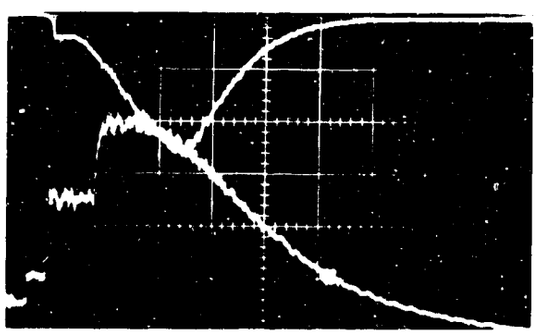

(e) Upper Trace - Photomultiplier Output
Lower Trace - Transducer Output
Sweep rate - 200 μ sec/cm
Helium/Argon (30% $CO - O_2$)
p_1 = 103.4 mm Hg

Figure 6. Carbon Monoxide Flame Experiments

change in specific heats has had very little or no effect on the incident shock velocity or on the level of the third plateau, compared to the tare run. However, the effect of combustion is evident on the third plateau where a superposed pressure due to the oxidation of CO can be observed to span about 250 microseconds. The ideal temperature, T_5, in the reaction zone, behind the reflected shock wave, is 2270°K for $p_4/p_1 = 40$, which exceeds the auto-ignition temperature of CO (924°K) by a factor of about 2½. The actual temperature is closer to 2000°K, determined from the Martin Marietta calibration curve (discussed below) and from the theoretical data on Figure 2. Hence, ignition induction commences at the shock front and lags about 250 microseconds prior to maximum burning. This is in agreement with the results of Sultzmann. Note that $p_1 = 20$ torr for these runs (rather than 103.4 torr), accounting for a reduced collision probability, hence no observable pressure rise due to auto ignition temperature behind the incident shock.

c. Optics

An attempt to verify the ignition induction period, by observing the total CO flame emission, was implemented by designing an optical system (Figure 7) with an RCA 931A photomultiplier tube located 90 degrees azimuthally from the end transducer in order to view light emitted from the slug of gas immediately downstream of the reflected shock wave. The sequence of oscilloscope records, (Figure 6, c, d, and e) shows a helium/argon tare run, a helium/30 percent CO/O_2 stoichiometric mixture diluted in argon, both swept at 50 μsec/cm, and a repeat of the oxidation run swept at 200 μsec/cm in order to display the entire history of events, all for $p_4/p_1 = 20$. As in the case of the $p_4/p_1 = 40$ runs, burning raises the level of the third and fourth plateaus whereas no change is observed nor predictable on the level of the first and second plateaus, the temperature in this case being about 130°K less than the auto-ignition temperature. However, in this case the initially set total charge pressure was about 5 times that of the earlier $p_4/p_1 = 40$ runs, (Figure 6a, b). That is $p_1 = 103.4$ torr so that the combined temperature and pressure effect can be observed in the initial photoemission rise (negative polarity, upper traces) over a period of about 10 microseconds. Evidently, the ignition induction period is complete by the time that the shock wave has arrived at the end transducer after reflection from the end plate.

d. Shock Tube Calibration

Approximately ideal air/air shock tube performance, shown in Figure 8 was accomplished experimentally after obtaining near ideal diaphragm rupture (petaling) using cellophane and scored aluminum foil diaphragms. This technique requires that p_4/p_1 be maintained at diaphragm pressure differences approaching the material yield point. Thus, the diaphragm ruptures with a minimum of material particles being lost to the stream and with a corresponding minimum energy transfer from the stream to the diaphragm particles. The transducer separation for these data was 17.80 cm.

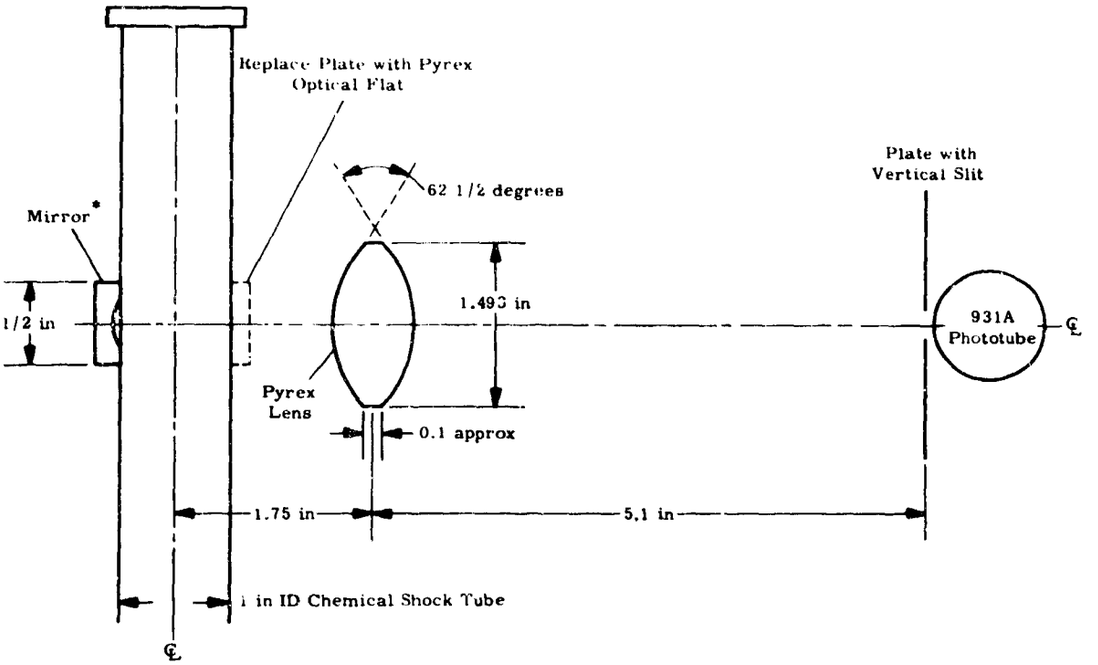

* Grind Spherical Radius – 0.56 in
Aluminum Mirror Surface Polished

Figure 7. Optical Emission Sensor

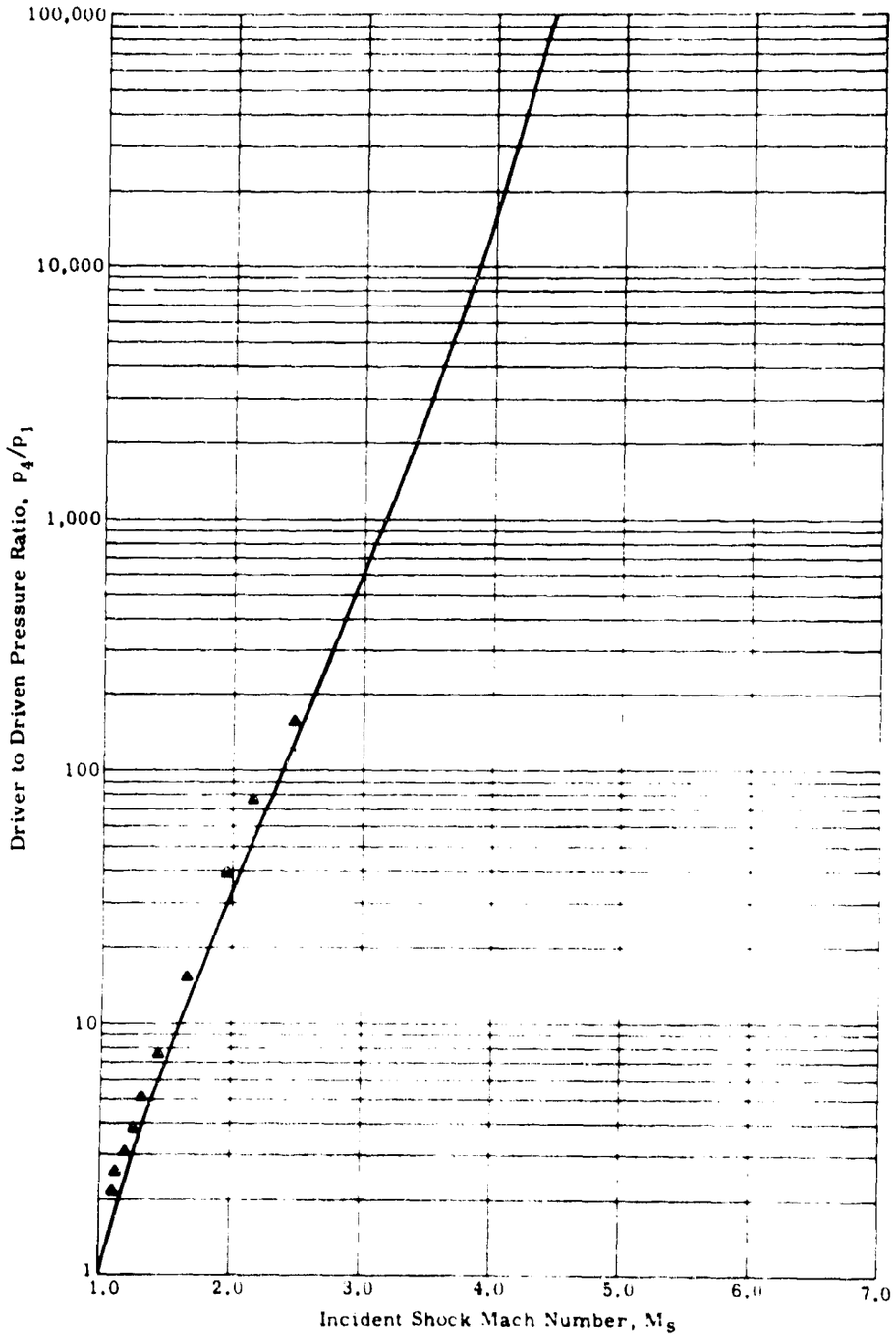

Figure 8. Air/Air Shock Tube Performance

Attempts have been made to eliminate the departure from ideal for the He/Ar calibration by running experiments at various transducer separations to increase the resolution (obtain an optimum ratio of transducer sensing element diameter to transducer spacing). The best resolution was obtained with the smallest transducer spacing tried. Consequently, the tare runs for a transducer spacing of 6.68 cm was used to define the standard calibration curve. This curve is shown in Figure 9 where the present experiments are compared to both theory and results of previous investigations.

e. Sources of Error, Data Scatter, and Uncertainties

The principal sources of error contributing to the departure of experimental shock tube performance from the ideal are:

1. Sensor resolution
2. Non-ideal diaphragm rupture
3. Boundary-layer effects
4. Laboratory environmental variations

Attempts to eliminate the first two sources of error listed have been discussed above. A correction, in the case of non-ideal rupture, is suggested but has not been attempted at this writing. It is suggested that the diaphragm may be weighed on an analytical balance both before and after a run. The energy balance required to accelerate diaphragm residue down the tube may then be used to correct for shock wave attenuation.

Shock wave attenuation due to the boundary layer is another factor which can be accounted for in order to correct the departure.

The data shown on Figure 8 indicates good repeatability, considering that each of the single data points plotted at a given p_4/p_1 represents two indistinguishable runs.

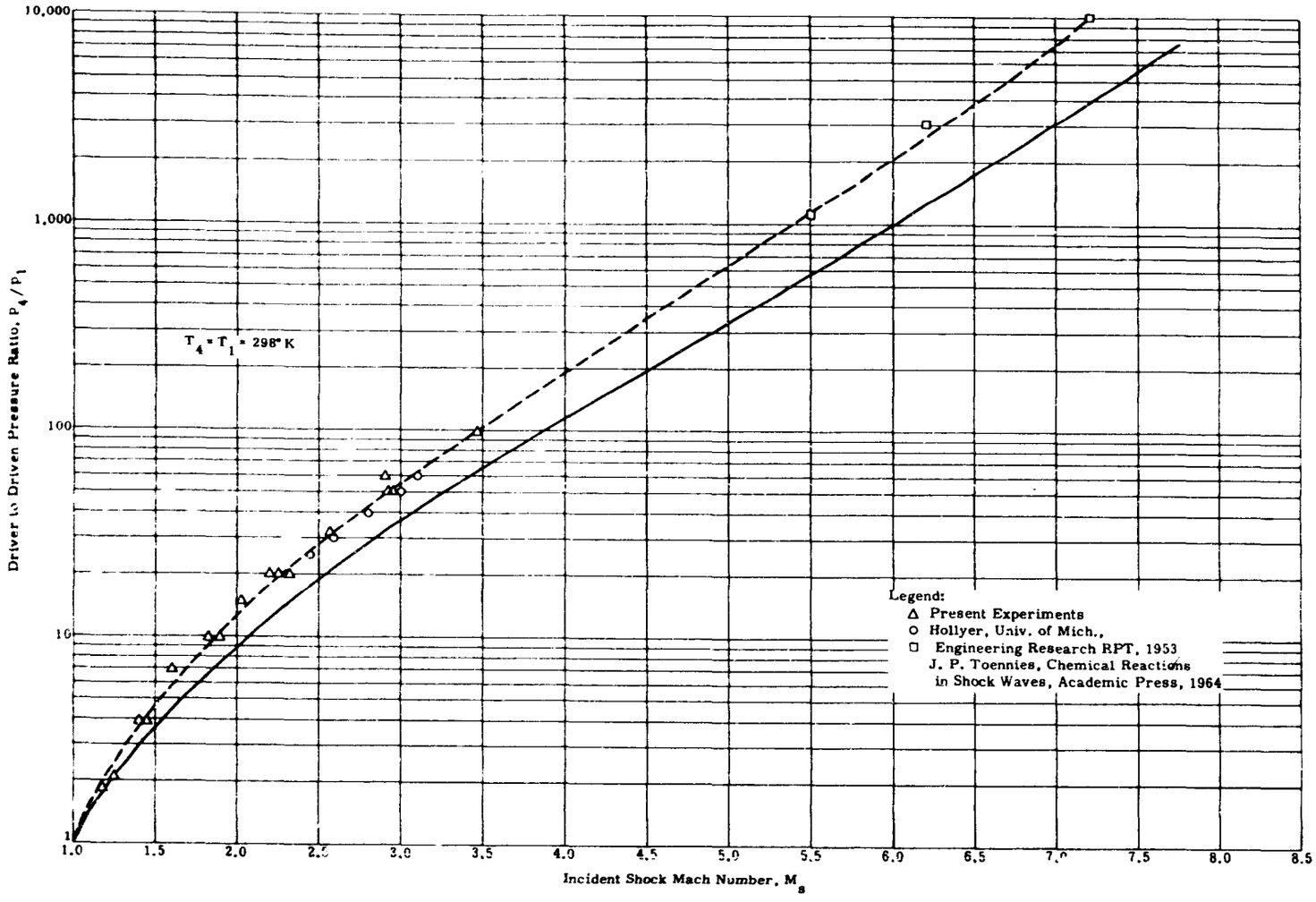

Figure 9. Helium/Argon Performance Calibration

II. TECHNICAL APPROACH

A. SELECTION OF FUELS

The selection of high energy fuels used in the experimental studies was predicated on existing thermochemical and kinetics data, commercial availability, and ease of synthesis. Prior literature survey, described in Reference 22, eliminated pentaborane and aluminum borohydride from immediate practical consideration because of their high costs. A considerable amount of research has been conducted on the boron hydrides, their stable adducts, and substitution alkyl compounds, (References 23 through 27). In Reference 23, for example, the aim of research has been to obtain a fundamental understanding of combustion and extinguishment for the diborane-oxygen (B_2H_6/O_2) and for the pentaborane-oxygen (B_5H_9/O_2) reactions. Ignition delay times for B_2H_6 and B_5H_9/oxygen mixtures diluted in argon were measured using a single pulse shock tube adapted to the tailored interface technique reported in Reference 28. Shock tube ignition of the $B_5H_9/O_2/Ar$ mixtures required slightly higher temperatures than those containing diborane, although static bulb experiments (Reference 23) indicate that pentaborane is more flammable than diborane.

For both compounds, test results show that ignition delay times are independent of the oxygen concentration throughout an equivalence ratio range from 0.5 to 2. This information is based on an equivalence ratio of 1 corresponding to a 1:6 pentaborane-oxygen ratio which could react completely according to

$$2\ B_5H_9 + 12\ O_2 \longrightarrow 5 B_2O_3 + 9\ H_2O;$$

and corresponding to a 1:3 diborane ratio for the overall reaction

$$B_2H_6 + 3\ O_2 \longrightarrow B_2O_3 + 3\ H_2O\ .$$

Because of the oxygen concentration independence of the ignition induction times and since the activation energies are close to those for pyrolysis, it was concluded in Reference 23 that pyrolysis is the rate controlling step in ignition.

Figure 10 presents thermochemical data in favor of the selection of B_2H_6 as a candidate for oxidation kinetics studies. Figure 10 shows the heat liberated in combustion of 1:3 mixtures of B_2H_6/O_2 over the temperature range 300-2300°K, compared to the heat liberated in combustion of a 2:1 mixture of H_2/O_2 (data taken from the JANAF tables, Reference 29). Thus, in applications where heat liberation per pound of total reactants is important, the reaction yielding boron oxide in the crystalline state produces 1300 Btu per pound more than the H_2/O_2 reaction at 300°K whereas the excess at 2200°K drops to 570 Btu per pound for B_2O_3 in the liquid state. Applications to supersonic combustion seem desirable.

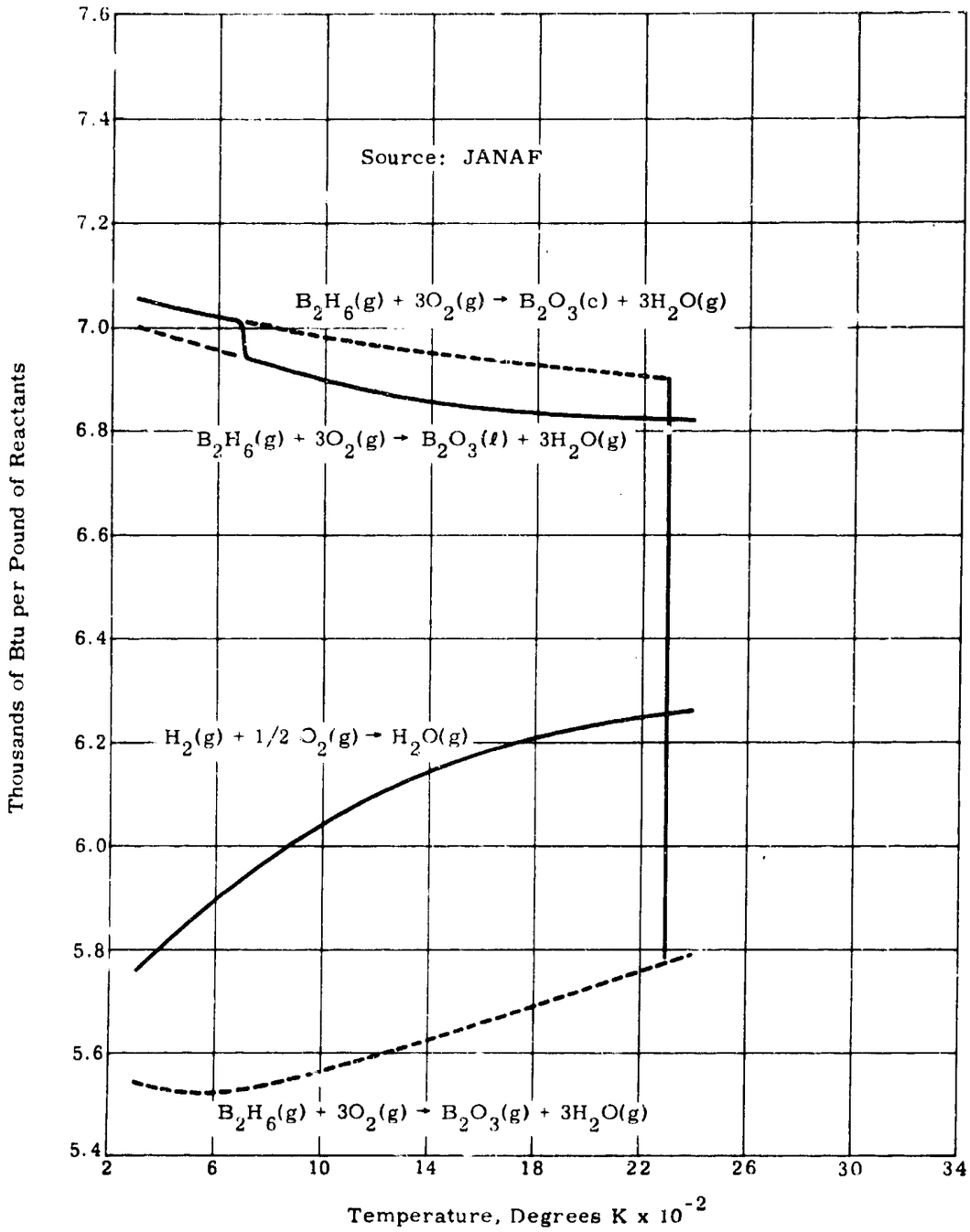

Figure 10. Heat of Combustion of B_2H_6/O_2 Compared to H_2/O_2

Clearly, the best way to proceed with a diagnostic method of investigation which one hopes to apply to the understanding of mechanisms and kinetics of a chemical system is to see how that method has been applied to the understanding of other systems. Literature search and problem solving began with the relatively well known hydrogen/oxygen (H_2/O_2) system, including brief digressions with the better known hydrogen/halide (H_2/X_2) and the nitrous oxide/hydrogen (N_2O/H_2) systems, all of which are branching chain mechanisms at temperatures above 600°K. The Martin Marietta reaction profile model computer program was used to try an H_2/O_2 reaction test case. Reaction profile models are now part of the molecular dynamicist's diagnostic tool kit, both in industry and at universities. The Orlando Division of Martin Marietta worked with Cornell University during the simultaneous development of very similar reaction profile models, thereby gaining insight to the problems that will arise when the Orlando Division proceeds to more complicated systems such as H_2/air, B_2H_6/O_2 and B_2H_6/air for computer diagnostics or engineering applications. The details of this work will be given in Part Two of this report.

Experimentally, the B_2H_6/O_2 system is more complex than those aformentioned because element number five, boron, has three electrons to share in combination with other elements, in contrast to more stable elements such as its neighbor, carbon. Diborane has six pairs of electrons to distribute among nine bond positions, that is, 2/3 of a single (pair) bond per bond. The molecule is therefore said to be electron deficient (on the average, 1/3 electron pair). This is the fundamental reason for the reactivity and, consequently, sometimes desirable quality of diborane as a high energy pyrophoric fuel. Also, this system has ten individual atoms (B_2H_6/O_2) to permute within the limits of certain allowed combinations. These limits may change in a way that is yet to be discovered. In contrast, after a decade of modern techniques including the use of shock tubes and reactor profile analysis, the H_2/O_2 system is now essentially fixed at eleven steps in its high temperature and homogeneous branching chain mechanism, with only four individual atoms to permute!

B. HYPOTHESIZED B_2H_6/O_2 MECHANISMS

It is generally conceded in the literature that B_2H_6/O_2 will exhibit a branched chain mechanism, but even the early hypotheses (e.g. Roth's thesis, Reference 30) have not been clearly verified beyond the first step, viz., $1/2\ B_2H_6 + O_2 \rightleftharpoons BH_3 + O_2 \rightarrow$

Roth and Bauer (References 31 and 32) postulated a mechanism for the B_2H_6/O_2 reaction (Reference 15) based on partial analogy with the H_2/O_2 at the second explosion limit, namely

$$B_2H_6 \rightleftharpoons 2\ BH_3$$

$$BH_3 + O_2 \rightarrow BH_2OH + O$$

$$O + B_2H_6 \rightarrow BH_2OH + BH_3$$

$$BH_2OH + B_2H_6 \rightarrow BH_3 + B_2H_5OH$$

$$BH_3 + O_2 + M \rightarrow HBO_2 + H_2 + M$$

$$BH_3 + B_2H_6 \rightarrow B_3H_7 + H_2$$

$$B_3H_7 \rightarrow \text{polymerization}$$

$$B_2H_5\ OH \rightarrow \text{further oxidation}$$

where M in the fifth reaction step is any third body. The mechanism was further modified by Goldstein (Reference 33) and has been studied by the group at Rensselaer under Bauer and Wiberly (Reference 34). Compared to the oxidation of hydrogen, the oxidation of diborane requires considerable study before its mechanism is understood as fully as H_2/O_2.

Recently, the shock tube work of Skinner et al (Reference 23) opened a new line of research for understanding the mechanism of flame inhibition in both H_2/O_2 and B_2H_6/O_2 reactions. The investigations of Koski at Johns Hopkins and Porter at Cornell have yielded low temperature mass spectra of BH_3 and other intermediate species in the B_2H_6/O_2 system (References 35 and 36).

Gobbett and Linnett (Reference 37) have studied the B_2H_6/O_2 system in a conventional reaction vessel at temperatures between 393 and 483°K, while Jolly and Schmitt (Reference 38) have studied the reacion of diborane with hydroxide in aqueous solutions, lending credence to the existence of $BH(OH)_2$ as an intermediate.

Based on stoichiometric data derived in these experiments, and from the available literature on the B_2H_6/O_2 system, the following reaction mechanism was postulated, consistent with thermochemical data shown on Table II:

		(ΔH) 298°K, kcal/mole	
	$B_2H_6 \rightleftharpoons 2BH_3$		+36.0
	$O_2 + BH_3 \longrightarrow H_3BOO \rightleftharpoons H_2BOOH \xrightarrow{k_1} H_2BO + OH$		
	$Ar + BH_2O \xrightarrow{k_2} BO + H_2 + Ar$		+ 6.0
	$Ar + OH + BO \xrightarrow{k_3} OBOH + Ar$	-154	
	$OH + BHO_2 \xrightarrow{k_4} BO_2 + H_2O$	-10	
	$OH + BH_3 \xrightarrow{k_5} BH_2 + H_2O$	-45	
(4 Center)	$O_2 + BH_2 \xrightarrow{k_6} BHO + OH$	-38	
	$O_2 + BHO \xrightarrow{k_7} BHO_2 + O$	-75	
	$H_2 + BO_2 \xrightarrow{k_8} BHO_2 + H$	-7	
	$2\ BHO_2 \xrightarrow{k_9} B_2O_3 + H_2O$		+11.0
H_2/O_2	$O + H_2 \xrightarrow{k_{10}} OH + H$		+ 2
	$Ar + 2H \xrightarrow{k_{11}} H_2 + Ar$	-104	
		-442.0	+55.0

Net: $3O_2 + B_2H_6 \longrightarrow B_2O_3 + 3H_2O$ (-386) -387.0

Observables $\langle OH;\ BO;\ BO_2;\ BH_2 \rangle$

Note: Prof. S. H. Bauer suggests that $BO_2 + BO_2H$ is more likely for the production of B_2O_3.

TABLE II

Thermochemical Data, H°_f*

	Molecule	°K 298	1000	1500	
	B	133	133	132	boron
	BH	106	105	104	boron monohydride
	BHO	-20±20	-21	-21.5	boron oxide hydride
	BHO_2	-134	-136	-137	metaboric acid
	BH_2	48±15	47	46	boron dihydride
	BH_2O_2	-114±1.	-115	-115	boron dihydroxide
	B_2H_2O				
	BH_3	25.5±10	22.6	21.5	boron trihydride
	BH_3O	-70.0±1	(J Phys. Chem. 68,		monohydroxyborane
	BH_3O_2	-153.8	27, 32, 64)		dihydroxyborane
	BH_3O_3	-237	240	-241	boric acid
	B_2	195±6	194	192	boron
	$B_2H_2O_3$	-200.4±3.5	(J. Phys. Chem. 68, 3164, '65)		
	B_2H_6	9.8±4	5.5	5.7	diborane
	B_2H_3O				
	B_2O_2	-109±2	-109.5	-110.5	dimeric boron monoxide
	B_2O_3	-199.14	-200	-201	boron oxide
	$B_3H_3O_3$	-291±10	-293.6	-293.5	boroxin
	$B_3H_3O_6$	-543±3	-542	-540	trimeric metaboric acid
	BO	11±10	9.88	8.76	boron monoxide
	BO_2	-75.27	-75.3	-75.6	boron dioxide
	$B_2H_4O_4$	-307	-309	-308	boron dihydroxide (dimeric)

*in kcal/mole, JANAF

Reaction steps in the chain include the thermal decomposition of B_2H_6, with dissociation energy of 1.62 eV (Reference 39) to give two moles of BH_3. Oxygen combines with BH_3 producing one of several isomers, $H_3BOO \rightleftharpoons H_2BOOH$ at high temperatures, or $HB(OH)_2$ at low temperatures. Following Berl (Reference 40) this step may contribute to the production of hydroxyl radical and H_2BO. Thermochemical data for the latter molecule is not yet available. It was, therefore, necessary to add the reaction steps leading to the production of boron monoxide, deleting the isomerization, to obtain the heat of reaction of 6.0 kcal/mole. The total heat liberated in the sequence of reaction steps summed to within 0.26 percent of the heat liberated in the net reaction.

The only high temperature rate obtained at this writing is the one for pyrolysis, Reference 23. Subsequent reaction steps which contribute to ignition induction may be determined through a search for readily observable free radicals such as OH or boron monoxide. Thus, a spectrospopic investigation of the ignition induction mechanism was initiated.

BLANK PAGE

III. SHOCK INDUCED IGNITION OF DIBORANE

The shock tube used to measure ignition induction time is described in Section I. A schematic of the shock tube, instrumentation, and recording setup is shown on Figure 11.

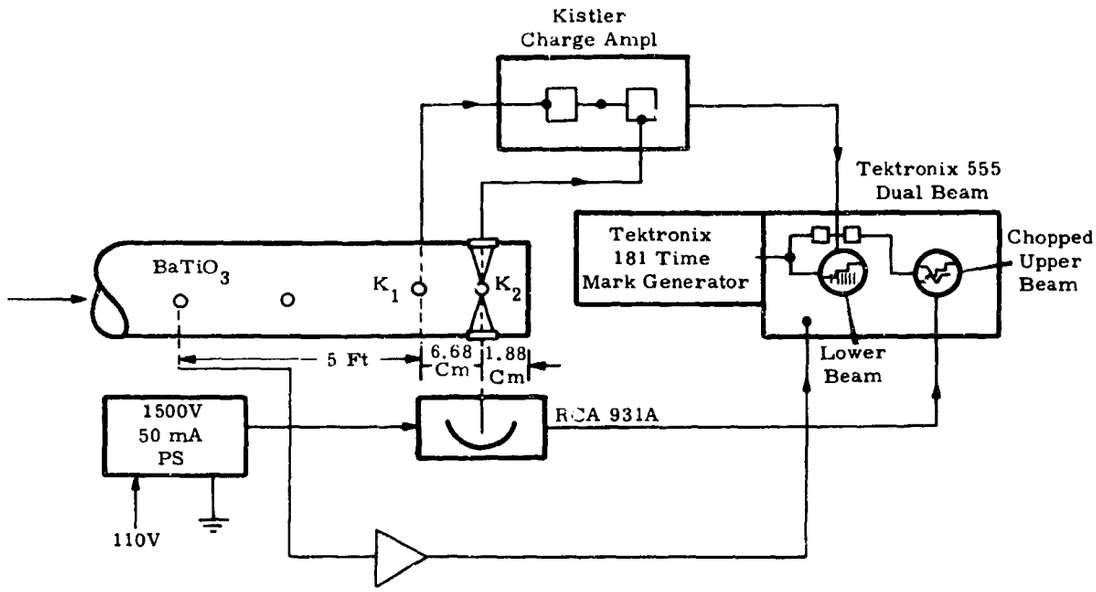

Figure 11. Instrumentation Schematic

Figure 12 illustrates the region of observation on a time-distance wave diagram, representative of events occurring axially in the shock tube following the time of diaphragm burst.

Measuring station (1) is defined at 1.88 cm from the shock reflection end plate of the driven tube. Overall length of the driven tube is 40 inches, from the diaphragm station to the end plate, for all subsequent experimental data presented. The driver tube length is continuously varied (Reference 7) to adjust the wave intersect position for optimum gas dynamic quench characteristics (i.e., cooling rates of 10^6°K/sec). Thus, the total shock tube length can be varied from about 4 feet 2 inches at the high-diaphragm burst-pressure ratio, P_{41} = 100, to about 7 1/2 feet at the low P_{41} = 5. Helium was used as the driver gas, to produce shock waves in argon.

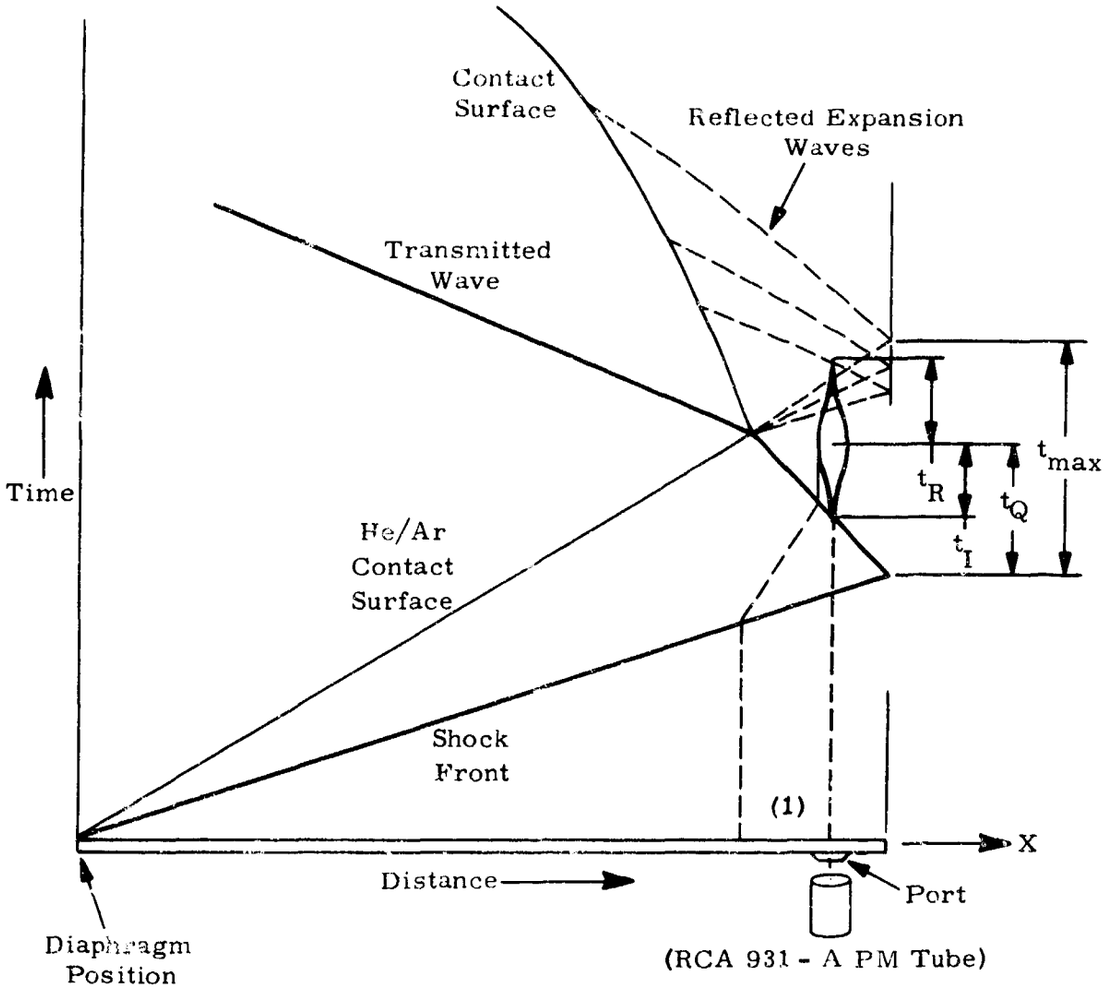

Figure 12. Wave Diagram - Flame Schematic

An RCA 931A photomultiplier (PM) is mounted at an observation port centered on measuring station (1). A Kistler 603 pressure transducer is also mounted at station (1), perpendicular to the observation port, so that both light and pressure intensities are observed simultaneously from the same homogeneous gas sample behind the reflected shock wave.

The flame-like schematic represents spatial extent of the intensity observed as a function of time, superimposed on the wave diagram. (Such flames have been observed in shock tubes using Schlieren photography.)

A. IGNITION INDUCTION MEASUREMENTS

Definition of ignition induction time, t_I, for the present measurements is shown as the incremental time from arrival of the reflected shock wave at the measuring port to the time of maximum light intensity at the measuring port (Figure 12).

Oscillogram traces from the experiments are shown in Figure 13 for the sequence of diaphragm burst pressure ratios P_{41} = 5, 5.5, 6, 6.5, 7, 8, 8.9, and 11.42, representing ideal reactor bath temperatures in the range 750 to 1175°K behind the reflected shock wave. The actual temperature range, after bulk correction for losses due to boundary layer and inefficient diaphragm burst, is believed to be 575 to 945°K ±50°K. The tolerance is obtained from literature values for the attenuation of shock waves in shock tubes of L/D approximately that used in this experiment. Data reduction for this series of runs is displayed on Table III.

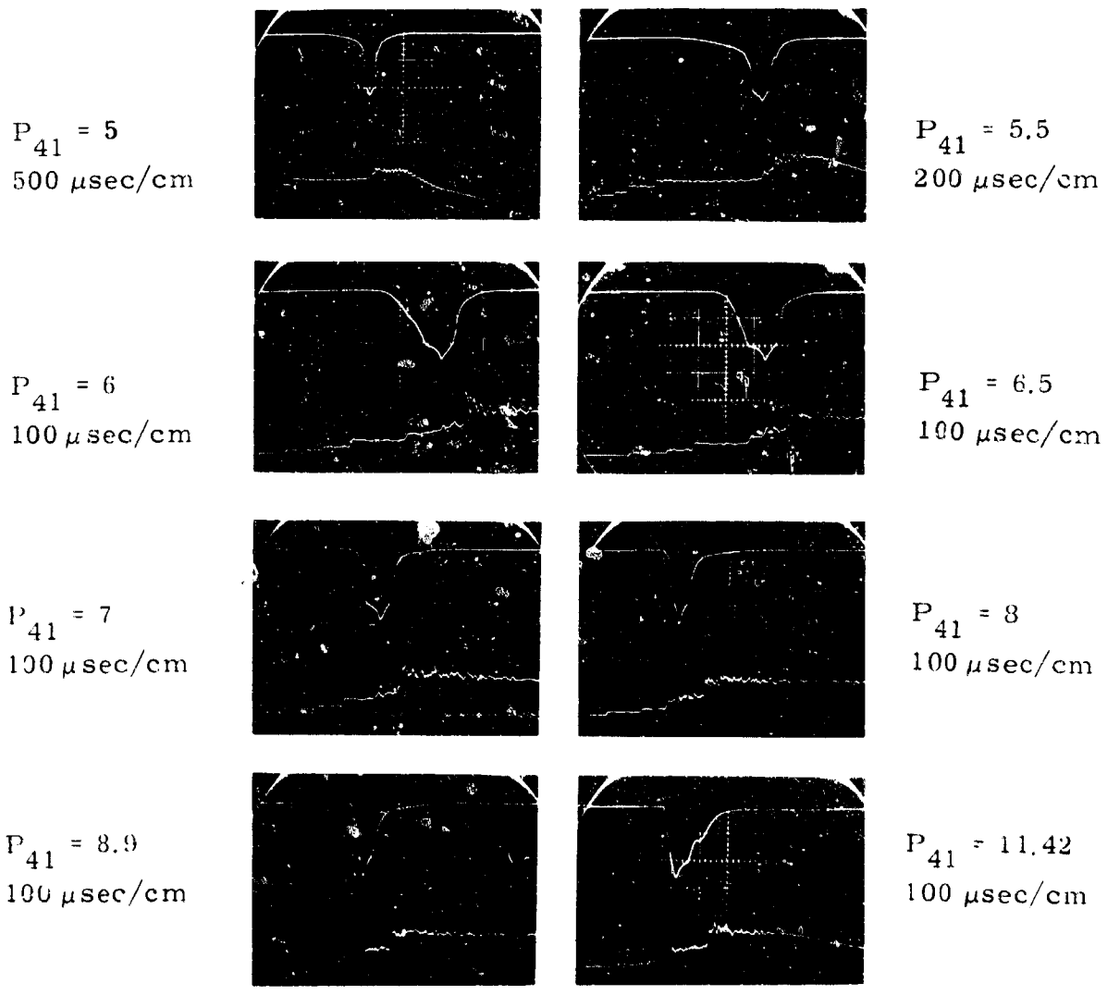

Figure 13. Oscillogram Traces, Ignition Induction Measurements of 1:3:96 B_2H_6:O_2:Ar, P_1 = 300 mmHg

TABLE III

Sample Run Chart

Run	Tube Configuration	Mixture	P41	P1 torr	Sweep μsec/cm	Δt1 μsec	Δℓ Transducer Spacing (.100 cm)	V1 Δℓ/Δt1 (msec⁻¹)	T1 Room Temp (°C)	a1 Sound Speed (msec⁻¹)	M1 Incident Shock Mach Number	T5 Reaction Temperature (°K)	10³/T5 (°K⁻¹)	Δτ, Ignition Delay (μsec)	Remarks
2.24.1	Short*	He/96% Ar B_2H_6/O_2 (S)	8.8	91	200	556.5	0.314	564	24	319	1.7675	820	1.220	200	
2			8.7	32		565		556			1.7420	804	1.244	318	
13														270	
2.23.4			8.9	90		562		558.5			1.750	809	1.237	280	
6														240	
5.3.20			8	100	50	125	0.0668	534.5			1.675	750.5	1.331	39.4	✓
22			8.9	90		120		557			1.747	807	1.239	16.5	✓
5.4.6			11.42	70		110.5*		605			1.893	929	1.0775	11.0	
4		He/Ar Tare				110 [2]		602.5			2.120 1.903	1085 936	0.9225 1.068		
5		He/96% Ar/ B_2H_6/O_2 (S)				110						906 936	1.068	11.0	
5.3.15			12.34	65		109.5*		610			1.911	945	1.0585	15.0	
14		He/Ar Tare				109.25		611			1.914				
5.4.8		He/96% Ar/ B_2H_6/O_2 (S)	5	160	500	147.5		453			1.420	575	1.739	1600	✓
9													1.739	2000	✓
5.2.3		He/Ar Tare			50	141 [2]		474			1.485				
5.2.4		He/Ar Tare	5.5	145.37	50	138		484.5			1.5185				
5.5.1		He/Ar Tare		145.00	200	134		498.5			1.561				
2		He/96% Ar/ B_2H_6/O_2 (S)				140		477.5			1.4975	620	1.622	656	Diffusion 1 hr ✓
4													1.622	762 [2]	Diffusion ≈ 3 hr ✓
5													1.622	980	3½ hr ✓
5.8.7													1.622	810	72 hr ✓
5.8.4		He/Ar Tare	6.0	133	100	131.5		508			1.591				
5.8.16		He/Ar Tare		130		135		495			1.55				P4 = 780 Torr
5.3.17		He/96% Ar/ B_2H_6/O_2 (S)		130		137		488			1.53	642.5	1.557	335	P4 = 780 Torr ✓
5.8.5		He/96% Ar/ B_2H_6/O_2 (S)		133		133		502.5			1.574	677.0	1.478	381	Diffusion 70½ hr ✓
5.8.2		He/96% Ar/ B_2H_6/O_2 (S)	7	115	100	130		514.5	23		1.61	701.5	1.426	137.5 [3]	✓
5.8.8		He/96% Ar/ B_2H_6/O_2 (S)	8	100	100	122		547.5			1.718	782	1.278	31	74 hr ✓
5.3.5		He/96% Ar/ B_2H_6/O_2 (S)				121.5		550			1.722	786	1.272	50	22 hr ✓
5.8.9		He/Ar Tare	8.9		200	550	0.314	571.5			1.790	840	1.19		
10		He/96% Ar B_2H_6/O_2 (S)		90										30	12 3/8 ✓A ✓
5.3.7		He/96% Ar/ B_2H_6/O_2 (S)			100	122* [2]	0.0668	548			1.718	782	1.278	39	✓
5.9.1		Non stoichiometric			50	121.75								34.5	Mixture less than 90 mm (S) ✓
5.5.6	Short	T	6.5 780	120	100	138	0.0668	484	23						
7		T								319	1.518	635	1.574	260	✓
8		T											1.574	243	✓
5.3.9		F	10	80		138		566	25		1.773	828	1.266	16.8	✓
5.8.13	Short	T	10			540	0.314	581.5	23		1.823				
12		T				542.5		579			1.8135	858	1.165	11.5	✓

T - Long tube
S - Short tube
(S) - Stoichiometric F/R = 1
* - Same as Tare
[n] - Number of repeats
T - Tare - He/Ar
F - 1.3.96 - B_2H_6 O_2 Ar
✓ - Points used for method of least squares determination of activation energy = 17.5 kcal

The incident shock wave velocity is measured as the difference between the first two pressure steps on the lower trace. The end of the wiggle between the second and third steps indicates the acoustical effect of shock wave reflection at the end plate. The third and fourth steps measure the reflected shock wave velocity. Pressure oscillations after this time are due to combustion. Note correlations with the (upper) photomultiplier trace.

To obtain measurements under approximately ideal conditions, the stoichiometric reactants (B_2H_6:O_2 = 1:3) are premixed at high dilution ratios in argon. Initial conditions, i.e., the initially set pressures in the driver and driven (reactor) sections of the shock tube, are then set according to the theory governing propagation of ideal shock waves in the inert diluent (Appendix B). Both measurement and theory show there is negligible error (Figures 14 and 15) in this procedure provided that diluent concentrations are sufficiently large and that the incident shock wave is sufficiently weak to preclude the onset of detonation modes. It follows that the equilibrium temperature T_2 downstream of the shock wave (Region 2 in shock wave nomenclature) is too small to provide significant interparticle collision frequency for ignition of the highly diluted fuel/oxygen gas mixture. This is verified experimentally with the PM which views the incident shock wave in the reaction section of the tube. Since no light is detected in the region of sensitivity of the PM, centered about 0.42 micron, until after shock reflection from the end plate and since there is no measurable difference between the incident shock wave velocity in the mixture or in the pure diluent for the same initial conditions, it follows that ignition occurs only after shock reflection for those initial conditions. (The observed effects here are entirely analogous to the observations with CO ignition.)

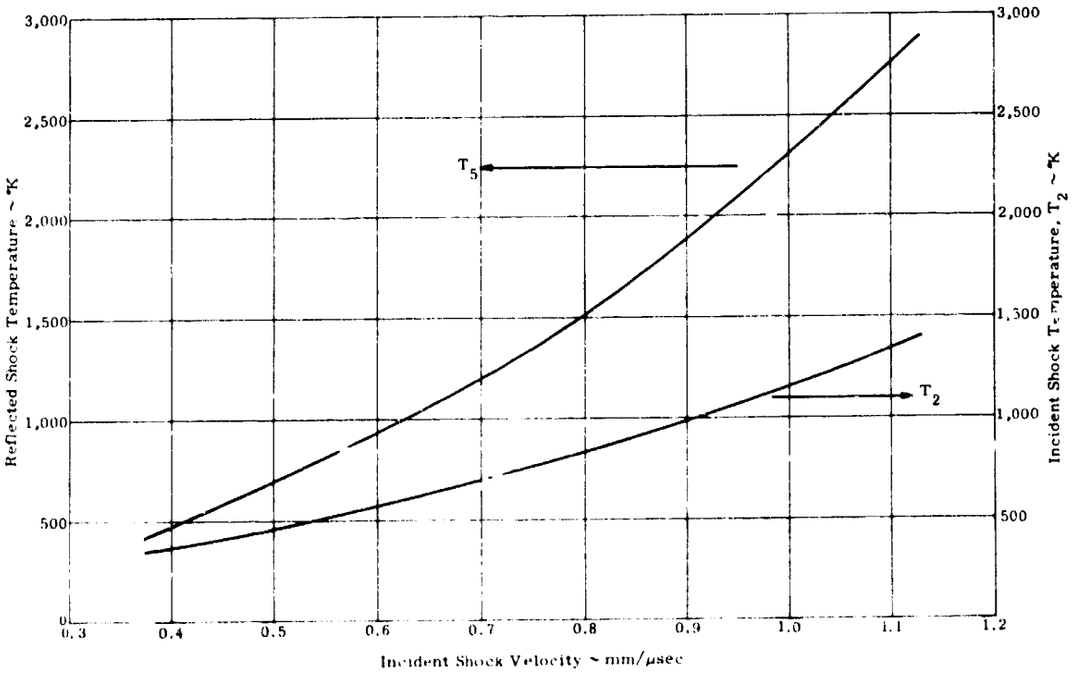

Figure 14. Shock Waves in Pure Argon, Initial Temperature = 298°K

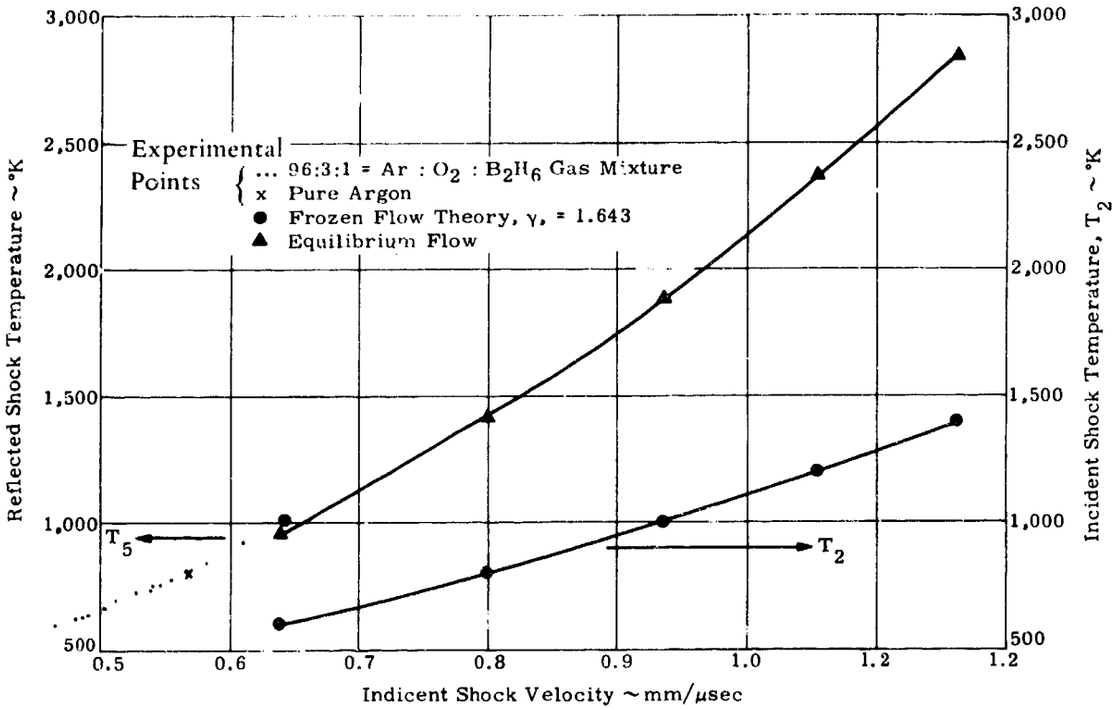

Figure 15. Shock Waves in Ar (96 Percent) + O_2 (3 Percent) +B_2H_6 (1 Percent); Initial Temperature = 298°K; Pressure = 500 mmHg

Under these conditions it may be assumed that the initial mixture mole fractions are unchanged in traversing the shock wave into Region 2. Figure 15 shows the equilibrium chemistry temperature calculations (Appendix B) which assume first, that flow is chemically frozen across the incident shock wave and, second, that equilibrium concentrations of intermediate species postulated in the chain mechanism on page occur downstream of the reflected shock wave. (Note that initial pressure variation does not significantly change T_5.) Martin Marietta experimental data is plotted on Figure 15. Comparison of these data show that the reported experimental temperatures T_5 lie above the equilibrium values by about 40°K at the highest measured velocity. This is not surprising in view of the fact that the experimental temperatures are deduced from ideal shock calculations for the pure diluent, Figure 14. Converting the measured incident shock velocity to Mach number (see Table III) and reading the calibration curve, the dashed line of Figure 9, shows good agreement with the initially set

pressure ratio P_{41} - as it should for the shock tube used. The departure between ideal and actual P_{41} at that Mach number implies a smaller value of T_5, in agreement with the equilibrium temperature of the mixture. This Martin Marietta calibration curve was used as a standard of agreement and as a basis of deducing the heat bath temperature.

Ignition induction for diborane is presented on Figure 16. Note that data of Skinner, et al (Reference 23) was obtained in a 3-inch diameter single-pulse tube patterned after the work of Glick, Squire, and Hertzberg (Reference 28), the driven section being 12 feet long and the driver variable between 6 and 28 feet. Thus, the L/D = 48 for Monsanto's driven tube is about the same (L/D = 40) as Martin Marietta's, indicating nearly equal incident shock wave attenuation characteristics. The present measurements appear to extend the data of Skinner et al by 2 orders of magnitude with approximately the same activation energy.

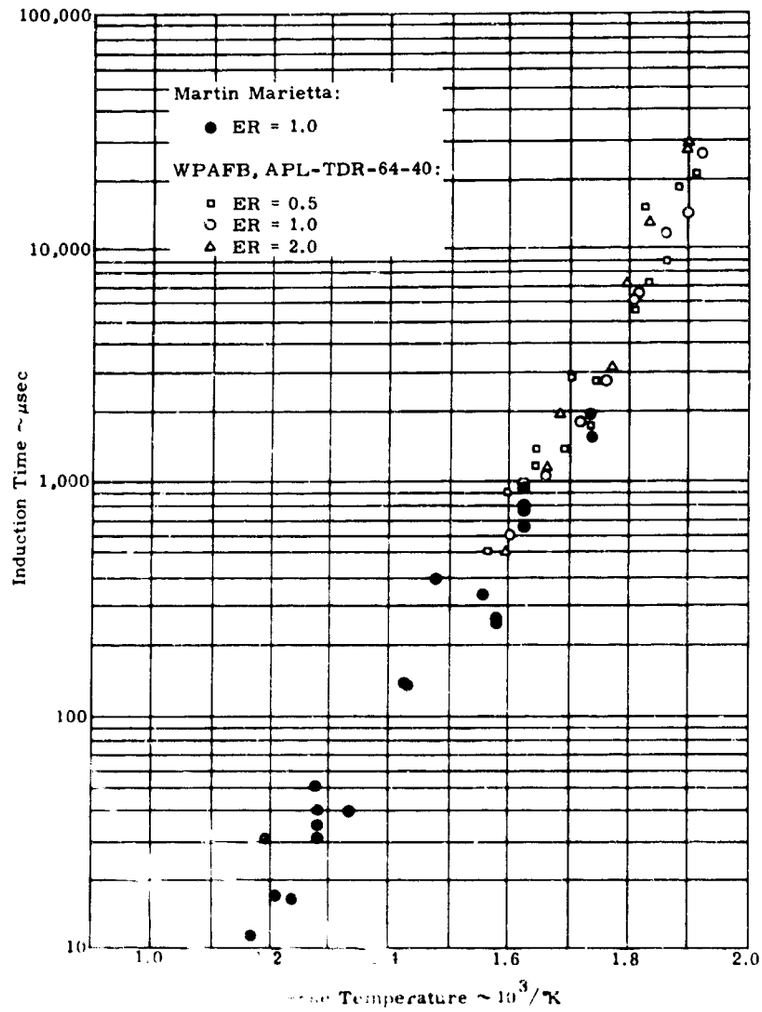

Figure 16. Diborane - Ignition Induction

The activation energy obtained for points indicated on Table III by a method of least squares calculation was 17.5 kcal compared to 21.1 kcal reported by the Monsanto group for E.R. = 1. Note that if Martin Marietta were to replot their data in agreement with the equilibrium temperature as noted above, but not in agreement with the calibration curve, Martin Marietta activation energy would be closer to Skinners, for then the 40°K, disagreement at the high temperature end would be removed, the disagreement (from equilibrium) at the low temperature being close to zero. However, if there is a decrease in the activation energy at high temperatures one may conclude that it is due to a possible change in mechanism between the high and low temperature regimes such that the system tends to be less reaction controlled at the high temperature.

The efficiency of Monsanto's tube is compared to Martin Marietta's and to the ideal He/Ar shock tube performance on the expanded scale shown on Figure 17 (expanded from Figure 9). The apparent better efficiencies obtained by Monsanto are attributed to their use of nitrogen gas to tailor the interface (acoustical impedance matching). However, Martin Marietta's greater departure from the ideal is not a prima facie cause of the slight departure from the activation energy curve established by the earlier investigators.

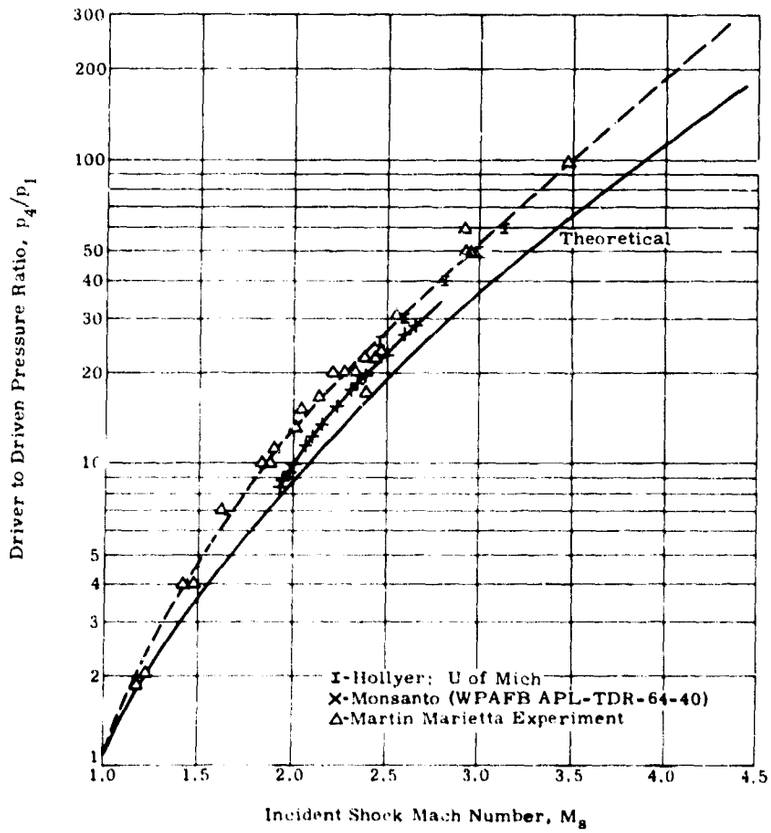

Figure 17. Helium/Argon Performance - Calibration

B. DETONATION LIMITS

Detonation studies, Figure 18, give further insight to differences between the greater volume tube (Monsanto) and Martin Marietta's 1-inch lower-volume tube. When attempts were made by the Monsanto group to measure ignition induction times of B_2H_6/O_2 at temperatures greater than 640°K for an equivalence ratio of 1 in a 99 percent diluent mixture, detonation of the gas mixture occurred behind the incident shock wave. The driver pressure in these experiments was 4400 mm Hg. These results showed that although the gas mixture behaves dynamically like pure argon (see Figures 14 and 15), complete reaction of the 1:3 mixture theoretically generates enough heat to raise the gas temperature by about 240°K at initial pressures of about 450 mm Hg. This would similarly occur at about 45 mm Hg (Figure 18) for the present studies as the detonation curve is, proportionally speaking, near its peak there. Note that the present study is conducted at initial pressures that are less than the Monsanto study by about one order of magnitude and with a driver pressure of 800 mm Hg so that shock strengths may be comparable and the temperature rise due to combustion will be less than 240°K, proportional to the enthalpies. The tailored interface technique, greater volume, and high initial pressures combined to exceed the explosion limits and to enhance the onset of detonation at greater temperatures, limits the amount of ignition induction data obtainable by the large volume tube at the high temperatures by as much as two orders of magnitude in the induction time. On the other hand, the low volume tube was high pressure limited and data could not be obtained with sufficient accuracy at the low temperatures. Departure in the calibration base curves (argon only) are due to acoustical impedance mismatch of the driver gases. To account properly for all differences it would be necessary to extrapolate data to infinite volume.

Figure 18. Comparison of Martin Marietta and Monsanto Deton

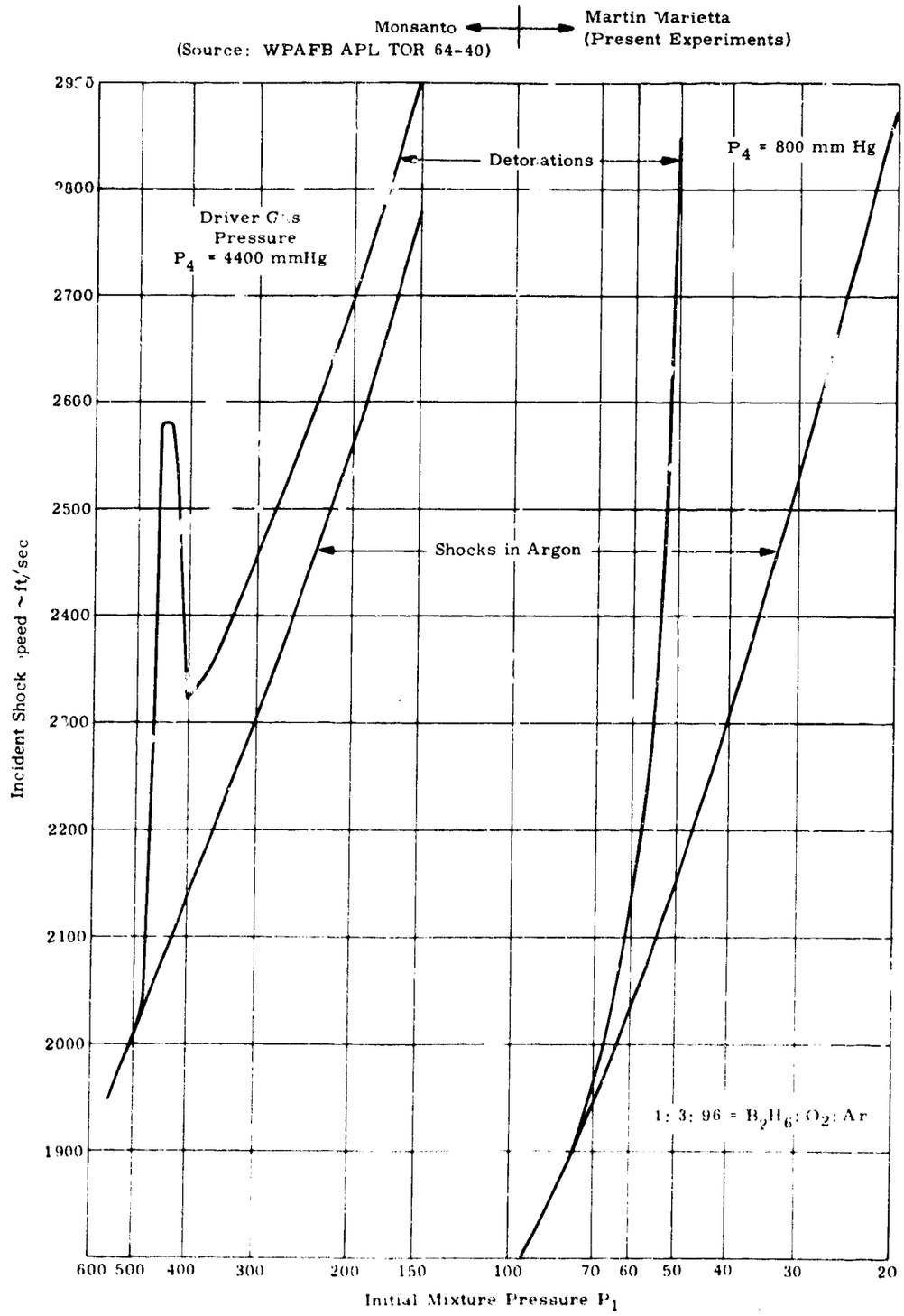

etonation Studies

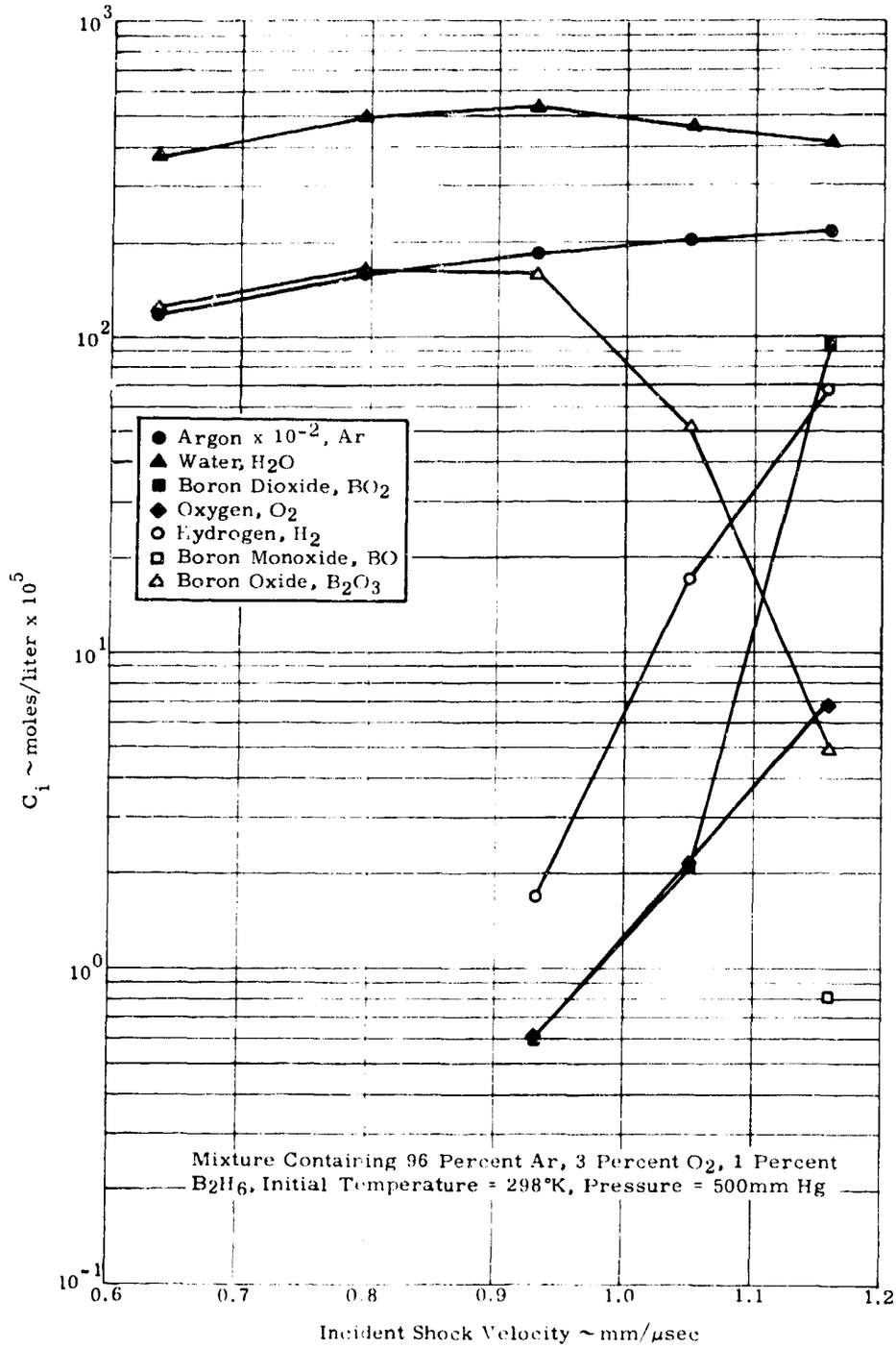

Figure 10. Computed Equilibrium Compositions in the Reflected Shock Wave Region Ar, H_2O, O_2, H_2, BO, and B_2O_3

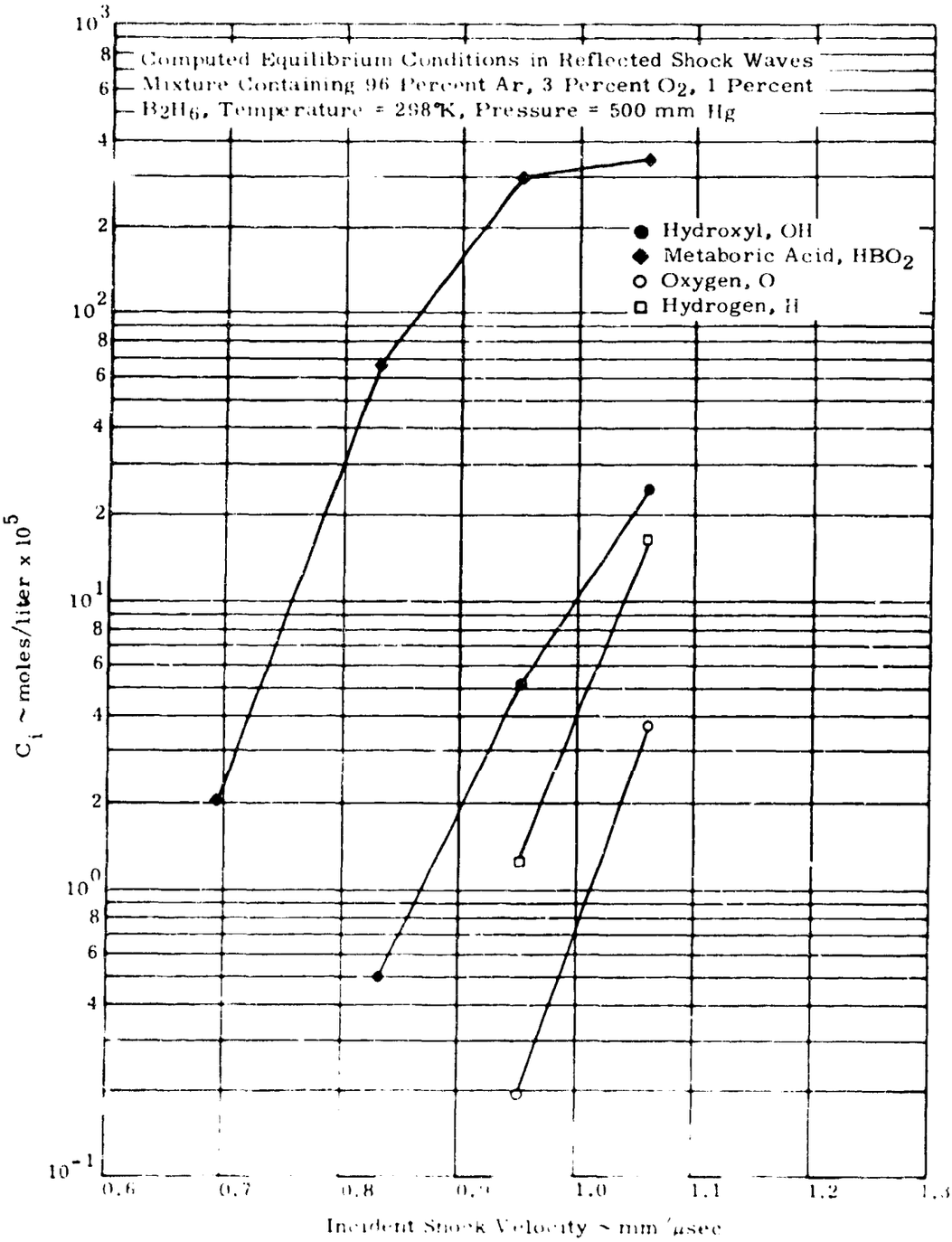

Figure 20. Computed Equilibrium Compositions in the Reflected Shock Wave Region OH, HBO_2, O, and H

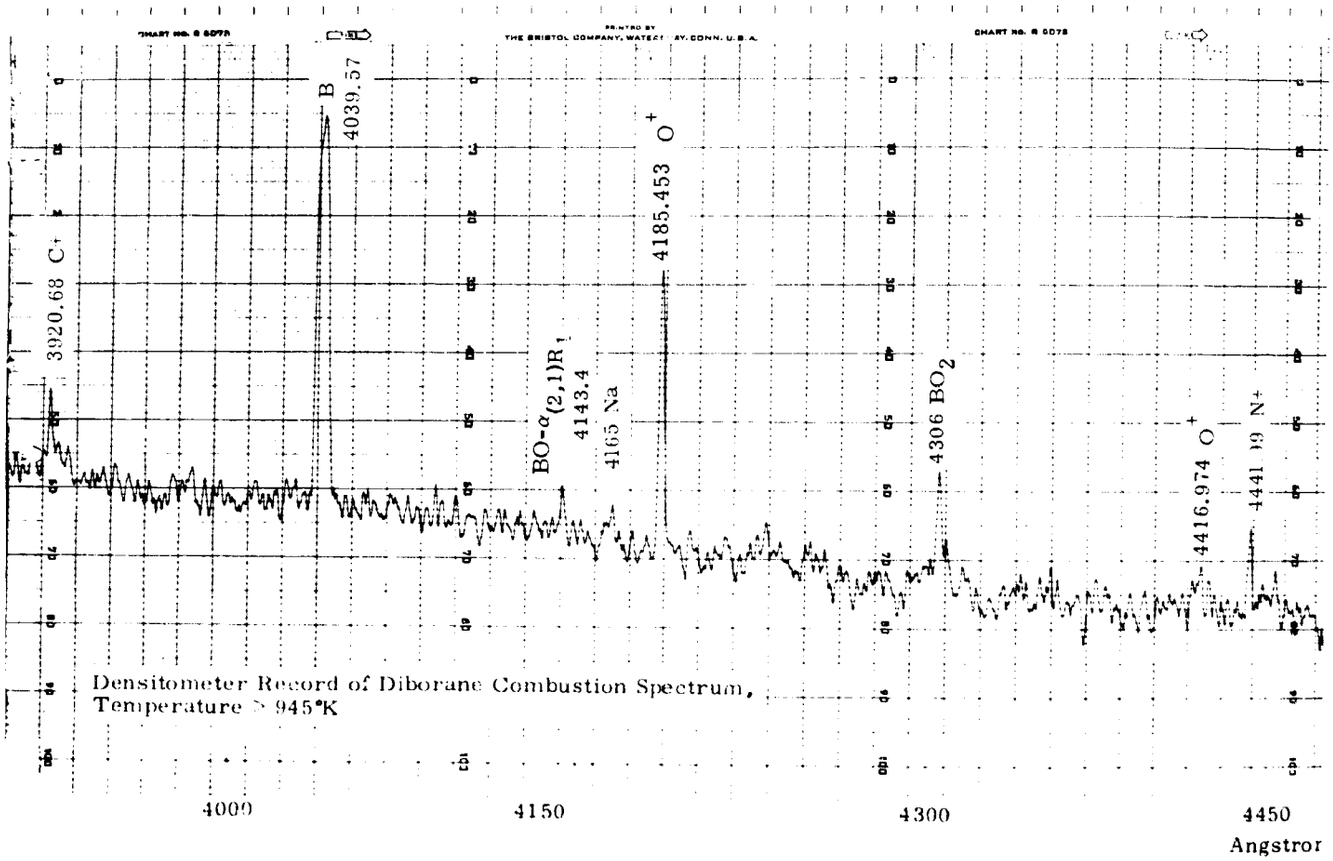

Figure 22. Densitometer Record of Diborane Combustion Spectrum; Temperature = 945°K

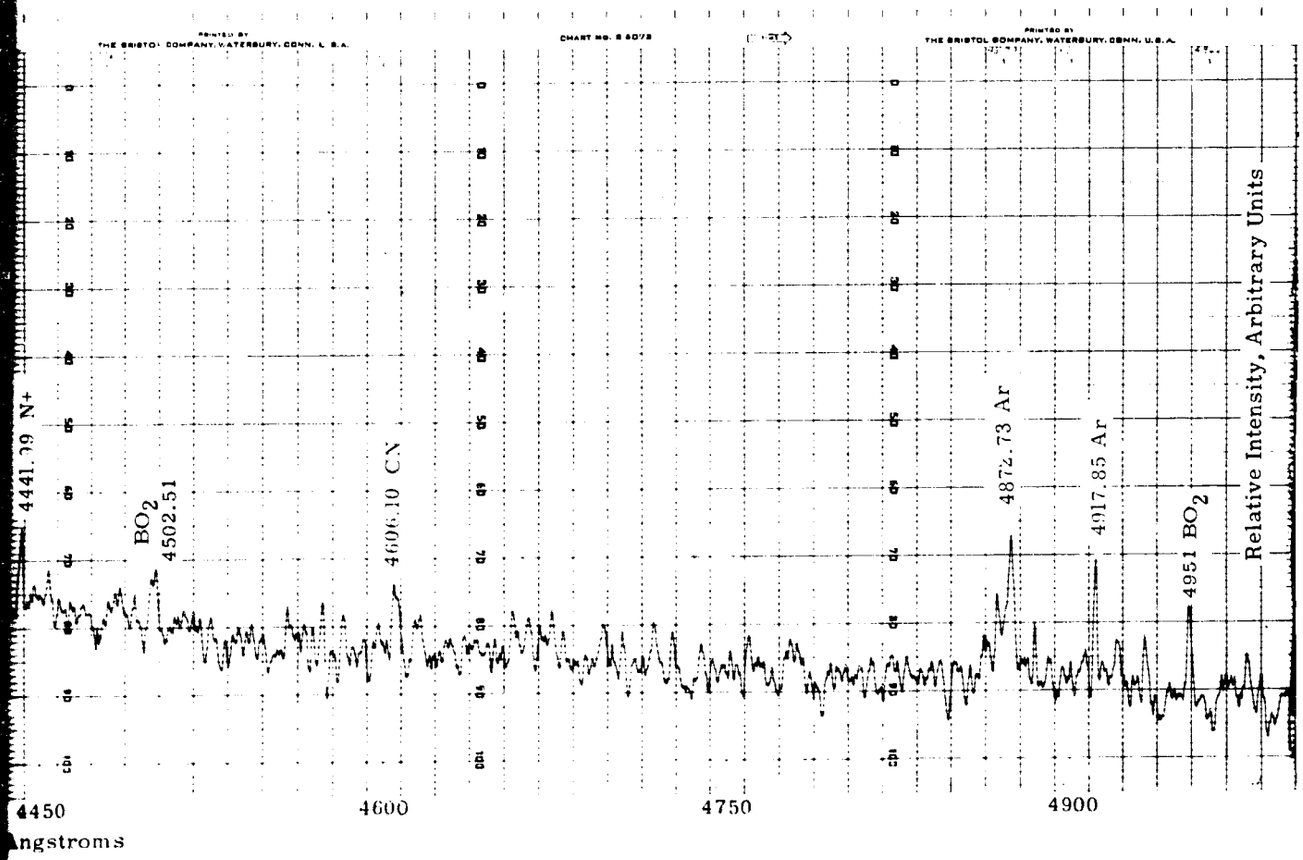
4441.09 N+
BO_2
4502.51
4606.10 CN
4872.73 Ar
4917.85 Ar
4951 BO_2
Relative Intensity, Arbitrary Units
4450
4600
4750
4900
Angstroms

TABLE IV

Wavelengths Identified, Spectrum I

System	$\lambda \sim \mathring{A}$ (Published)	Measured	Order	Ref	Relative Intensity
BO - β	2581.60	(84.01)	3	2	5.0
O	2641.53	(40.18)	2	1	5.5
BO - β	2713.80	(15.10)	2	2	2.0
N_2-Kaplan	2740.00	(40.60)	3	2	1.5
NO - λ	2763.30	(64.00)	3	2	1.0
BO - β	2999.60	(97.51)	3	2	>1.5
OH	3063.60	(64.11)	3	2	5.5
BH	3098.90	(96.10)	2	2	>1.0
Ar	3165.30	(65.50)	2	1	1.5
Ar^+	3393.75	(94.30)	2	1	2.0
BN	3809.30	(11.10)	1	2	1.5
C^+	3920.68	(20.78)	1	1	2.0
B	4039.57	(39.75)	1	1	10.0
N^+	4133.61	(33.65)	2	1	1.0
CO_2	4137.60	(38.44)	2	2	2.4
N_2	4141.80	(41.90)	2	2	2.0
BO - α	4143.40	(43.05)	1	2	1.5
Na	4165.00	(65.00) min	1, 2	1	2.0
0+	4185.456	(85.63)	1	1	6.0
$^{10}BO_2$	4305.89	(04.88)	1	3	5.0
BH	4331.60	(34.65) max	2	2	2.5
0^+	4416.97	(18.10)	1	2	2.0
N^+	4441.99	(41.10)	1	1	2.0
$^{11}BO_2$	4502.51	(01.10)	1	3	2.5
CN	4606.10	(04.78)	1	2	2.5
Ar	4872.73	(73.61)	1	1	5.5
Ar	4917.85	(17.97)	1, 2	1	4.0
$^{10}BO_2$	4951.05	(51.10)	1	3	4.5

References:

1. G. R. Harrison, M.I.T. Wavelength Tables, Wiley, 1956.
2. R. W. B. Pearse and A. G. Gaydon, The Identification of Molecular Spectra, Third Ed., Chapman and Hall, 1963.
3. J. W. C. Johns, "The Absorption Spectrum of BO_2", Can J of Physics 39, pp 1738-68, 1961.

The third order spectrum on the same photographic plate was also analysed and was found to yield the hydroxyl (0,0) bandhead $^2\Sigma - {}^2\pi$ transition line at 3064 Å to fair precision (1.7 percent of 30 Å) and with 55 percent of maximum intensity. OH was not observed in first order because it was obscured by the noise level there. In second order the OH line was not sufficiently intense to be obtained below the 100 percent transmission level of the record. It is to be noted that OH emission has not been observed in steady flames during the slow burner combustion of stoichiometric B_2H_6/O_2 mixtures, References 23 and 43. However, emission evidently exceeded absorption by OH during some or most of the 19 repeat runs producing the spectrum under analysis.

A grey gas, Reference 41, analysis was performed, using an absorption coefficient of 8.6 x 10^4 cm^2/mole (Reference 42) for OH at temperatures in excess of 1100°K. The calculations show that the absolute emission intensity at 1160 °K is about 0.001 Watts/cm^2, while at 3480 °K it increased to about 50 Watts/cm^2. We conclude that in the detonation mode, the local temperatures may reach sufficiently large values to promote large populations of excited OH so that emission exceeds absorption as observed in the present experiment. The presence of OH, even in third order, tends to qualitatively verify both the prediction of early mechanism, postulated on page 19, and the equilibrium composition shown on Figure 20.

Generally, the present observations are found in agreement with emission spectra obtained from diborane/air and diborane/NO flame studies by Wolfhard, et. al., Reference 43, and oxy-diborane flame studies by Skinner's Group, Reference 23. For example, the intermediate species BH, BO-α, β and BO_2 were observed in all the flame studies. Hydroxyl radical was observed in the non-stoichiometric flames. However, the range of (non-detonative) temperatures in which OH absorption dominates over emission by excited OH is still to be determined. This is desired so that one may minimize the guesswork in proceeding with quantitative absorption measurements. At an equilibrium temperature of 1000 °K in the non-detonative mode OH will probably absorb, according to present calculations and to data of References 44 and 45; but if the OH concentrations are as low at 1000 °K as indicated on Figures 15 and 20, the absorption measurements may be limited by instrument sensitivity, Reference 46. It is important to note that the actual non-equilibrium OH concentrations to be measured will be one to two orders of magnitude greater than those shown by the equilibrium calculations on Figure 20. The OH absorption experiment was designed and is discussed in Appendix A.

PART TWO

MATHEMATICAL INVESTIGATIONS

BLANK PAGE

I. BACKGROUND

Research resulting from the desire to utilize the processes of heat release at high power density levels has greatly enhanced the understanding of phenomena in high speed gas dynamics. Thus, problems in combustion dynamics and reëntry physics have received increasing attention by various specialists who are finding a common field of interest called gas-wave-dynamics (References 47 and 48). This new field depends on experimental methods and theoretical developments in spectroscopy, chemical kinetics, statistical turbulence, and radiative energy transfer. Investigative methods are identical, both in combustion dynamics and reentry physics.

In the presently sponsored AFOSR investigation of high energy fuel chemistry special attention is directed to the further understanding of gas-wave-dynamics in supersonic combustion. Applications of interest in supersonic combustion include development of the supersonic combustion ramjet and the use of external burning for increased maneuvering capability of tactical, strategic, and manned reentry vehicles.

Two possible modes of supersonic combustion have been identified for study, e.g., supersonic diffusion flames and detonations (Reference 49). The former is largely deflagrative burning, characterized by the mixing requirement; whereas the latter assumes the reactive components are premixed, giving rise to the simplest explanation, in terms of Chapman-Jouguet detonations, that the local Mach number of the burned gas behind the detonation wave is unity. A third mode of supersonic combustion is possible that in which the supersonic diffusion flame achieves the condition of a standing (stationary) detonation wave in the reactive flow as it is swept downstream (References 49, 50).

The necessity for including the exact kinetic processes in the burning region, in order to understand the various modes of supersonic combustion, has led investigators to depend upon better known mechanisms such as the branched H_2/O_2 reaction (References 50, 51). Thus, a better understanding of the structure of stationary waves has evolved (References 15 and 52 through 56). It is presently suggested, for example, that ignition delay in the stationary (stable) detonation of H_2 is related to the distance between the burning region and the shock wave created by pressure pulses from this region, i.e., one concept of a detonation wave which has gained much acceptance is that of the shock wave followed by a burning region. However,

the study of standing detonation waves where a free boundary is used, such as in the work of Nicholls, and detonations in tubes have shown some interesting differences. Whereas in a free boundary, the detonative flow may be largely of the "laminar" type, in a tube the reactive flow following a running detonation wave becomes "turbulent" giving rise to a non one-dimensional spin mode (References 56, 57, and 58).

The origin of spin appears to be related to the scale of irregularities (turbulence) in the burning region. It is opined that the turbulence scale depends on the particular reactants, the necessary activated state being achieved in a manner different (perhaps more efficient) than in the "laminar" case. As this turbulence scale is increased, transverse acoustical waves coalesce because of superposition at the walls, giving rise to the shock waves observed within the detonative transition region (References 59 and 60). Since these irregularities are not prima facie random, perhaps due to anisotropy induced by the mean flow, the strong waves enhance, rather than cancel the motion creating an angular momentum, or spin (Reference 61). In the case of free boundary waves, the transverse acoustical disturbances are present due to combustion but are free to propagate out of the region of influence; this may also account for the "laminar" structure of a standing detonation wave.

There appears to be some uncertainty as to the most efficient mode of supersonic combustion for a given application. However, it does seem likely that attempts to utilize standing detonation waves in external burning may require a better understanding of the scale of irregularities due to the presence of the boundary. In any case, the concepts of ignition induction and the acceptance of shock tube kinetics as a means of establishing both reaction mechanism and ignition induction have been established.

II. REACTION PROFILE MODEL

In the study of reaction rates and mechanisms of complex systems, it is expedient to have a means to determine the reaction profile, i.e., a method whereby the time rate of change of each reacting species may be evaluated. Such an analysis requires the simultaneous solution of the gas dynamical equations of change and the species production equations. In the case of shock tube studies the equations of change reduce to the Rankine-Hugoniot relations, and in the case of competitive reactions a series of simultaneous differential equations describing the relaxation processes must be solved. Hence the kinetic rate constants and the mechanisms of the reactions must be known or estimated. In addition, a knowledge of the coupling of the chemical kinetics with other relaxation processes such as vibration should, in principle, be known since often it is found that the chemical reaction rates are affected by changes in the internal energy modes of the species. Generally such effects are ignored initially until there is good reason to verify these effects experimentally. If it can be demonstrated that the vibrational relaxation time is of the order of or less than the chemical relaxation time for example, then provision must be made to account for this effect. Often coupling between different relaxation modes may be neglected if the temperature is not too high. In addition to these effects, temperature and pressure variations within the reaction zone will also affect the reaction rates; however, the pressure variation is usually small and, in shock tube work, the temperature in the reaction zone is very nearly constant if sufficient diluent is used.

Duff (Reference 51) and Duff and Davidson (Reference 62) have given a method whereby the reaction profiles may be computed for nondetonative shock tube work or the effects of estimated rate constants and proposed reaction mechanisms may be evaluated. The gas dynamical equations and the equation of state are solved subject to the initial conditions, i.e., the temperature and pressure behind the shock prior to reactions, the concentration of all species at the same point, and a function of pressure and density related to the shock velocity.

The values for the rate constants may be obtained from the literature (if available) by estimation, or by studies made in the shock tube. The latter method is usually done by following the time rate of change of a

property of a species i as the reaction proceeds. From these data a theoretical curve containing adjustable parameters may be fitted to the experimentally observed data and the rate constants found from the fitted values of the parameters (Reference 63). A more sophisticated method is to develop an algebraic function of the measured property which is linear with time. Values of the property can then be taken from the data at various intervals and plotted against time so that the slope can be related to the rate constant (References 64 and 65).

Duff's reaction profile model was constructed for inviscid flow, accounting for chemical kinetics.

Subsequent formulation is aimed at the more sophisticated approach; following Marrones' (Reference 66) extension of Duff's idea, i.e., to include vibrational relaxation processes and chemical kinetics, with their cross couplings, the next step is to include the effects of collisional transport properties.

III. MATHEMATICAL FORMULATION

The objective is to develop the theory of planar shock wave propagation in a reactive medium, taking into account the structure that may arise due to interaction effects of chemical kinetics with collisional transport properties and energy transfer mechanisms. These effects superpose on the general class of inviscid reaction profile models such as Duff's and, more recently, Marrone's (Reference 66). Planar detonation wave structure theories, which account for the interaction effects, were investigated by Hirschfelder's group (References 67 and 68), by Adamson (Reference 69) and, more recently, by Petrone (Reference 70). In references 67 and 68 the type of reactions studied was limited to the exothermic, irreversible and reversible unimolecular reaction respectively, with transport properties grouped as constant values of the Lewis and Prandtl numbers. Adamson found an approximate analytical solution to the same problem, neglecting diffusion. Petrone considered a single reaction describing the decomposition of a homogeneous condensed explosive and included but one transport property, namely artificial viscosity, solving the time dependent one-dimensional Lagrangian equations. Finally, a non-exothermic reaction problem was investigated by Scala and Gordon (Reference 71) who obtained an exact numerical solution to the two-dimensional, time dependent Navier-Stokes equations for the supersonic flow past a blunt body where the effects of temperature dependent transport properties and where a system of two dissociation-recombination bimolecular reactions are treated.

In the present development we proceed with a general endothermic or exothermic scheme, following Marrone, where the chemical source matrix will be adapted to any branching chain mechanism and where an explicit dependence of chemical reactions is introduced into the transport properties subroutines.

A. EQUATIONS OF MOTION

The development of chemical reactions in a branching chain mechanism may be strongly vibration-dissociation coupled, particularly in the initial stages of thermal decomposition during the ignition delay period. Thus, the equations describing processes in the reaction zone downstream of a shock wave must account for such chemical-mechanical couplings. These relationships were discussed for a general multicomponent system in Reference 72

and have been reduced to a system of first order, ordinary, integro-differential equations including collisional transport, radiation energy transfer and chemical source terms governing the mass and energy transfer phenomena of a quasi steady-state, one-dimensional, chemically-relaxing, multicomponent gas.

In their simplest form these equations are:

$$\rho v = A \tag{1}$$

and

$$\rho_i v = B + m_i N_o \int \nu(T) \frac{kT\, e^{-\epsilon_i/kT}}{2\pi\hbar} dy - j_i \tag{2}$$

for mass transfer;

$$\rho v^2 = C + \frac{4}{3}(\mu \frac{dv}{dx} - \sigma T^4/c) - p \tag{3}$$

for momentum transfer, and

$$\frac{1}{2}\rho v^3 = D + \frac{4}{3}\mu v \frac{dv}{dx} + \kappa \frac{dT}{dx} + p \sum_{i=1}^{N} \sum_{j=1}^{N} \frac{n_j D_i^T}{n^2 m_i \mathcal{D}_{ij}} (v_i - v_j)$$

$$-4\sigma \int \alpha(y)\, T^4\, dy - \sum_i^N j_i h_i - \rho v h \tag{4}$$

for energy transfer. A, B, C, and D are constants; the ϵ_i's are the reaction activation energies, α is the Planck mean absorption coefficient, and other symbols are defined in Appendix C.

Diffusion mass flux j_i and velocities v_i of chemical species are related to the concentration, pressure, and temperature gradients according to

$$j_i = \rho_i v_i = m_i n_i v_i; \tag{5}$$

that is, the diffusion velocity is given by (Reference 72):

$$v_i = \frac{n^2}{n_i \rho} \sum_j^N m_j D_{ij} \left\{ \frac{dX_j}{dx} + (X_j - \rho_j/\rho) \frac{d \ln p}{dx} \right\}$$

$$- \frac{1}{n_i m_i} D_i^T \frac{d \ln T}{dx}. \tag{6}$$

B. CHEMICAL EQUILIBRIA AND RELAXATION PROCESSES

The specific enthalpy for chemical species is

$$h_i = \left\{ 1 + \bar{e}_i / R_i T \right\} R_i T \tag{7}$$

where $\bar{e}_i$ is the specific energy content per unit mass and the bracketed quantity is the reduced enthalpy function

$$\beta(T) = \frac{h(T)}{p/\rho} = \frac{\gamma(T)}{\gamma(T)-1}, \tag{8}$$

a temperature dependent function of the ratio of specific heats, γ, suggested in Reference 73 for applications where the state of the gas may deviate from thermal equilibrium. Considering Equations (7) and (8) the reduced enthalpy is

$$\beta(T) = 1 + \sum_f e_f \tag{9}$$

where e_f is a dimensionless specific energy content per degree of freedom, f, of the atomic or molecular system of interest. For example, the energy distributions for ideal gases in equilibrium are described by

$$\beta = \frac{\gamma}{\gamma-1} = 1 + \frac{f}{2} \tag{10}$$

Thus,

$$\sum_f e_f = \frac{f}{2} \tag{11}$$

where f = 3 and 5 respectively for atomic and diatomic molecules in accordance with equipartition.

1. Statistical Considerations

These classical considerations from kinetic theory are not sufficient in the case of very strong shock waves, nor in the case of detonation waves,

and possibly not in the case of some deflagrations, especially those due to the burning of high energy pyrophoric fuels. It is therefore necessary to consider the microscopic model for the distributions of chemical species among the various energy levels excited in the combustion processes. From statistics,

$$e_f = T \frac{\partial \ln}{\partial T} Q_f \tag{12}$$

where the partition function Q_f is given by the product of individual partition functions,

$$Q_f = \left\{ Q^{(tr)} Q^{(rot)} Q^{(vib)} Q^{(int\ rot)} Q^{(el)} Q^{(nucl)} \right\}_f \tag{13}$$

associated with the translational, rotational, vibrational, electronic and nuclear excitations of chemical species. Each partition function is computed by an expression of the form

$$Q = \sum_j g_j e^{-E_{ij}/kT} \tag{14}$$

where the E_{ij} are the j energy eigenvalues of chemical species i, and the g_j are the degeneracies of these eigenvalues in the jth state.

For shock excited processes it is known that the translational and rotational degrees of freedom of atomic and/or diatomic mixtures equilibrate after about 3 to 5 and 10 to 300 interparticle collisions respectively, with increasing shock wave strength. Thus, it is safe to say that equipartition holds, in general, for translation. This is easily proven because

$$Q^{(tr)} = \text{volume} \times \left(\frac{m_i k T}{2\pi \hbar^2} \right)^{3/2} \tag{15}$$

which yields, for all molecules,

$$e_f = \frac{3}{2} \tag{16}$$

in agreement with the result from Equation (11). The solution to Schrödinger's equation for the rotational energy eigenvalues of a rigid diatomic rotator is

$$E_{ij} = \hbar^2 j(j+1)/2I \tag{17}$$

and the degeneracies are

$$g_j = 2j + 1. \tag{18}$$

Thus

$$Q^{(rot)} = \sum_{j=0}^{\infty} (2j+1)e^{-\hbar^2 j(j+1)/2I\,kT} \tag{19}$$

for a rigid rotator. Equation (19) is most easily summed by the substitution of integration for summation, see Reference 74,

$$Q^{(rot)} = \int_0^{\infty} e^{-z\hbar^2/2I\,kT}\,dz = \frac{2I\,kT}{\hbar^2}. \tag{20}$$

Equations (12) and (13) then yield

$$e_f = \frac{3}{2} + 1 = \frac{5}{2}, \tag{21}$$

again in agreement with Equation (11). These results are useful provided the vibrational levels of a diatomic gas are not appreciably excited. When the vibrational contribution is included,

$$e_f = \frac{5}{2} + \frac{u(T)}{e^{u(T)} - 1}, \tag{22}$$

where

$$u(T) = \omega\hbar/kT. \tag{23}$$

With increasing shock strength,

$$u(T) \ll 1, \tag{24}$$

equation (22) reduces to

$$e_f = \frac{7}{2} \tag{25}$$

for the "fully" equilibrated classical diatomic molecule. Corrections for the case of a nonrigid, vibrating rotator are given, for example, in References 74 and 75. Equation (22) then becomes

$$e_f = \frac{5}{2} + \phi(\alpha, \beta)/u(T) + \frac{u(T)}{e^{u(T)} - 1} \quad , \tag{26}$$

where α and β are spectroscopic parameters of the chemical species. Here the similarity to classical kinetic theory ends.

Indeed, it may end prior to the effects noticable when the anharmonic effect ϕ is accounted for. This is because electronic states may be excited prior to the full vibrational equilibrium. Accounting for the electronic excitation, and the heat of formation,

$$e_f = \frac{5}{2} + \phi\, u^{-1} + \frac{u}{e^{u} - 1} + \frac{1}{R_i T} \frac{\sum_{\ell=1}^{m} E_{i\ell}\, g_{i\ell}\, e^{-E_{i\ell}/kT}}{\sum_{\ell=1}^{m} g_{i\ell}\, e^{-E_{i\ell}/kT}} + \frac{\overline{e_f^{\,o}}}{R_i T}, \tag{27}$$

where ℓ is the energy eigenstate above the ground state and where T is the equilibrium temperature.

2. Relaxational Processes

When the state of a molecular system is changed suddenly, as in the case of shock or detonation waves, a finite time is required before the system reaches its new equilibrium position. This relaxation time, τ, is determined by the efficiency of collisional energy transfer between the various degrees of freedom of the system. The value for τ was first obtained in Reference 76. It is

$$\tau = \left\{ k_{1,0}(1 - e^{-h\nu/kT}) \right\}^{-1} \quad . \tag{28}$$

For the present, consider only the case of vibrational non-equilibrium. Then, the rate equation that determines the deviations from equilibrium is

$$\frac{d\bar{e}_i}{dt} = \frac{\bar{e}_f - \bar{e}_i}{\tau_i} - \frac{\left\{ \overline{E}_i(T, T_{v_i}) - \bar{e}_i \right\}}{[X_i]} \left(\frac{d[X]_i}{dt} \right)_{fwd} + \frac{\overline{G}_i(T) - \bar{e}_i}{[X_i]} \left(\frac{d[X]_i}{dt} \right)_{back} \tag{29}$$

where T_{v_i} is the vibrational temperature obtained by solving the harmonic oscillator relation,

$$e_i = \frac{h\nu/k}{\exp\left(h\nu/kT_{v_i}\right) - 1} \tag{30}$$

The first term in equation (29) was first given in Reference 73 to describe the rate of change of vibrational energy due to collisions. The second term accounts for the fact that the average vibrational energy of the system is reduced due to dissociation, while the third term accounts for the increase due to recombination. Thus, vibrational and dissociative nonequilibrium processes have been coupled according to Reference 77.

Important vibrational relaxation times, τ, for high temperature air species are

1 For Oxygen:

$$\tau'_{O_2} = \frac{1.6188 \times 10^{-3}}{p'} \exp\left[\frac{101.444}{(T')^{1/3}}\right] \tag{31}$$

2 For Nitrogen:

$$\tau'_{N_2} = \frac{1.11531 \times 10^{-5}}{p'} (T')^{0.5} \exp\left[\frac{154}{(T')^{1/3}}\right] \tag{32}$$

$\tau' \sim$ seconds
$p' \sim$ dynes/cm^2
$T' \sim$ °K

C. EQUATION OF STATE

For a real gas, the equation of state is

$$p = Z\rho RT, \tag{33}$$

where Z is the compressibility. Z = 1 in the case of an ideal gas and will be assumed so in most instances.

Equations (1) through (7) and (27) through (33) must be solved simultaneously for the usual flow variables $\rho(x)$, $v(x)$, $p(x)$, $T(x)$, $h(x)$ and $X_i(x)$.

The species mole fractions $X_i(x)$ obtained as a function of the distance x behind the shock wave, in a one-dimensional combustion process, constitutes the desired reaction profile model.

D. KINETICS

In the case of combustion processes that are rate controlled, the diffusion mass flux may vanish identically. Equations (1) and (2) may then be rearranged as follows:

$$dX_i/dx - X_i \sum_i^N \overline{M}_i \; dX_i/dx \langle\overline{M}\rangle = N_o \dot{W}_i/nv \qquad (34)$$

Equation (34) may then be inverted, as shown in Reference 78, by matrix techniques into a secular equation relating the column matrix of mole fraction derivatives, the N- component species mole fraction matrix of rank N, and the column matrix of N chemical source terms $\dot{W}_i$ defined in Reference 72 as the mass rate of production of species.

E. SAMPLE CALCULATIONS

When collisional transport and radiative energy transfer mechanisms are suppressed, the Martin Marietta program reverts to the CAL subroutine. This subroutine may be used to compute the nonequilibrium chemical effects due to highly exothermic, branching chain reactions during shock ignition.

In this case Equations (1) through (6) are altered by setting μ, κ, D_i^T, α and D_{ij} equal to zero, differentiating Equations (1) through (4) with respect to the distance y following the shock front, neglecting the radiative pressure term in Equation (3), and substituting for the integral term in Equation (2) the chemical source matrix required. The calculation then proceeds exactly as described in Reference 66.

The chemical system used in this study is the hydrogen/oxygen branching chain mechanism. Table V lists rate constants used for the assumed mechanism. These were obtained from the work of Henrici and Bauer, Reference 79. The result of the seven species, eight reaction H_2/O_2 ignition induction calculation is shown on Figure 23 (solid line terminated by circled points). Vibrational-dissociation coupling was assumed unimportant for these calculations. The activation energy agreed very well with that obtained by Hersh, Frey and Gerstein, Reference 80, whose calculations are exprapolated from the low temperature region. The calculated activation energy seems to be in slight disagreement with that measured by Schott and Kinsey, Reference 3. Departures in the ignition induction times may be explained in terms of initial pressure and diluent, Reference 81.

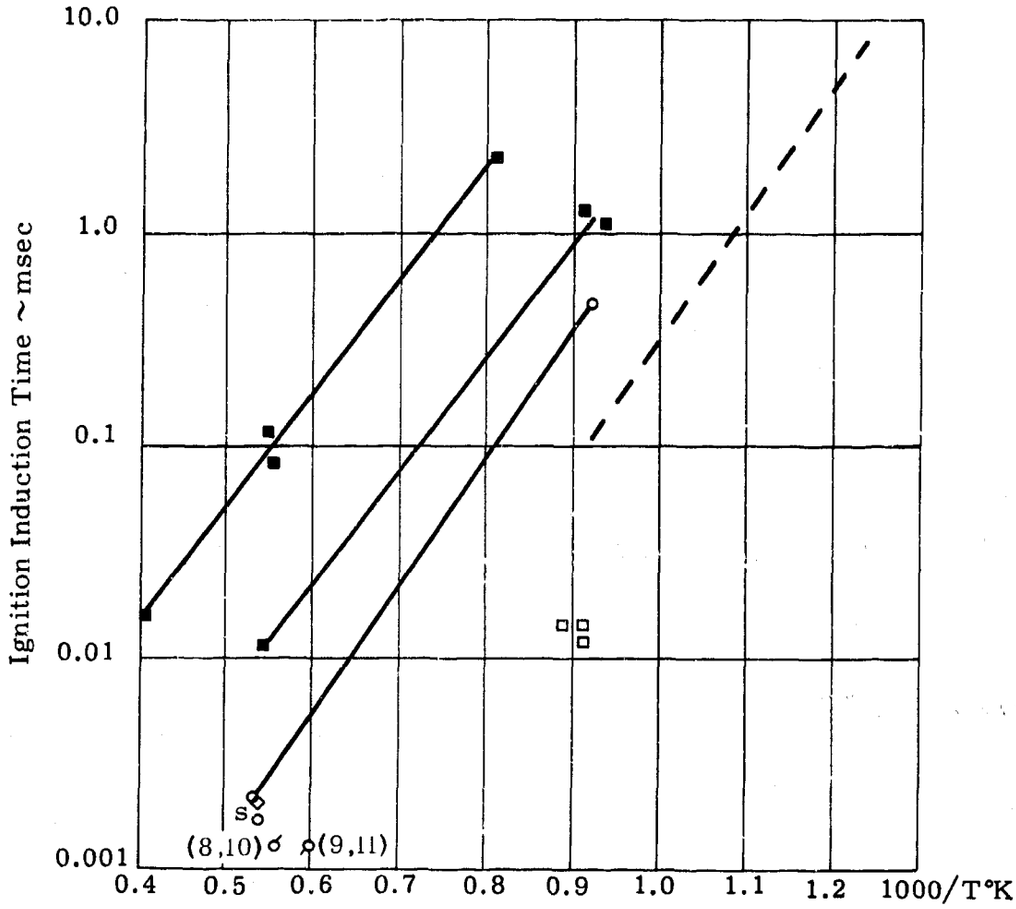

	O_2:	H_2:	Ar	P_o
Experimental				5-10 cm Hg
■ Schott and Kinsey				
Upper Line	0.5:	1:	98.5	
Lower Line	2:	1:	97	
◻ Urtiew and Oppenheim $3O_2 + 4H_2$	42.8:	57.2:	0	
Calculated:				
○, ○, ○ Present Work	2:	1:	97	1 Atm
◇ Cornell University				
- - - Hersh, Frey, and Gerstein	3.34:	6.66:	90	

Note: ○ 8 Species, 10 Reactions
○ 9 Species, 11 Reactions
S Suppress Termolecular Reactions

Figure 23. Hydrogen/Oxygen Ignition Induction

TABLE V

Rate Constants for Assumed H_2/O_2 Mechanism

Reaction	Rate Constant* (cc mole^{-1} sec^{-1})	Reference
$H_2 + M \rightarrow 2H + M$	$2.23 \times 10^{12} \times T^{1/2} \exp(-92\,600/RT)$	a
$O_2 + M \rightarrow 2O + M$	$3.6 \times 10^{18} \times T^{-1} \exp(-118\,000/RT)$	b
$H_2 + O_2 \rightarrow 2\,OH$	$2.51 \times 10^{12} \exp(-39\,000/RT)$	c
$H + O_2 \rightarrow OH + O$	$7.75 \times 10^{13} \exp(-14\,450/RT)$	d
$O + H_2 \rightarrow OH + H$	$10^{13} \exp(-8\,800/RT)$	e
$OH + H_2 \rightarrow H_2O + H$	$2.3 \times 10^{13} \exp(-5\,150/RT)$	f
$OH + OH \rightarrow H_2O + O$	1.55×10^{12}	g,h
$H_2O + M \rightarrow H + OH + M$	$5 \times 10^{14} \exp(-105\,000/RT)$	i

*The rate constants shown have been determined for M is argon.

a. A. L. Myerson and W. S. Watt, J. Chem. Phys. 49, 425 (1968).
b. K. L. Wray, in Progress in Astronautics and Rocketry, F. R. Riddel, Ed. (Academic Press Inc., New York, 1962), Vol. 7, p. 181.
c. Value suggested by G. L. Schott.
d. D. Gutman and G. L. Schott, J. Chem. Phys. 46, 4576 (1967).
e. I. M. Campbell and B. A. Thrush, Trans. Faraday Soc. 64, 1265 (1968).
f. W. E. Wilson, Western States Section Meeting, The Combustion Institute, LaJolla, Calif., 1967, Report on the Establishment of Chemical Kinetics Tables, Chemical Propulsion Information Agency, April 1967.
g. W. E. Wilson and J. T. O'Donovan, J. Chem. Phys. 47, 5455 (1967).
h. The reference quoted gives no temperature dependence. In earlier work (F. Kaufman and F. P. Del Greco, Symp. Combust. 9th Cornell Univ., Ithaca, N. Y., 1963, 659 (1953)) it was suggested that the activation energy cannot be more than (1-2) kcal/mole. In our calculations we used the room-temperature value without an activation energy.

Calculations (points) are also shown for eight species, ten reaction and nine species, eleven reaction models assumed. These contained the termolecular reaction $H + O_2 + Ar \rightarrow HO_2 + Ar$, and the collisional dissociation reaction.

$$OH + Ar \rightarrow O + H + Ar.$$

Suppressing the termolecular reaction had the effect of increasing the ignition induction time as shown at a nominal temperature of 1820°K. The same calculation, repeated at Cornell University produced a still higher value of the ignition delay time at 1855°K. This is attributed to machine differences since the same model was used. Otherwise, differences in the model used, though deemed adequate for ignition processes does tend to make a great difference in the ignition time and may produce errors in the activation energy. This was discovered after performing a calculation with the nine species, eleven reaction model of Reference 82.

The output lists species concentrations variation with distance downstream of the shock front, or as a function of time from the front. The reverse of each reaction is accounted for in the CAL subroutine. For these calculations the induction time is defined as the time for maximum OH concentration. The (final) equilibrium temperature occurring in the reaction is used to obtain the ignition induction plot. Figure 24 shows the OH concentration envelope for all reactions from which the maximum OH concentration was obtained at 2.35 μsec, for an equilibrium temperature of 1855°K. Figure 25 gives the positive Q_{ij} (i = OH) matrix elements which represent the instantaneous net rates of formation of species i in reaction j. The envelope of the absolute values of all such matrix elements for OH, viz Figure 24, was used to obtain the ignition induction time.

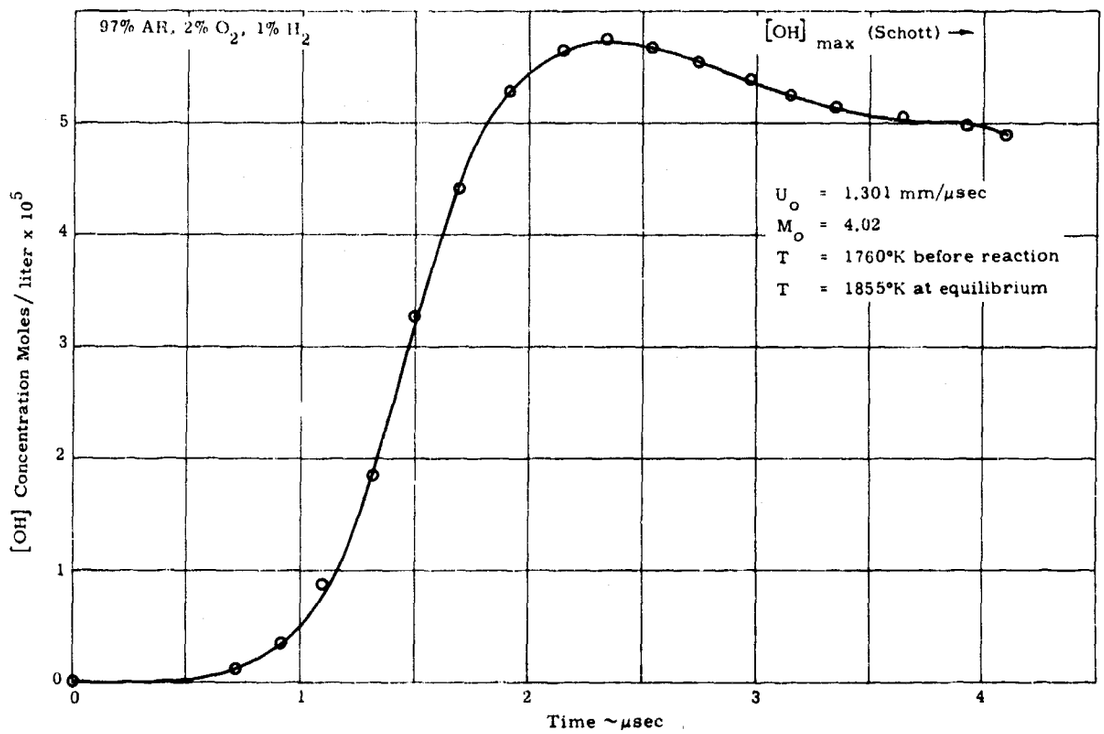

Figure 24. Envelope of [OH] Concentration versus Time

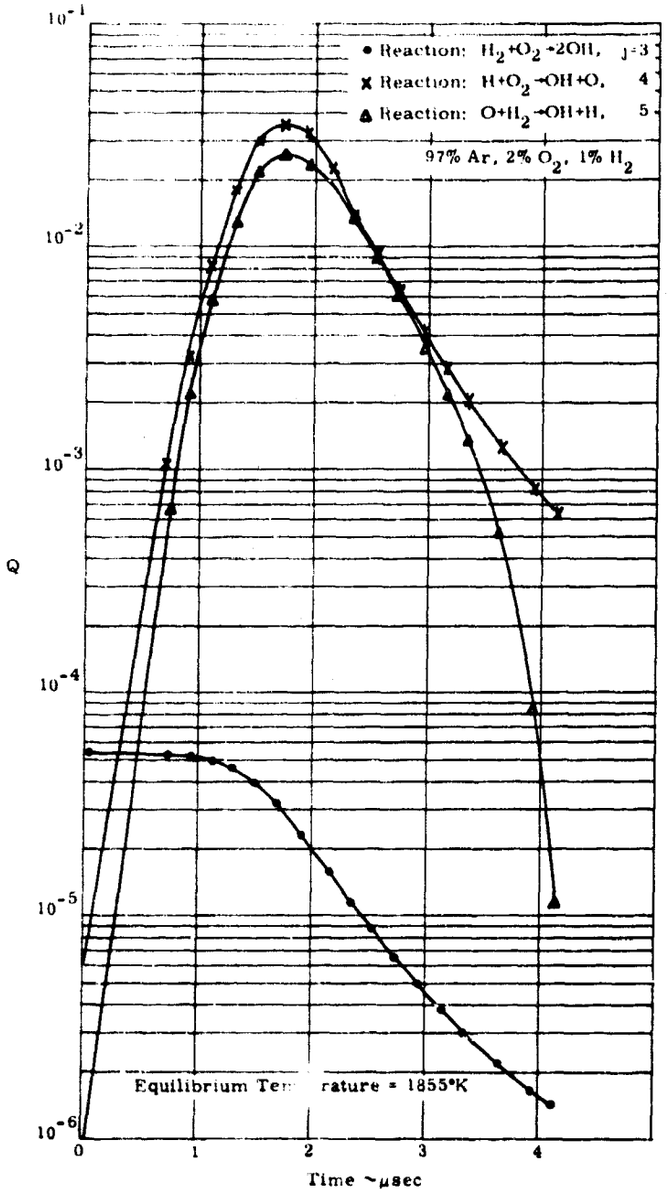

Figure 25. Rate of Production of OH, $Q_{OH,j}$ versus Time of Several Reactions in the Hydrogen/Oxygen Chain

IV. EXTENDED MODEL

Of immediate interest to the Martin Marietta Corporation is the chemically coupled shock wave, reaction profile model now coded. This model is constructed with arbitrary endothermic and exothermic chemical source input. It includes as principal subroutine, the quasi-steady state, one-dimensional, inviscid, reacting air chemistry model of Reference 66. As such, this subroutine is ready for use in high temperature, chemical nonequilibrium problems, both endothermic and exothermic, provided that radiative energy and collisional transport effects are unimportant. A number of practical engineering problems presently require the CAL (subroutine) inviscid model to supplement:

1 Propulsion,

2 Heat shield, and

3 Communications

systems design of advanced, high acceleration vehicles.

The CAL subroutine is used as a diagnostic device for determination of reaction rate data within the framework of self consistent, branched-chain reaction mechanisms (Reference 79). To better achieve such evaluations, Reference 66 is being extended to include the interacting effects of finite rate chemical reactions, radiative energy, and collisional transport properties of high temperature multicomponent systems. To the degree that collisional transport models are known, Reference 83 for example, for purposes of calculating the multicomponent viscosity, diffusion, and thermal conductivity coefficients, the proposed extension is complete. However, even the simplest radiative energy transfer model proposed, in the optically thin limit, will be of limited use due to the paucity of photon absorption coefficient data, particularly in the chemiluminescent regions of interest. Recently there has been a great demand, and corresponding activity, to obtain these data, along with refinements of the radiative energy transfer models, both at the optically thin and thick limits and within the framework of a precise molecular band structured model, see Reference 84.

It is believed that the extended model will play a significant role in design problems of interest to the Nation's aerospace engineering effort because, in addition to the determination of chemical nonequilibrium effects, it will also be possible to estimate:

1 Radiative heating due to the rocket motor and the heat shield

2 Effects of viscosity, diffusion, and thermal conductivity, for applications where the nondimensional transport property parameters (Schmidt and Prandtl numbers) are variable

3 The generation and populations of free photoelectrons that contribute to plasma noise effects, disrupting communication signals.

A. EQUATIONS CODED

It is desired to investigate the interacting effects of multicomponent collisional transport properties, radiative energy transfer and chemical kinetics. It is known, Reference 83 for example, that collisional momentum and mass transfer are locally independent of chemical kinetics; but depend on the previous history of physico-chemical processes in the flow through the local multicomponent molecular weight and temperature. In a reacting flow, particularly where supersonic combustion may give rise to steep temperature and concentration gradients, it is important to access this mutual interaction. Collisional energy transfer is far more complicated than the other two transport properties because of internal energy exchanges between species occupying varied excited energy states, Reference 85 to 92, in addition to the energy transport dependence on chemical kinetics and prior history of processes. These combined energy transport phenomena are grouped into the coefficient of thermal conductivity.

Starting with general equations applicable to chemical reactions in flow systems we obtained a system of first order, ordinary integro-differential equations accounting for collisional transport, radiation energy transfer, and chemical source terms governing transfer phenomena in a quasi-steady state, one-dimensional, chemically (and vibrationally) relaxing, multicomponent gas. Thermodynamic expressions accounting for the contributions of excited vibrational and electronic states, including anharmonicity, have been incorporated into the energy equation, whereas Landau-Teller-Hertzfeld-Treanor and Marrone theory is used to account for coupled vibrational-dissociative nonequilibrium, (refer to Equation 1-33), see References 66 and 93.

In their present form, the equations have been further developed to adopt Treanor's modification to the Runge-Kutta method (Reference 94). A matrix of Runge-Kutta coefficients has been programmed from the following set of 17 equations, and machine logic has been developed for the overall program:

$$\frac{d\epsilon_j}{dy} = \frac{\epsilon_{j_\infty} - \epsilon_j}{\lambda_j} + \left\{ \left[\frac{\theta_{v_j}}{\exp\left(\frac{\theta_{v_j}}{T_{m_j}}\right) - 1} - \frac{N_j \theta_{v_j}}{\exp\left(\frac{N_j \theta_{v_j}}{T_{m_j}}\right) - 1} \right] - \epsilon_j \right\} \cdot$$

$$\cdot \sum_{i=1}^{r} \frac{A_{ij} Q_{ij}}{\gamma_j \rho U \chi_i} - \left\{ \left[\frac{1}{2} (N_j - 1)\, \theta_{v_j} \right] - \epsilon_j \right\} \cdot$$

$$\cdot \sum_{i=1}^{r} \frac{A_{ij} Q_{ij}}{\gamma_j \rho U} \frac{1 - \chi_i}{\chi_i} \qquad j = f + 1, \ldots, g \tag{35}$$

$$\frac{d\Gamma_j}{dy} = \frac{1}{\rho U} \sum_{i=1}^{r} Q_{ij} \qquad j = c + 1, \ldots, s \tag{36}$$

$$\frac{dX_j}{dy} = U(MW) \sum_{\alpha=1}^{s} \left\{ \frac{1}{D_{j\alpha}} \left[X_j \Gamma_\alpha - X_\alpha \Gamma_j \right] \right\} \tag{37}$$

$$MW = \sum_{\alpha=1}^{s} (MW)_\alpha X_\alpha \tag{38}$$

$$\frac{d(MW)}{dy} = \sum_{\alpha=1}^{s} (MW)_\alpha \frac{dX_\alpha}{dy} \tag{39}$$

$$\gamma_j = X_j/(MW) \tag{40}$$

$$\frac{d\gamma_j}{dy} = \frac{1}{(MW)} \frac{dX_j}{dy} - \frac{X_j}{(MW)^2} \frac{d(MW)}{dy} \tag{41}$$

$$j_j = \rho U (MW)_\alpha \left[\Gamma_j - \gamma_j \right] \tag{42}$$

$$\frac{dj_j}{dy} = \rho U (MW)_\alpha \left[\frac{d\Gamma_j}{dy} - \frac{d\gamma_j}{dy} \right] \tag{43}$$

$$-\frac{dp}{dy} = \frac{\rho}{U}\frac{dU}{dy} \tag{44}$$

$$\rho = \frac{1}{U} \tag{45}$$

$$\frac{dp}{dy} = \frac{\rho}{(MW)}\frac{dT}{dy} - \frac{p}{(MW)}\frac{d(MW)}{dy} + \frac{p}{\rho}\frac{d\rho}{dy} \tag{46}$$

$$p = T\rho/(MW)\Lambda \tag{47}$$

$$\frac{dT}{dy} = \dot{T} \tag{48}$$

$$\begin{aligned}\frac{d\dot{T}}{dy} = \frac{d^2T}{dy^2} &= \frac{\rho U}{\Lambda\kappa}\sum_{\alpha=f+1}^{g}(n_\alpha - 1)\gamma_\alpha\frac{d\epsilon_\alpha}{dy} + \frac{U(MW)}{\kappa}\frac{dp}{dy} - \frac{p}{\rho}\frac{d\rho}{dy}\sum_{\alpha=1}^{s}\gamma_\alpha c_{p_\alpha} \\ &+ \frac{\rho U}{\Lambda\kappa}\sum_{\alpha=1}^{s}\sum_{j=1}^{s}\left[\frac{h_\alpha}{s} - \frac{\Lambda(MW)^2}{\rho}p\gamma_j c_{p_j}\right]\frac{d\gamma_j}{dy} - \frac{4\mu}{3\kappa}U\frac{d\dot{U}}{dy} - \frac{4\mu}{3\kappa}\left(\frac{dU}{dy}\right)^2 \\ &+ \frac{\rho U^2}{\kappa}\frac{dU}{dy} + \frac{4\sigma T^4 k_P}{\kappa} + \frac{1}{\Lambda\kappa}\sum_{\alpha=1}^{s}\frac{h_\alpha}{(MW)_\alpha}\frac{dj_\alpha}{dy} + \frac{1}{\Lambda\kappa}\sum_{\alpha=1}^{s}\frac{j_\alpha c_{p_\alpha}}{(MW)_\alpha}\frac{dT}{dy}\end{aligned} \tag{49}$$

$$\frac{dU}{dy} = \dot{U} \tag{50}$$

$$\frac{d\dot{U}}{dy} = \frac{d^2U}{dy^2} = \frac{3}{4\mu}\frac{dp}{dy} + \frac{3\rho U}{4\mu}\dot{U} \tag{51}$$

These equations are used to compute, in order of their appearance, the rate of change (with respect to distance y from the shock front) of

ϵ_j = the vibrational energy of jth species, calories/mole;

Γ_j = $\gamma_j u_j/u$, concentration of jth species, moles/unit mass, including the effect of multicomponent diffusion through the ratio of species velocity u_j to mass averaged velocity, u;

X_j = mole fraction of jth species;

(MW) = total molecular weight at a point y downstream of the shock front due to the production and recombination of species, including the effect of the rate of change of their concentrations, gms/mole;

γ_j = concentrations of jth species, moles/unit mass;

j_j = mass flux, gm/cm^2s;

ρ = mass density, gm/cc;

p = pressure, $dynes/cm^2$;

T = temperature, degrees Kelvin;

$\dot{T}$ = rate of change of temperature with respect to y;

$\dot{U}$ = rate of change of mass averaged velocity with respect to y.

B. VIBRATION - DISSOCIATION COUPLING MODEL

The nonpreferential vibrational energy model, Equation (35), is derived in Reference 93 and is included in the principal (C.A.L.) subroutine, where

λ_j = the vibrational relaxation distance of jth species, cm;

θ_j = the characteristic vibrational temperature of jth species, °K;

$T_{m_j}^{-1}$ = $T_V^{-1} - T_T^{-1}$ is a temperature parameter, $°K^{-1}$, relating the vibrational and translational temperatures;

N_j = the number of vibrational energy levels of jth species;

Λ_{ij} = 1 or zero, is the vibrational coupling of jth species to the ith reaction depending upon which reaction will be affected by the vibration-dissociation coupling process;

Q_{ij} = is the mole-volumetric rate of production of jth species from the ith reaction;

χ = is the degree of nonequilibrium of the ith reaction.

In the nonpreferential model, dissociation is hypothesized to occur with equal probability from any level of vibrational excitation of jth species. However, recent theoretical arguments, References 95 and 96, suggest that dissociation is coupled preferentially to the upper vibrational levels of excited molecules. Thus, a preferential vibrational energy model is also included in the CAL subroutine. Presently, such models exist only for diatomic molecules.

C. COLLISIONAL TRANSPORT PROPERTIES

1. Mass Transfer - The Diffusion Coefficients

Equation (37) requires an expression for calculating the multicomponent diffusion coefficient, $D_{j\alpha}$. For this prupose, Reference 83 gives

$$u_o' L D_{j\alpha} = \frac{K^{\alpha j} - K^{jj}}{(MW)_\alpha \, \|K\|} \sum_{\kappa=1}^{s} X_\kappa (MW)_\kappa, \ cm^2/s \tag{52}$$

where $\|K\|$ is the determinant of

$$K_{j\alpha} = \frac{X_j}{\left[\mathcal{D}_{j\alpha}\right]_1} + \frac{(MW)_\alpha}{(MW)_j} \sum_{\kappa \neq j}^{s} \frac{X_\kappa}{\left[\mathcal{D}_{j\kappa}\right]_1}, \tag{53}$$

u_o' and L are dimensional velocity and scale parameters in the CAL subroutine, the $K^{\alpha j}$ are the minors of $\|K\|$, the $K_{jj} = 0$, and the first approximation to the binary diffusion coefficient is computed from the formula

$$p(y)\left[\mathcal{D}_{j\alpha}\right]_1 = (0.002628) \sqrt{\frac{T^3 \left[(MW)_j + (MW)_\alpha\right]}{2(MW)_j (MW)_\alpha}} \Big/ \sigma_{12}^2 \, \Omega_{12}^{(1,1)}(T_{12}^*) \tag{54}$$

Equation (54) shows that the binary diffusion coefficient varies directly with the 3/2 power of the local translational temperature and varies inversely with the local pressure, the square of the collision diameter σ_{12} and the collision integral $\Omega_{12}^{(1,1)}(T_{12}^*)$, where $T_{12}^* = kT/\epsilon_{12}$ is the reduced temperature, ϵ_{12}/k is the potential parameter in °K, and k is Boltzmann's constant. Equation (54) was checked out for self diffusion, Table VI.

TABLE VI

Comparison of Calculated and Observed Self Diffusion Coefficients at 1 atm*

Gas	T(°K)	$\mathcal{D}'$ $cm^2 s^{-1}$ Present	Ref 83	Experimental ($cm^2 sec^{-1}$)
AR	353.2	0.249	0.245	0.249 ± 0.003
	273.2	0.157	0.154	0.156 ± 0.002
				0.158 ± 0.002
	77.7	0.0136	0.133	0.0134 ± 0.0002
N_2	353.2	0.273	0.273	0.287 ± 0.009
	273.2	0.174	0.174	0.185 ± 0.006
				0.172 ± 0.002
	77.7	0.0161	0.0161	0.0168 ± 0.0003

*Check 1 P581 using Equation (3.2-46) Reference 83.

Collision diameters and integrals are tabulated in References 83 and 97 for like particle encounters (single species gas). The collision diameters are averaged for pairs of interacting (unlike) molecules, according to Reference 83,

$$\sigma_{12} = \frac{1}{2}(\sigma_1 + \sigma_2) \tag{55}$$

where the σ_j are obtained from Tables I-A, page 1110, Reference 5 and Table 1, Reference 97. The required collision integrals are obtainable as a function of T_{12}^*, where the potential parameter for pairs of interacting molecules is, again according to Reference 83,

$$\epsilon_{12} = \sqrt{\epsilon_1 \epsilon_2} \tag{56}$$

2. Momentum Transfer - The Viscosity Coefficients

For a single species gas the first approximation to the viscosity coefficient, from Reference 83, is

$$[\mu]_1 \times 10^6 = 26.693 \frac{\sqrt{T(MW)_j}}{\sigma_j^2 \, \Omega^{(2,2)}(T^*)} \tag{57}$$

is tabulated extensively for molecular species of interest in Reference 21. The first approximation to the multicomponent viscosity coefficient, required in Equations (49) and (51), is given by Reference 83:

$$\mu = -\begin{vmatrix} H_{11} & H_{12} & \cdots\cdots & H_{1s} & X_1 \\ H_{12} & H_{22} & \cdots\cdots & H_{2s} & X_2 \\ \vdots & \vdots & & \vdots & \vdots \\ H_{1s} & H_{2s} & & H_{ss} & X_s \\ X_1 & X_2 & & X_s & O \end{vmatrix} \times \begin{vmatrix} H_{11} & H_{12} & \cdots\cdots & H_{1s} \\ H_{12} & H_{22} & \cdots\cdots & H_{2s} \\ \vdots & \vdots & & \\ H_{1s} & H_{2s} & \cdots\cdots & H_{ss} \end{vmatrix}^{-1} \tag{58}$$

where the diagonal elements are

$$H_{jj} = \frac{X_j^2}{[\mu]_1} + \sum_{\substack{\kappa = 1 \\ \kappa \neq j}}^{s} \frac{2X_j X_\kappa}{[(MW)_j + (MW)_\kappa]} \frac{RT}{p[\mathcal{D}_{j\kappa}]_1} \left[1 + \frac{3}{5}\frac{(MW)_\kappa}{(MW)_j} A_{j\kappa}^*\right] ; \tag{59}$$

the off-diagonal elements are,

$$H_{j\alpha} = -\frac{2N_j N_\alpha}{\left[(MW)_j + (MW)_\alpha\right]} p \frac{RT}{\left[\mathcal{D}_{j\alpha}\right]_1} \left[1 - \frac{3}{5} A^*_{j\alpha}\right], \; j \neq \alpha; \tag{60}$$

the collision integral ratio is

$$A^*_{j\alpha} \equiv \Omega^{(2,2)*}/\Omega^{(1,1)*}, \tag{61}$$

tabulated in Tables I-N and VII-E (pages 1128 and 1176 respectively) of Reference 83 for the Lennard-Jones and Buckingham potentials; and the (molar) universal gas constant is

$$R = k\tilde{N} = 8.313404 \times 10^7 \text{ ergs/°K/mole},$$

3. Energy Transfer - The Thermal Conductivity Coefficients

Reference 83, page 1196, recommends use of the formula

$$\kappa = \left[\kappa_{mix}\right]_1 + \kappa_{int} + \kappa_{react} \tag{62}$$

with which to estimate thermal conductivity due to a multicomponent mixture of polyatomic, polar and nonpolar molecules in chemical nonequilibrium, and under flow conditions where local thermodynamic equilibrium (l.t.e.) holds; i.e., where collisional and radiative processes do not appreciably alter the distribution of molecular velocities from the Maxwell-Boltzmann distribution at the local bath temperature.

The first term on the right hand side of Equation (62) is the first approximation to the coefficient of thermal conductivity, not including the effects of internal energy transfer between excited states occupied by interacting molecules, nor the energy transfer effects of chemical kinetics, but accounting for the transformation of internal energy into translational motion; i.e., for a multicomponent gas,

$$\left[\kappa_{mix}\right]_1 = 4 \begin{vmatrix} L^{11}_{11} \cdots\cdots L^{11}_{1s} & X_1 \\ \vdots \qquad\qquad \vdots & \vdots \\ L^{11}_{s1} \cdots\cdots L^{11}_{ss} & X_s \\ X_1 \cdots\cdots X_s & 0 \end{vmatrix} \begin{vmatrix} L^{11}_{11} \cdots\cdots L^{11}_{1s} \\ \vdots \qquad\qquad \vdots \\ L^{11}_{s1} \cdots\cdots L^{11}_{ss} \end{vmatrix}^{-1} \tag{63}$$

where, in the nomenclature of Reference 66, the diagonal elements are,

$$L_{\alpha\alpha}^{11} = -\frac{4X_\alpha^2}{[\kappa_\alpha]_1} - \frac{16T}{25p}\sum_{k\neq\alpha}\left\{X_\alpha X_k\left[15(MW)_\alpha^2/2 + 25(MW)_k^2/4 - 3(MW)_k^2 B_{\alpha k}^* + 4(MW)_\alpha (MW)_k A_{\alpha k}^*\right]\Big/\left[(MW)_\alpha + (MW)_k\right]^2 \left[\mathcal{D}_{\alpha k}\right]_1\right\}, \tag{64}$$

the off-diagonal elements are,

$$L_{\alpha j}^{11} = \frac{16T}{25p}\frac{X_\alpha X_j (MW)_\alpha (MW)_j}{\left[(MW)_\alpha + (MW)_j\right]^2 \left[\mathcal{D}_{\alpha j}\right]_1}\left[\frac{55}{4} - 3B_{\alpha j}^* - 4A_{\alpha j}^*\right];\ \alpha\neq j \tag{65}$$

and the first approximation thermal conductivity coefficient for a single component gas, including the effect of internal energy exchange with the translational modes, is

$$\left[\kappa_j\right]_1 = \frac{1}{4}\left\{(15 - 6\xi_j)\tilde{\gamma}_j - (15 - 10\xi_j)\right\} c_{v_j}\left[\mu_j\right]_1 / (MW)_j - \left\{2\left[\mu_j\right]_1/\pi\right\}\left\{\frac{5}{2} - \xi_j\right\}^2 \sum_k (c_v)_k Z_k/(MW)_k. \tag{66}$$

The first term on the right hand side of Equation (66) represents the first approximation to the thermal conductivity for polyatomic gases where it was assumed that the internal energy of a molecule does not depend on the molecular velocity, and that the exchange of internal and translational energy occurs sufficiently rapid so that l.t.e. holds at each point of the flow. The second term represents the correction, for nonpolar gases, by Mason and Monchick (Reference (86)

where

$(c_v)_k$ is the specific heat of the kth internal mode and

Z_k is the number of collisions required to exchange a quantum of energy of this mode with the translational degrees of freedom.

Experimental data for a number of common gases were examined in Reference 86 where it is concluded that better agreement between experiment and theory occurs at temperatures less than about 400°K when Equation (66) is used to correlate data. However, at high temperatures two compensating effects take place in that the translational conductivity is less than the value predicted by the first term on the right hand side of Equation (66) while the reciprocal Schmidt number,

$$\xi_j = \rho \mathcal{D}/\mu \tag{67}$$

is greater than unity; i.e., greater than the Eucken correction, Reference 83, which was used prior to the theoretical prediction by Mason and Monchick. Further, since only a few of the large number of relaxation times needed to evaluate Z_k are known, a reciprocal Schmidt number value of $\xi = 1.32$ is used in the present work in order to use the data computed for the first term of Equation (32) tabulated in Reference 97. The actual form of Equation 66 used for monatomic gases check out is Equation 8.2-31 of Reference 83, see Table VII. The Eucken correction was used for polyatomic gases, Table VIII. Equation 63-66 were used to check out the binary gas mixtures shown on Figure 26 and Table IX. An option to compute the exact value of $[\kappa_j]_1$ is included in the program for those cases where the relaxation times have been measured (diatomic gases) and to be consistent with the relaxation phenomena calculation included within the framework of the Vibration-Dissociation Coupling Model (the CAL subroutine) above.

TABLE VII

Thermal Conductivity

Thermal Conductivity of Monatomic Gases: Comparison of Experimental Values with those Calculated Using Equation (8.2-31)*

$X\ 10^7$ in cal cm^{-1} sec^{-1} deg^{-1}

°K	Helium		Neon		Argon		Kryston		Xenon	
	Calculated	Experimental	Calculated	Experimental	Calculated	Experimental	Calculated	Experimental	Calculated	Experimental
90.2	1726	1655	496	489	140	141	68		40	
194.7	2839	2706	870	876	297	293	149	152	85	91
273.2	3534	3390	1097	1097	398	385	206	190	120	123
		3406		1110		390		208		124
		3438				394				
		3510								
373.2	4329	4165	1340	1357	509	506	271	272	161	168
491.2	5173	4947	1589	1595	622	614	339	340	204	208
579.1	5752	5504	1770	1789	699	685	384	388	233	237

*Check 1 P573 Reference 83

TABLE VIII

Thermal Conductivity

Thermal Conductivity of Polyatomic Gases: Comparison of Experimental Values with those Calculated Using Formula (8.2-33)*

X 10^7 in cal cm^{-1} sec^{-1} deg^{-1}

T °K	Hydrogen		Oxygen		Carbon Dioxide		Methane		Nitrous Oxide	
	Calculated	Experimental	Calculated	Experimental	Calculated	Experimental	Calculated	Experimental	Calculated	Experimental
100	1589	1625	224	216			254	254		
150									327	321
200	2994	3064	435	438	183	227	508	522	456	425
273	3871	3965	568	584	267	349	696	734	578	567
		4040		577		360		720		
300	4099	4227	614	635	300	398	764	819	618	619

*Check 2 P574 Reference 83.

TABLE IX

Thermal Conductivity

Comparison of Calculated and Experimental Values for Binary Gas Mixture Using Equation (8.2-42) and Mix Formula on Page 1196*

Helium - Argon			X 10^5 in cal cm^{-1} sec^{-1} deg^{-1} Hydrogen - Carbon Dioxide			Hydrogen - Argon		
Percent of Lighter Constituent	Experimental	Calculated	Percent of Lighter Constituent	Experimental	Calculated	Percent of Lighter Constituent	Experimental	Calculated
0.0	3.89	3.98	0.0	3.60	3.91	0.0	3.90	3.99
27.04	7.42	7.43	10.0	5.10	5.10	9.0	5.50	5.58
45.37	10.77	10.81	14.2	5.70	5.67	18.0	7.30	7.37
8[illegible].68	23.20	24.43	25.0	7.70	7.33	40.0	12.60	12.88
94.61	29.39	30.84	35.5	10.00	9.30	60.0	18.70	20.00
100.00	33.86	35.24	50.0	13.50	12.85	80.2	27.00	30.87
			75.0	22.70	23.10	100.0	40.00	48.99
			90.0	31.50	34.97			
			100.0	40.40	48.49			

*Check 3 P576-578 Reference 83.

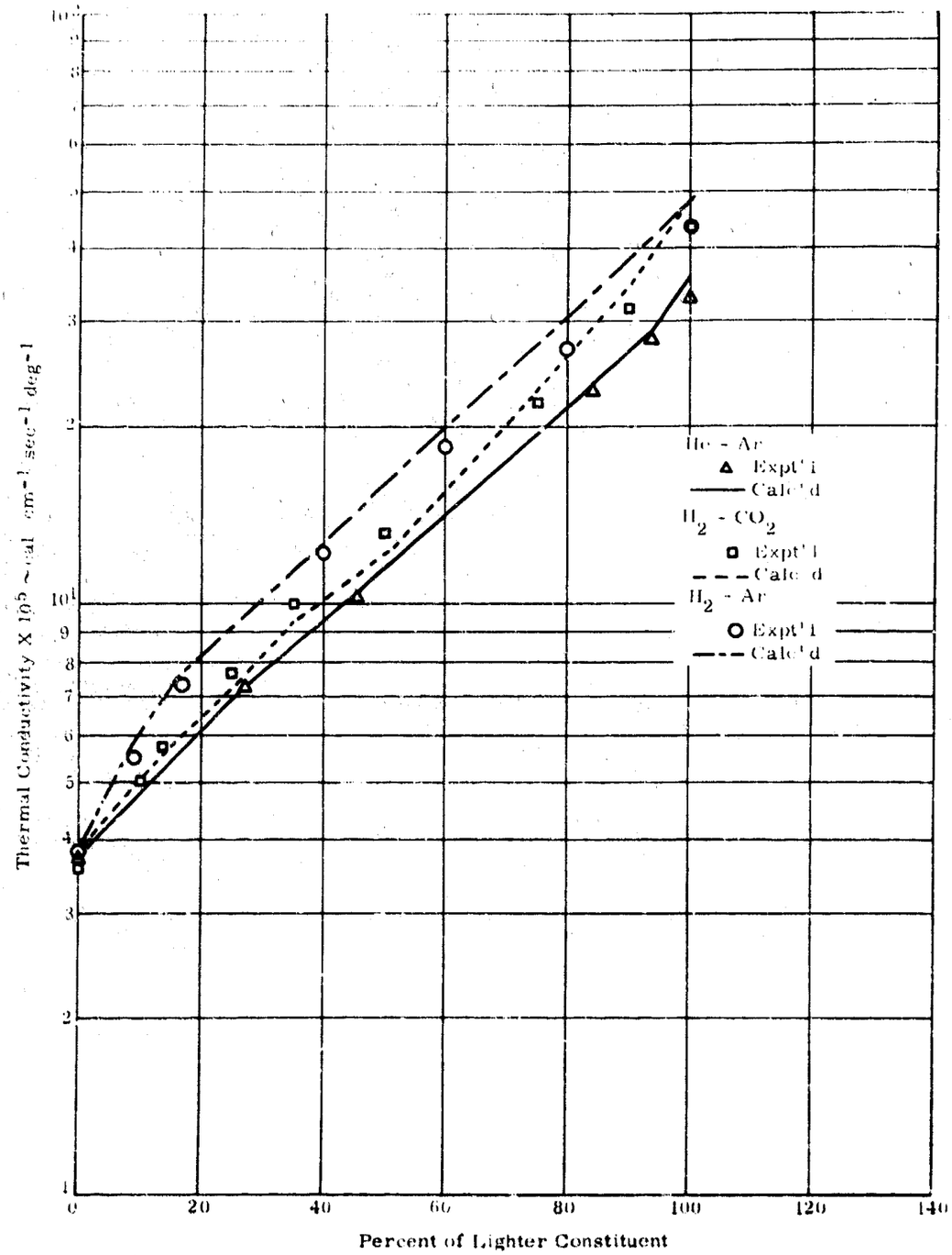

Figure 26. Check Calculation of Thermal Conductivity for Various Binary Systems

The second term on the right hand of Equation (62) is, according to Reference 83, page 1196 and Reference 87,

$$\kappa_{int} = \sum_{j=1}^{s} \left\{ \frac{X_j \left(\xi_j \left[\mu_j \right]_1 c_{p_j} / (MW)_j - \left[\kappa_j \right]_1 \right)}{\sum_{k=1}^{s} X_k \left[\mathcal{D}_{jj} \right]_1 / \left[\mathcal{D}_{jk} \right]_1} \right\}, \tag{68}$$

where

c_{p_j} is the specific heat at constant pressure of the jth gas component (species) and

$\mathcal{D}_{jj}$ is the coefficient of self diffusion of the jth species, derivable from Equation (54).

According to Butler and Brokaw, Reference 90, who have shown that for a set of s chemical species $[M]$ participating in r chemical reactions which can be written stoichiometrically

$$\sum_{j=1}^{s} \nu_{ij} [M] = 0; \; i = 1,2,\ldots,r \tag{69}$$

it follows that the third term of Equation (62) is

$$\kappa_{ract} = -\left(RT^2\right)^{-1} \begin{vmatrix} A_{11} \ldots\ldots A_{1r} & \Delta\tilde{H}_1 \\ \vdots \qquad \vdots & \vdots \\ A_{r1} \ldots\ldots A_{rr} & \Delta H_r \\ \Delta\tilde{H}_1 \ldots\ldots \Delta\tilde{H}_r & 0 \end{vmatrix} \begin{vmatrix} A_{11} \ldots\ldots A_{1r} \\ \vdots \qquad \vdots \\ A_{r1} \ldots\ldots A_{rr} \end{vmatrix}^{-1} \tag{70}$$

where

$$\Delta\tilde{H}_i = \sum_{j=1}^{s} \nu_{ij} \tilde{H}_j \tag{71}$$

is the enthalpy change of the ith reaction and the $\tilde{H}_j$ are the species enthalpies referred to a common base. The determinant elements are

$$A_{ij} = \sum_{k=1}^{s-1} \sum_{\ell=k+1}^{s} \left\{ (RT/\mathcal{D}_{k\ell} p)\, X_k X_\ell \left[(\nu_{ik}/X_k) - (\nu_{i\ell}/X_\ell) \right] \cdot \right.$$
$$\left. \cdot \left[(\nu_{jk}/X_k) - (\nu_{j\ell}/X_\ell) \right] \right\}. \tag{72}$$

If the chemical reactions are slow, the thermal conductivity, Equation (70) depends on the boundary conditions, see Reference 83 (page 1197), References 91 and 92.

D. RADIATIVE ENERGY TRANSFER

The scope of present work includes investigation of gas dynamically coupled radiative energy transfer, with particular emphasis on applications in supersonic combustion. Such coupled interactions are included within the framework of the reaction profile model, the sources being due to chemiluminescence and inelastic collisional encounters among the reactants.

Beginning with the simplest approximation, that of the optically thin gas, the energy conservation term expressing the divergence of radiative flux in Equation (49) is (see References 98 and 99)

$$\frac{\partial q_j^R}{\partial x_j} = 4\, k_P \sigma T^4 \tag{73}$$

where

$$k_P = \frac{\pi}{\sigma T^4} \int_0^\infty k_\nu B_\nu \, d\nu, \ \mathrm{cm}^{-1} \tag{74}$$

is the Planck mean absorption coefficient,

$$B_\nu(T) \equiv \frac{2h\nu^3/c^2}{e^{h\nu/kT} - 1} \tag{75}$$

is the Planck function which, integrated over all frequencies gives

$$\int_0^\infty B_\nu(T)\, d\nu = \sigma T^4/\pi \ . \tag{76}$$

The Stefan-Boltzman constant is

$$\sigma = \frac{2\pi^5 k^4}{15 h^3 c^2} = 5.6697 \times 10^{-5} \text{ erg/cm}^2 {}^\circ\text{K}^4 \text{s}; \tag{77}$$

the absorption coefficient is

$$\begin{aligned} k_\nu &= \rho \eta_\nu^* \\ &= \rho \eta_\nu (1 - e^{-h\nu/kT}), \end{aligned} \tag{78}$$

and the spectral intensity is

$$I_\nu = k_\nu B_\nu . \tag{79}$$

To evaluate the Planck mean-absorption coefficient, combine Equations (74) - (78) to obtain

$$k_P = \frac{15}{\pi^4} \int_0^\infty \zeta^3 e^{-\zeta} d\zeta / \mathcal{K}(\zeta) \tag{80}$$

where

$$\zeta = h\nu/kT \tag{81}$$

and

$$\mathcal{K}(\zeta) = (\rho \eta_\nu)^{-1} \tag{82}$$

is the radiative mean-free-path.

Two alternate methods of determining absorption coefficients (e.g., reciprocal Equation (82)) or spectral intensities (Equation (79)) are available to evaluate the required integral, Equation (88). The first method requires a direct experimental measurement of $1/\mathcal{K}$ over the wavelength range of interest, at the equilibrium temperature. Such measurements are not available for the special case of interest; i.e., the combustion of pyrophoric fuels. The second method depends on quantum mechanics. In this case, measurements of oscillator strengths, transition frequencies and spectral constants are still, for the most part, required. Further, as is pointed out

by Herzberg, Reference 100, a knowledge of the excited states of intermediate species is of great importance in the determination of chemiluminescence and in understanding the occurrence of elementary processes; i.e., the elementary chemical kinetic steps in the reaction mechanism. These problems may be approached as follows.

1. Local Thermodyanic Equilibrium

Chandrasekhar's hypothesis of local thermodynamic equilibrium, Reference 101, is an important concept applied in the calculation of gas dynamically coupled spectral intensities and radiative energy transfer. According to this hypothesis, at each point (ρ, T) of the flow field, one defines a gas at temperature T and specie density ρ such that ρ is the population of excited energy states of that gas in true thermodynamic equilibrium at temperature T. That is, the state populations are locally defined by a Boltzmann distribution, exp (-E/kT). The condition of local thermodynamic equilibrium does not require that the radiation field be in equilibrium with the flow field nor is chemical equilibrium a requirement for thermodynamic equilibrium on a local basis.

A subroutine code for calculation of the spectral intensities of species in nonequilibrium high temperature gas is required. The reaction energies and populations of continuum states obtained from the CAL subroutine must be taken into account. The following section gives a review of the basic formulation and recently accepted approximations for calculation of spectral intensities of diatomic species in either equilibrium or chemical nonequilibrium in the optically thin limit.

2. Review of Basic Formulism

The radiation process in a model sample of high temperature gas may be regarded as the emission of photons of spectral frequencies $\nu = c/\lambda$ caused by electronic (orbital) transitions of a molecule from an initial state of energy E_n to a final state of energy E_m: where $E_n > E_m$ is the condition that radiation of frequency $(E_m - E_n)/h = \nu_{nm}$ be emitted. The rate of emission of photons of energy $h\nu_{nm}$ from a single source in the sample is called the radiation intensity I_ℓ (watts/molecule). Classically, the intensity of the radiation field is determined by Fourier analyzing the spectrum due to a dipole source. For a single (orbital) electron, the time averaged intensity corresponding to the ℓth Fourier component of frequency $\ell\nu$ (accounting for two polarizations of the field) is

$$I_\ell = \frac{4}{3}(2\pi\ell\nu)^4 |p_\ell|^2/c^3 \qquad (83)$$

where p_ℓ is the Fourier coefficient of the dipole moment. Now, of all molecules in the sample which occupy the initial state, let A_{nm} be the fraction which participates in the transition from state n to state m per second. Then, on a statistical basis

$$I_\ell = A_{nm} h\nu_{nm}. \tag{84}$$

Comparing Equations (83) and (84) obtains the Einstein coefficient; i.e., the transition probability

$$A_{nm} = \frac{64\pi^4}{3h} \left(\frac{\nu_{nm}}{c}\right)^3 \left|\langle m \left| p_k \right| n \rangle\right|^2 \tag{85}$$

where Fourier terms of Equation (83) have been formally replaced by the matrix elements of the dipole moment; e.g.,

$$\langle m \,|p_k|\, n\rangle \equiv \int\int\int \psi^*(m)\, p_k\, \psi(n)\, d\tau \tag{86}$$

The state eigenfunctions ψ are obtained by solving the time-independent Schroedinger equation, given the appropriate potential function. One must sum Equation (85) over all states m which have energy $E_m < E_n$ to obtain the total probability per unit of time that state n will undergo spontaneous depopulation through emission of light photons. The fact that spontaneous transitions incur isotropic radiation, while induced emission (such as in Raman spectra) is aligned with the incident field, leads to the Einstein probability B_{nm} that the system will undergo a induced emission from n to m under the influence of an external field. On the other hand, induced absorption $m \rightarrow n$ is also likely; thus, accounting for possible degeneracies g_k in the electronic states of a molecule, the Einstein coefficient for induced absorption is,References 102 and 103.

$$B_{mn} = \frac{1}{8\pi hc} \left(\frac{c}{\nu_{nm}}\right)^3 \left(\frac{g_n}{g_m}\right) A_{nm} = \left(\frac{g_n}{g_m}\right) B_{nm} \tag{87}$$

Since the intensities of molecular electronic transitions from an upper state n to a lower state m are determined by the transition probability A_{nm} in emission or B_{nm} in absorption, one can theoretically find the emission intensity from Equations (84), (85) and (86) after multiplying (84) by the number density N_m of molecules populating the lower electronic state. However, the absolute intensity of electronic transitions is usually

determined experimentally from the absorption spectrum because of the general difficulty of finding N_m. The development chosen here is the absorption spectrum approach to facilitate inclusion into the program of new measurements of physical data that appear in the literature.

Now, the spectral intensity due to an optically thin slab of gas is given approximately by Kirchoff's law; viz,

$$I_\lambda = B_\lambda k_\lambda \tag{88}$$

where k_λ is the absorption coefficient, and

$$B_\lambda = \frac{c}{4\pi} \frac{8\ hc}{\lambda^5} \left[\exp(hc/kT\lambda) - 1\right]^{-1} \tag{89}$$

is the Planck energy density rate per steradian. In that hc/kT is large, Wien's approximation is good. Therefore, Equations (88) and (89) combine to give

$$I_\lambda = \frac{2hc^2 k_\lambda}{\lambda^5} \exp(-hc/kT\lambda). \tag{90}$$

Given the absorption coeffieient k_λ relating the energy density I_o (incident per unit time on a "one-dimensional" sample of gas) to the transmitted energy,

$$I_\lambda = I_o e^{-k_\lambda \Delta x} \tag{91}$$

one integrates over the pertinent bandwidth interval to obtain the absorption intensity, Reference 104,

$$\begin{aligned} I &= \int (I_o - I_\lambda) d(1/\lambda) \\ &= I_o \Delta x \int k_\lambda d\,\nu/c = I_o N_m B_{mn} h\nu_{nm} \frac{\Delta x}{c} . \end{aligned} \tag{92}$$

Therefore, the integrated absorption coefficient is

$$\int k_\lambda d\nu = N_m B_{mn} h\nu_{nm} \equiv N_m \pi r_o cf, \tag{93}$$

where N_m is the number density of molecules populating the lower electronic state, r_o is the classical electron "radius", e^2/mc^2, and the "f-number" is defined by Equations (85), (87), and (93). In terms of the matrix elements of the dipole moment

$$f = \frac{8\pi^2 m\nu_{nm}}{3hc^2} \left| \langle m|p_k|n\rangle \right|^2 \tag{94}$$

Equation (60) is the "electronic oscillator strength" f, a dimensionless quantity that can be found experimentally and is most important to the calculation of both transition probabilities and spectral intensities.*

Differentiating Equation (59) yields the absorption coefficient

$$k_\lambda = N_m \pi r_o c \frac{df}{d\nu} \tag{95}$$

Penner, Reference 106, approximates the derivative in the following manner. Assuming all transitions from lower energy levels are to the lowest upper energy level, the derivative is equal to the total oscillator strength times the rate of change of the fraction of molecules that are in an excited energy state

$$E = E_o - hc/\lambda \equiv hc\left(\frac{1}{\lambda_{oo}} - \frac{1}{\lambda}\right).$$

Thus,

$$\frac{df}{d\tilde{\nu}} = f \frac{d}{d\tilde{\nu}} \exp\left[-\frac{hc}{kT}\left(\frac{1}{\lambda_{oo}} - \frac{1}{\lambda}\right)\right] \quad ; \tilde{\nu} \equiv \frac{1}{\lambda}$$

i.e.,

$$\frac{df}{d\tilde{\nu}} = \frac{hc}{kT} f \exp\left[-\frac{hc}{kT}\left(\frac{1}{\lambda_{oo}} - \frac{1}{\lambda}\right)\right] . \tag{96}$$

*Bethe and Salpeter, Reference 105, shows that for hydrogen-like atoms of nuclear charge $Z \ll 137$, the dipole approximation holds and $\Sigma_m f = 1$.

The present formulation uses an approach, originally applied to NO absorption spectra, Reference 107 which is in essential agreement with Penner. That is, employing the rotating oscillator model for diatomic molecules, the rate of change of the excited population varies directly with the Franck-Condon electronic transition probability for a single vibrational mode with average rotational overtones. Thus, introducing rotational and vibrational partition functions Q_r'', Q_v'' in the lower (double primed) state, Keck, et al., Reference 108, show

$$\frac{df}{d\tilde{\nu}} = \frac{q_{v'v''}\, e^{-(E_{r'} + E_{v'})/kT}}{Q_{r''}\, Q_{v''} \left| B_e' - B_e'' \right|} \qquad f \exp\left[-\frac{hc}{kT}\left(\frac{1}{\lambda_{oo}} - \frac{1}{\lambda}\right)\right]. \quad (97)^*$$

Substituting Equation (97) into (95) yields the absorption coefficient for a particular vibrational transition and averaged rotational structure. Thus,

$$k_\lambda = \frac{\pi\, r_o\, f\, N_m\, e^{-hc(\tilde{\nu}_{oo} - \tilde{\nu})/kT}}{Q_{r''}\, Q_{v''} \left| B_e' - B_e'' \right|} \qquad q_{v'v''}\, e^{-(E_{r'} + E_{v'})/kT} \quad (98)$$

A summation of Equation (98) over all vibrational transitions which can occur at the wavelength λ will give the absorption coefficient at λ for the electronic transition involved:

$$k_\lambda = \frac{\pi\, r_o\, f\, N_m\, e^{-hc(\tilde{\nu}_{oo} - \tilde{\nu})/kT}}{Q_{r''}\, Q_{v''} \left| B_e' - B_e'' \right|} \qquad \sum_{E_r' \geq 0} q_{v'v''}\, e^{-(E_{r'} + E_{v'})/kT} \quad (99)$$

A close inspection of the exponential term $E_{r'}$ will reveal the simple expression for the manner in which the summation is to be executed†. Consider a vibration band whose rotational structure degrades to the red, i.e., greater λ. The summation, in this case, should be over all vibrational bands for which the band head $\lambda_{v'v''}$ is equal to or smaller than the wavelength in question ($\lambda_{v'v''} \leq \lambda$). Reversing the case for vibration bands which degrade to the violet, the summation applies to all band heads equal to or greater than the wavelength in question ($\lambda_{v'v''} \geq \lambda$). Further, it may

*Most symbols not defined are the accepted notation; e.g., v and r for vibrational and rotational quantum numbers.

†The summation accounts for branching of the spectra, see Reference 109.

be noted from the spectrographic constants involved, that the quantity $(B_e' - B_e'')$ will be positive for all bands degrading to the violet, and negative for those degrading to the red. Substituting these facts into the expression for $E_{r'}$ it is easily verified that the summation for both types of degrading is that over all transitions for which $E_{r'} \geq 0$, i.e.,

$$E_{r'} = \frac{hc\, B_e'}{B_e' - B_e''} (\tilde{\nu} - \tilde{\nu}_{v'v''}) \geq 0 . \tag{100}$$

Finally, Equation (99) may be substituted into Equation (90) obtaining the spectral intensity

$$I_\lambda = \frac{2\pi\, r_o\, hc^2\, N_m f\, e^{-\frac{hc\tilde{\nu}_{oo}}{kT}}}{Q_{r''}\, Q_{v''} \left| B_e' - B_e'' \right| \lambda^5} \sum_{E_{r'} \geq 0} q_{v'v''}\, e^{-(E_{r'} + E_{v'})/kT} \tag{101}$$

A factor ϕ is incorporated in the derivation of Reference 108, which may be extracted from the above expression. In terms of ϕ, Equation (101) is written in the compact form,

$$I_\lambda = 2\pi\, r_o\, hc^2\, \phi\, \lambda^{-5}\, N_m\, f\, \frac{hc}{kT} \exp(-hc\tilde{\nu}_{oo}/kT) \tag{102}$$

where

$$\phi = \frac{kT}{hc} \frac{1}{Q_{r''}\, Q_{v''}\, B_e' - B_e''} \sum_{E_{r'} \geq 0} q_{v'v''}\, e^{-\left[\frac{E_{r'} + E_{v'}}{kT}\right]} \tag{103*}$$

Rotational and vibrational partition functions for the lower state population are

$$Q_{r''} = \frac{kT}{hc\, B_e''} \tag{104}$$

to a good approximation, and

*The notation $E_{r'} \geq 0$ under the summation sign in the expression for ϕ implies that all terms will be added into the sum except those for which $E_{r'} < 0$.

$$Q_{v''} = \left[1 - \exp\left(-\frac{hc\,\omega_e''}{kT}\right)\right]^{-1} \tag{105}$$

exactly.

The (Fortrat) averaged rotational energy level of the emitting state is

$$E_{r'} = \frac{hc\,B_e}{B_e' - B_e''}\left(\frac{1}{\lambda} - \tilde{\nu}_{v'v''}\right) \tag{106}$$

where

$$\tilde{\nu}_{v'v''} = \tilde{\nu}_{oo} + (E_{v'} - E_{v''})\frac{1}{hc}\,; \tag{107}$$

the vibrational energy of the emitting state is

$$E_{v'} = hc\,(\tilde{\nu}_{v'} - \tilde{\nu}_{o'}). \tag{108}$$

Assuming the rotating oscillator model for diatomic molecules,

$$\tilde{\nu}_{v'} = \omega_e'(v' + 1/2) - \omega_e'\,x_e'\,(v' + 1/2)^2 + \omega_e'\,y_e'\,(v' + 1/2)^3 \tag{109}$$

therefore,

$$\tilde{\nu}_{o'} = \frac{\omega_e'}{2} - \frac{\omega_e'\,x_e'}{4} + \frac{\omega_e'\,y_e'}{8}. \tag{110}$$

Likewise, for the absorbing or lower state,

$$E_{v''} = hc\,(\tilde{\nu}_{v''} - \tilde{\nu}_{o''}), \tag{111}$$

$$\tilde{\nu}_{v''} = \omega_e''(v'' + 1/2) - \omega_e''\,x_e''\,(v'' + 1/2)^2 + \omega_e''\,y_e''\,(v'' + 1/2)^3 \tag{112}$$

and

$$\tilde{\nu}_{o''} = \frac{\omega_e''}{2} - \frac{\omega_e''\,x_e''}{4} + \frac{\omega_e''\,y_e''}{8}. \tag{113}$$

Including the Free-Bound Radiation, e.g., References 110 and 111

$$I_\lambda = 2hc^2 \lambda^{-5} N_m \sigma e^{\left[-\frac{hc\tilde{\nu}}{kT}\right]}, \tag{114}$$

where σ is the photodetachment cross-section, cm^2.

Note that spectral intensities calculated with this subroutine can be used to predict the optically thin limit radiation signature of shock layers and trails that are predominantly composed of N_2, O_2, and NO in chemical equilibrium (or in chemical nonequilibrium when the populations of excited states are known).

BLANK PAGE

APPENDIX A

OPTICAL ABSORBIMETRY OF THE B_2H_6/O_2 SYSTEM

Specific radiation absorbimetry measurements are to be made, with microsecond resolution, to monitor the appearance and disappearance of the hydroxyl (OH) radical, postulated as a chain carrier intermediate in the high temperature oxidation of diborane (B_2H_6).

The reactor to be used is a one-inch diameter chemical shock tube with helium gas driving shock waves in argon, generating temperatures from 500 to 1000°K in the region behind the reflected shock wave. The source of OH radiation to be used is a flash lamp containing water vapor. The source radiation absorption will be measured in the homogeneous gas sample behind the reflected shock wave in argon at initial pressure near 76 mm Hg and containing the reactants, B_2H_6 and O_2, in amounts of the order of 1 percent by volume.

These measurements will give the change in the concentration of OH with time. From this it may be possible to deduce the effective activation energy and corresponding reaction rate (s) leading to a better understanding of the high temperature reaction kinetics of B_2H_6 oxidation. It may also be possible to verify the postulated chain mechanism following ignition induction.

Measurement of the OH concentration is to be made by ultraviolet light absorption, using a flash lamp as the source of characteristic OH radiation. The OH radical was selected for this study because of its known relative high stability and very high optical absorption coefficient (about 2.3×10^6 cm^2/mole). The integrated absorption coefficient for OH, over a selected number of rotational lines, will be measured by comparing the observed absorption with the computed OH concentration at equilibrium.

Using an analytical technique developed at Cornell University - beginning with Bauer, Schott and Duff (1958), the concentration of a specific chemical species as a function of time at high temperatures may be obtained for species with fine line absorption spectra, such as the OH radical. This can be done by using as a source an intense fine line emission spectrum generated by exiting the species which one wishes to observe in the sample.

In this case the source of OH radiation is a pulsed discharge through a short capillary containing water vapor at a pressure of about 10 mm Hg (Figure 27). The lamp is viewed through the ring-shaped anode. The electrical circuit for this flash lamp consists of a 3.7 microfad capacitor charged to 10 kilovolts in series with a 1.5 kilohm resistor and an 8 millihenry choke (Figure 28). This circuit produces a light pulse which rises in about 300 microseconds and is nearly constant for the following 1 millisecond, during which absorption measurements are made. The entire experimental setup is shown schematically on Figure 29.

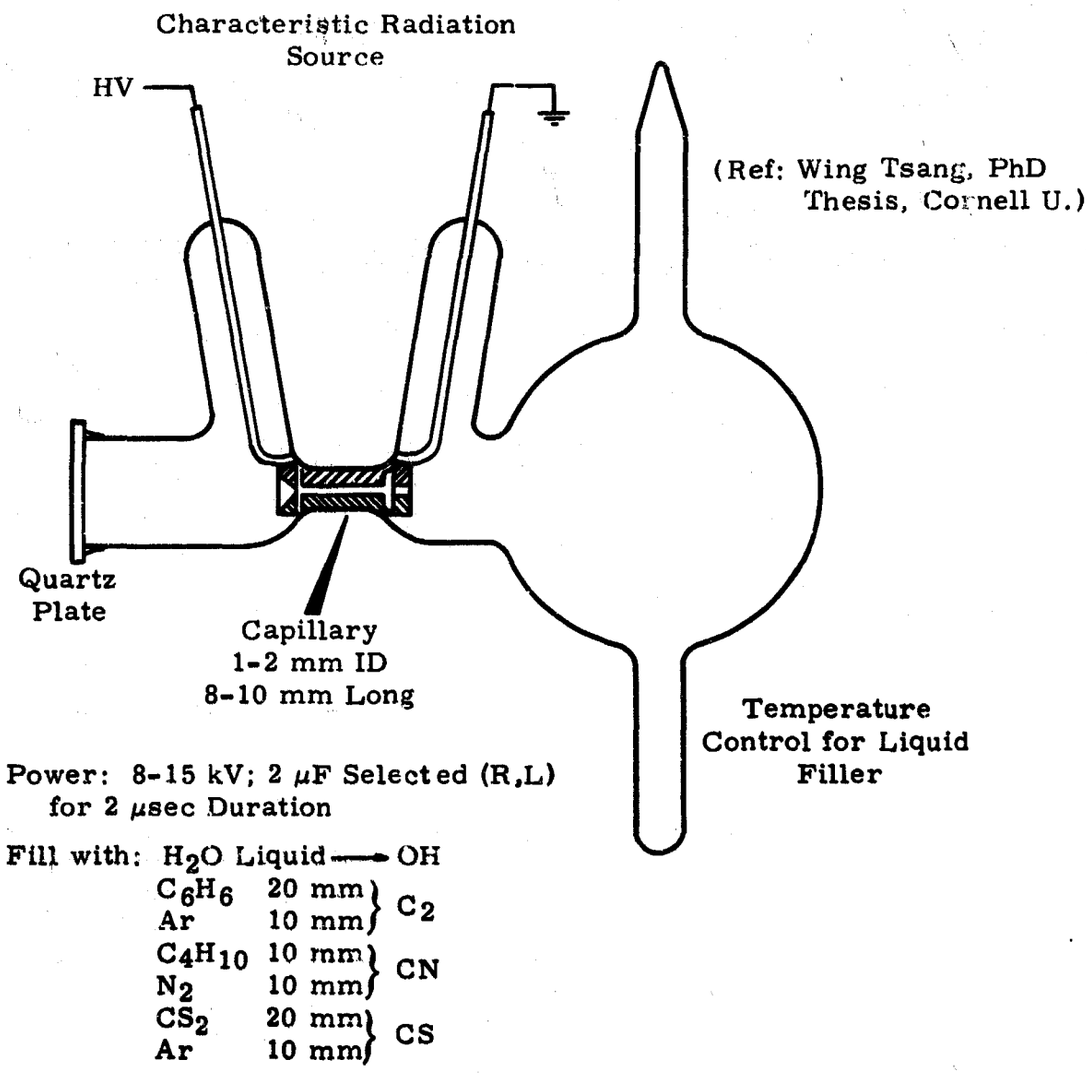

Figure 27. Characteristic Radiation Source Lamp

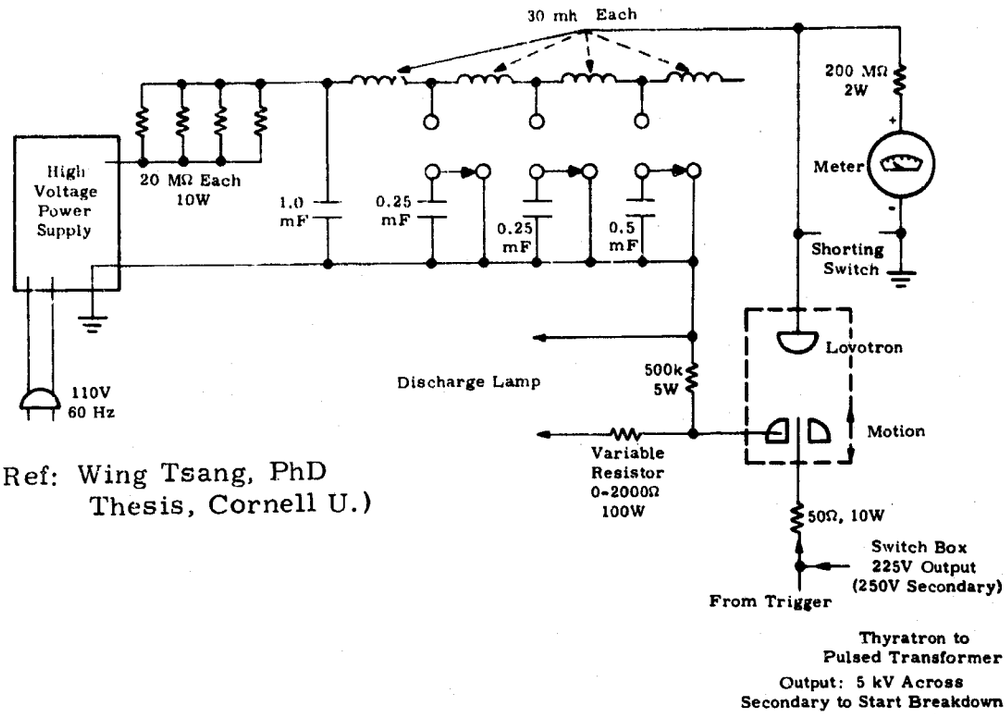

(Ref: Wing Tsang, PhD
Thesis, Cornell U.)

Figure 28. Schematic of High Voltage Capacitor Bank and Lovotron Switch to be Used for Energizing the Characteristic Radiation Source

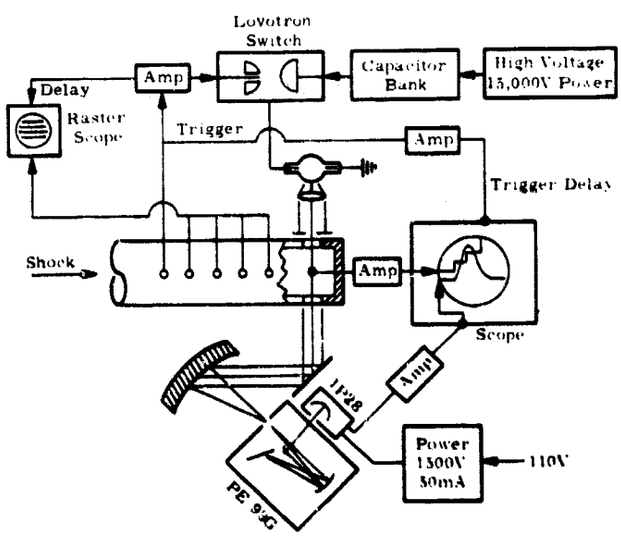

Figure 29. Absorptivity Measurement Instrumentation

BLANK PAGE

APPENDIX B

A SHOCK WAVE ANALYSIS

One-dimensional conservation equations were used for computation of flow variables in the chemical equilibrium region downstream of shock waves traversing a multicomponent gas mixture.

A. ONE-DIMENSIONAL CONSERVATION EQUATIONS

These equations are:

$$\rho_1 u_1 = \rho_2 u_2 \tag{1}$$

for miss conservation,

$$p_1 + \rho_1 u_1^2 = p_2 + \rho_2 u_2^2 \tag{2}$$

for momentum conservation, and

$$h_1 + \frac{1}{2} u_1^2 = h_2 + \frac{1}{2} u_2^2 , \tag{3}$$

for energy conservation. The terms ρ, u, p, and h are the gas density, velocity, pressure and specific enthalpy designated upstream (subscript 1) and downstream (subscript 2) of the shock wave. Since the specific enthalpy

$$h = e + p/\rho \tag{4}$$

introduces a fifth variable, namely the internal energy, e, per unit mass of gas component, essentially a function of temperature, the system of equations to be solved requires equation (4) in order to calculate enthalpy and an equation of state,

$$p = \rho RT = NkT, \tag{5}$$

to calculate temperature. N is the total number density of ν-component species, $N = \sum_{i=1}^{\nu} N_i$ and the density $\rho = \sum_{i=1}^{\nu} m_i N_i$.

Rearranging equation (3) and introducing equation (1)

$$\frac{1}{2} u_1^2 = (h_2 - h_1) + \frac{1}{2} (\rho_1/\rho_2)^2 u_1^2$$

then

$$\frac{1}{2}u_1^{\,2}\left[1-(\rho_1/\rho_2)^2\right] = (h_2 - h_1)$$

hence

$$u_1^{\,2}\left[1-(\rho_1/\rho_2)^2\right] = 2(h_2 - h_1)\,. \tag{6}$$

Rearranging equation (2), introducing equation (1)

$$\rho_1 u_1^{\,2} = (p_2 - p_1) + \rho_2(\rho_1/\rho_2)^2\, u_1^{\,2}$$

thus

$$u_1^{\,2} = (p_2 - p_1)/\rho_1 + (\rho_1/\rho_2)\, u_1^{\,2}$$

then

$$u_1^{\,2}\left[1-\rho_1/\rho_2\right] = (p_2 - p_1)/\rho_1\,. \tag{7}$$

Dividing equation (6) by equation (7)

$$1 + \rho_1/\rho_2 = 2\rho_1(h_2 - h_1)/(p_2 - p_1)$$

then

$$1 + \rho_1/\rho_2 = 2(\rho_1/p_1)\,\frac{(h_2 - h_1)}{(p_2/p_1 - 1)} \tag{8}$$

Introducing the equation of state and its ratio from region 1 to region 2 across the incident shock wave one obtains from equation (5) and equation (8)

$$1 + \rho_1/\rho_2 = \frac{2(h_2 - h_1)/R_1T_1}{\left(\rho_2/\rho_1\right)\dfrac{R_2T_2}{R_1T_1} - 1} \tag{9}$$

$$= \frac{2(h_2 - h_1)}{R_2T_2(\rho_2/\rho_1) - R_1T_1}\,.$$

From equation (5) the gas constant is defined (for equilibrium temperature T) as

$$R\cancel{T}\sum_{i=1}^{\nu} m_1N_i = k\cancel{T}\sum_{i=1}^{\nu} N_i \tag{10}$$

i.e.,

$$R = N_o k \sum_{i=1}^{\nu} N_i / \sum_{i=1}^{\nu} N_i M_i = N_o k / \sum_{i=1}^{\nu} X_i M_i$$

then

$$R = N_o k/\overline{M} = 8.3143 \times 10^7/\overline{M} \text{ ergs/°K/gm} \tag{11}$$

where the molecular weight

$$\overline{M} = \sum_{i=1}^{\nu} X_i M_i \tag{12}$$

is obtained by averaging the ν-component molecular weights over their mole fraction $X_i = N_i/N$. (13)

Equation (9) becomes

$$1 + \rho_1/\rho_2 = \frac{2(h_2 - h_1)\,\overline{M}_2}{N_o k\left[T_2(\rho_2/\rho_1) - T_1 \dfrac{\overline{M}_2}{\overline{M}_1}\right]} \tag{14}$$

thus, solving for ρ_2/ρ_1

$$N_o k(T_2/\overline{M}_2)\left[\rho_2/\rho_1 - \frac{T_1}{T_2}\,\frac{M_2}{M_1}\,(1 + \rho_1/\rho_2) = 2(h_2 - h_1)\right] \tag{15}$$

where the enthalpy may be obtained from JANAF tabulations according to

$$h_2 - h_1 = (H_2/\overline{M}_2 - H_1/\overline{M}_1)\,\text{JE7} \tag{16}$$

and at T = 298°K, $H_1(298) \equiv 0$. Therefore, equations (15 and (16) become

$$N_o k T_2\left[\rho_2/\rho_1 - \frac{T_1}{T_2}\,\frac{M_2}{M_1}\right](1 + \rho_1/\rho_2) = 2H_2\text{JE7}\,. \tag{17}$$

Let $N_o k T_2 \equiv \alpha$; then, expanding (17):

$$\alpha + \alpha\,\rho_2/\rho_1 - N_o kT_1\left(\frac{\overline{M}_2}{\overline{M}_1}\right)\frac{1}{(\rho_2/\rho_1)} - N_o kT_1\left(\frac{\overline{M}_2}{\overline{M}_1}\right) = 2H_2JE7$$

$$\alpha(\rho_2/\rho_1)^2 + \left[\alpha - 2H_2JE7 - N_o kT_1\left(\frac{\overline{M}_2}{\overline{M}_1}\right)\right]\rho_2/\rho_1 - N_o kT_1\left(\frac{\overline{M}_2}{\overline{M}_1}\right) = 0$$

therefore,

$$\rho_2/\rho_1 = -\left[\alpha - 2H_2JE7 - N_o kT_1\left(\frac{\overline{M}_2}{\overline{M}_1}\right)\right]/2\alpha$$

$$+\left\{\left[\alpha - 2H_2JE7 - N_o kT_1\left(\frac{\overline{M}_2}{\overline{M}_1}\right)\right]^2 + 4\alpha N_o kT_1\left(\frac{\overline{M}_2}{\overline{M}_1}\right)\right\}^{\frac{1}{2}}/2\alpha \tag{18}$$

where

$$\beta = \alpha - 2H_2JE7 - N_o kT_1\left(\frac{\overline{M}_2}{\overline{M}_1}\right) \tag{19}$$

and

$$\gamma = N_o kT_1\left(\frac{\overline{M}_2}{\overline{M}_1}\right) . \tag{20}$$

Note:

$$J = 4.1840 \text{ joules/calorie}, \; N_o k = 8.3143E7 \text{ ergs/°K/mole}, \tag{21}$$

and

$$H_2 = \sum_{i=1}^{\nu_2} X_i^{(2)} h_i^{(2)} + H_o^{(2)} \text{ calories/mole} \tag{22}$$

where the $h_i^{(2)}$ are enthalpies for the individual ν_2 stable components in the equilibrium region downstream of the incident shock wave and $H_o^{(2)}$ represents the bond energy or heat of dissociation of the system. From equations (6) and (16), the incident shock velocity, is obtained, namely,

$$u_1 = \sqrt{2H_2JE7/\overline{M}_2\left[1 - \frac{1}{(\rho_2/\rho_1)^2}\right]} . \tag{23}$$

B. COMPUTATION PROCEDURE

The following procedures will be used:

1 Initial conditions are specified as p_1 and $T_1 = T_{RM}$ (usually 298°); ν_1 components at T_1 are given, along with their mole fractions (or partial pressures). ν_2 components are specified according to stoichiometery.

2 T_2 is the equilibrium temperature required, with ν_2 equilibrium concentrations at T_2 determined from a free-energy minimization subroutine, following that of Reference 112 and 113.

a In the computation scheme, obtain the molecular weights:

$$M_1 = \sum_{i=1}^{\nu} X_i^{(1)} M_i^{(1)} \text{ and } M_2 = \sum_{i=1}^{\nu_2} X_i^{(2)} M_i^{(2)} ,$$

where the ν_2 mole fractions, $X_i^{(2)}$, are determined through iteration required to satisfy the free energy minimization (equilibrium constants) and mass balance constraints. The concentrations may then be computed according to

$$c_i^{(2)} = (X_i^{(2)} \rho_2/\overline{M}_2)E3, \text{ moles/liter} . \tag{24}$$

b Obtain H_2 from equation (22), with

$$h_i^{(2)} \equiv H^\circ - H^\circ_{298}$$

taken from JANAF thermochemical tables or computed using the method of References 112 and 113 available as an optional alternate subroutine to Martin Marietta program shock (Fϕ 018).

c The gas dynamical quantity ρ_2 is obtained from equations (18), (19) and (20) and ρ_1 is determined from the initial conditions specified. A second iteration loop is required between the main program (Shock) and the equilibrium subroutine so that ρ_2 is simultaneously satisfied by equations (18) and the ν_2 equilibrium concentrations, i.e., the final pressure p_2 obtained at the specified equilibrium temperature T_2 must satisfy the gas dynamical relation from equation (7):

$$p_2/p_1 = 1 + \frac{u_1^2}{p_1/\rho_1}\left[1 - \frac{1}{\rho_2/\rho_1}\right] \tag{25}$$

to be calculated after finding ρ_2/ρ_1 and H_1 from equations (18) and (23)

C. OTHER CALCULATIONS REQUIRED

Consider the shock tube just before and after diaphragm burst.

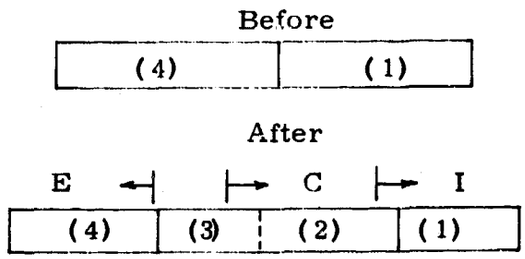

The initially set pressures are p_1 for the gas mixture in region (1) and p_4 in the high pressure helium driver gas region (4). After diaphragm burst, the incident shock wave I is driven to the reflection end plate by contact surface C, while an expansion wave E moves in the opposite direction. Gas particles flow from (1) to (2) so that the excess gas velocity in region (3) is, according to Ref :

$$u_3 = u_1 - u_2 = \frac{2a_4}{\gamma_4 - 1}\left[1 - (p_3/p_4)^{\frac{\gamma_4 - 1}{2\gamma_4}}\right] \tag{26}$$

$$= u_1(1 - \rho_1/\rho_2) \tag{27}$$

where equation (1) was used in the last step.

Since the pressures are equal across the contact surface, $p_2 = p_3$, equations (26) and (27) may be rearranged to give the diaphragm burst pressure ratio.

$$p_{41} = p_{21}\left[1 - \frac{\gamma_4 - 1}{2}\,\frac{u_1(1 - \rho_1/\rho_2)}{a_4}\right]^{-\frac{2\gamma_4}{\gamma_4 - 1}} \tag{28}$$

where equation (25) may be written

$$p_{21} = 1 + \gamma_1 M_1^2\left(1 - \frac{1}{\rho_2/\rho_1}\right). \tag{29}$$

The parameters

$$\gamma_1 = \frac{c_{p_1}}{c_{v_1}} = \frac{\sum_{i=1}^{\nu_1} X_i^{(1)} c_{p_i}^{(1)}(T_1)}{\sum_{i=1}^{\nu_1} X_i (c_{p_i}^{(1)} - R_o)} \tag{30}$$

and

$$M_1 = u_1 / \sqrt{\gamma_1 R_o T_1 / \overline{M}_1} \tag{31}$$

are the ratio of specific heats and the Mach number respectively. Equation (29) may be used alternately for frozen flow calculations (no chemical reactions) using the formulas given for ρ_2/ρ_1, for fixed γ and M, Reference 114. The frozen flow temperature, T_2, will be greater than the corresponding value of the equilibrium temperature at the same value of the incident shock velocity.

Program Shock, which in part was obtained through Cornell University, computes equations (18), (23), (25) and (28) simultaneously to determine the diaphragm burst pressure ratio as a function of u_1 or M_1. For ideal (frozen flow) diaphragm burst, the equation used (Reference) is

$$p_{41} = p_{21} \Big/ \left[1 - \frac{\gamma_4 - 1}{\gamma_1 + 1} \sqrt{\frac{\gamma_1 T_1 \overline{M}_4}{\gamma_4 T_4 \overline{M}_1}} \left(M_1 - \frac{1}{M_1}\right) \right]^{\frac{2\gamma_4}{\gamma_4 - 1}} \tag{32}$$

The equilibrium calculations for flow across the reflected shock wave follow an iterative procedure similar to the one outlined above. The value of $(T_5)_{EQ}$ is obtained through a second double iteration in program Shock which requires a stoichiometric mass balance and free energy minimization constraint. However, the pure helium/argon gas couple used in the shock tube design requires no consideration of chemistry so that the ideal shock relations were used for that purpose.

APPENDIX C

LIST OF SYMBOLS

A_{ij}	denotes vibrational coupling of jth species to i^{th} reaction
$B_\nu(T)$, $B_\lambda(T)$	Planck functions
c	velocity of light, cm/s
c_{p_j}	specific heat at constant pressure of jth species, $c_{p_j} = c'_{p_j}/R'_o$* (nondimensional)
c_{v_j}	specific heat at constant volume of jth species
D_{ij}	multicomponent diffusion coefficient
$\mathcal{D}_{ij}$	binary diffusion coefficient
$\mathcal{D}_{\alpha\alpha}$	self diffusion coefficient
e	electronic charge
$E_{r'}$	rotational energy of the emitting state relative to the ground (lowest upper) state of the electronic band, ergs
$E_{v'}$	vibrational energy of the emitting state relative to the ground state of the electronic band, ergs
$E_{v''}$	vibrational energy of the lower state, ergs
f	electronic oscillator strength, or f-number, dimensionless
h, $\hbar$	Planck's constant, $\hbar = h/2\pi$, erg sec
h_j	enthalpy of jth species including heat of formation; (dimensionless) $h_j = h'_j/R'_oT'_o$
I_λ	intensity in watts/cm^3/steradian/micron
j_j	species diffusion flux = $\rho_j U_j$
k	Boltzmann's constant
k_P	Planck mean absorption coefficient
L	reference length

*Primes denote dimensional quantities.

$M_j \equiv [M]$	denotes j^{th} species
(MW)	molecular weight of gas mixture defined by Equation (4)
$(MW)_j$	molecular weight of jth species
m_j	number of electronic levels included for j^{th} species
$m = \rho U$	mass flow rate
m	electron mass
N_j	number of vibrational energy levels of jth species
$\tilde{N}$	Avogadro's number = 6.023×10^{23} per AMU
N_m	number of molecules (per cm^3) populating the lower electronic state
n_j	number of atoms per species
p	pressure; $p = p'/\rho_o'(U_o')^2$ (nondimensional)
$Q_{r''}(T)$	rotational partition function of the lower state
$Q_{v''}(T)$	vibrational partition function of the lower state
Q_{ij}	mole-volumetric rate of production of M_j from reaction i
$q_{v'v''}$	Franck-Condon factor for the transition from v' to v'' (square of the overlap integral), dimensionless
R_o'	universal gas constant (R_o' = 1.98647 cal/mole °K in CAL subroutine)
T	equilibrium gas temperature, °K
T_{m_j}	parameter of jth species having units of temperature
U	velocity; $U = U'/U_o'$ (nondimensional)
V_j	vibrational coupling factor of jth species
X_j	mole fraction of jth species
y	coordinate normal to shock; $y = y'/L$ (nondimensional)
Z_k	number of collisions per mode
Γ_j	concentration of jth species, moles/unit mass including effect of diffusion flux, Equation (8)
γ_j	concentration of jth species in moles per unit mass (see Equation (6))
$\tilde{\gamma}_j$	ratio of specific heats for j^{th} gas
ϵ_j	vibrational energy of jth species; $\epsilon_j = \epsilon_j'/R_o T_o'$ (nondimensional)

ζ	defined by Equation (47)
θ_{v_j}	characteristic vibrational temperature of jth species
κ	coefficient of thermal conductivity
Λ	nondimensionalizing term, see Reference 4 (the CAL subroutine) $\Lambda = (U'_o)^2 MW'_o/R'_o T'_o$
λ_j	vibrational relaxation distance of jth species
λ	wavelength
μ	coefficient of viscosity
ν_v	wavenumber of the vth vibrational level, cm^{-1}
$\nu_{v'v''}$	wavenumber for the vibrational transition between the states v' and v'', cm^{-1}
ν_{oo}	wavenumber of the (0,0) vibrational transition, cm^{-1}
ν_{ij}	stoichiometric coefficients of jth species in i^{th} reaction
ξ	reciprocal Schmidt number
ρ	density; $\rho = \rho'/\rho'_o$ (nondimensional)
σ	photodetachment cross-section, cm^2; collisional diameter
χ_i	degree of nonequilibrium of ith reaction
ω_j	vibrational frequency of jth molecule
B_e, ω_e, $\omega_e x_e$, $\omega_e y_e$	Spectral constants. The ' refers to the excited electronic or emitting state and the '' refers to the lower electronic or absorbing state.

Subscripts

∞	refers to vibrational equilibrium
o	free stream conditions ahead of shock wave
i	pertaining to i^{th} reaction
j	pertaining to j^{th} species
n	pertaining to n^{th} electronic level
v	pertaining to v^{th} vibrational level
r	pertaining to r^{th} rotational level

REFERENCES

1. Bauer, S. H., Schott, G. L., and Duff, R. E., J. Chem Phys, 28, 1089-96

2. Gardiner, W. C., Jr., Morinaga, K., Ripley, D. L., and Takeyama, T., J. Chem Phys, 48, 1665-73, 1968

3. Schott, G. L., and Kinsey, J. L., J. Chem Phys 29, 1177, 1958

4. Schott, G. L., J. Chem Phys, 32, 710-16, 1960

5. Gaydon, A. G., and Hurle, I. R., "The Shock Tube in High-Temperature Chemical Physics," Reinhold, 1963

6. Bauer, W. H., and Wiberley, S. E., "Explosive Oxidation of Boranes, "Advances in Chemistry Series," (32), 115-126, 1961

7. Lifshitz, A., Bauer, S. H., and Resler, E. L., Jr., J. Chem Phys 38, 2056-63, 1963

8. Greene, E. F. and Toennies, J. P., "Chemical Reactions in Shock Waves," Academic Press, 1964

9. Bradley, J. N., "Shock Waves in Chemistry and Physics," John Wiley and Sons, Incorporated, 1962

10. Strehlow, R. A. and Cohen, A., J. Phys Fluids, 5, 96, 1962

11. Gaydon, A. G., "The Use of Shock Tubes for Studying Fundamental Combustion Processes," Plenary Lecture of the 11th Symposium (Int'l) on Combustion, The Combustion Institute, Pittsburgh, Pennsylvania, 1967

12. Bauer, S. H., "Shock Waves," Annual Review of Physical Chemistry, 16, 245-296, Table III, Annual Reviews, Inc., 1965

13. Volvodskii, V. V., and Soloukhin, R. J., Tenth Int'l Symposium on Combustion, 279-283, The Combustion Institute, Pittsburg, Pa., 1965

14. Miyama, H. and Takeyama, T., J. Chem Phys, 41, 2287, 1964

15. Belford, R. Linn and Strehlow, R. A., "Shock Tube Technique in Chemical Kinetics," to be published in Annual Review of Physical Chemistry, 20, Annual Reviews, Inc., 1969

16. Palmer, H. B., Knox, B. E., and McHale, E. T., AIAA Journal, 1, 1195-98, 1963

17. Tschuikow-Roux, E., J. Phys Fluids, 8, 821-25, 1965

18. Strehlow, R. A., J. Phys Fluids Supplement I, 12, I-96, 1969

19. Mark, H.,"The Interaction of a Reflected Shock Wave with the Boundary Layer in a Shock Tube," NACA TM 1418

20. Klepeis, J. E., M. Sc. Thesis, Graduate School of Aeronautical Engineering, Cornell University, Ithaca, N. Y., 1961

21. Sulzmann, K. G. P., Meyers, B. F., and Bartle, E. R., Journ Chem Phys, Vol 42, 3969, (1965)

22. Chinitz, W., A Survey of Fuels Suitable for External Combustion Applications, General Applied Science Laboratory, Incorporated, Technical Memorandum 109, June 1964

23. Skinner, G. B., Snyder A. D., and Ringrose, G. H., A Research Program for Understanding the Mechanisms for Flame Inhibition, Air Force APL-TDR-64-40, January 1964

24. Adams, R. M. (Ed), Boron, Metallo-Boron Compounds and Boranes, Interscience, 1964

25. Lipscomb, W. N., Boron Hydrides, Benjamin, 1963

26. Advances in Chemistry Series, Boron-Nitrogen Chemistry, An International Symposium, American Chemical Society, Washington, D. C., 1964

27. Hughes, R. L., Smith, I. C. and Lawless, E. W., "Production of The Boranes and Applied Research," Ed. Holzmann, R. T., Applied Research, 1967

28. Glick, H. S., Squire, W., and Hertzberg, A., "A New Shock Tube Technique for the Study of High Temperature Gas Phase Reactions," Fifth (International) Symposium on Combustion, Reinhold Publishing Company, 1955

29. JANAF Interim Thermochemical Tables, Dow Chemical Company, Midland, Michigan, 1965

30. Roth, W., PhD Thesis, Rensselaer Polytechnic Inst., 1954

31. Roth, W. and Bauer, W. H., "Combustion of Diborane-Oxygen Mixtures at the Second Explosion Limit," 5th Int'l Sym on Combustion, Reinhold, 1955

32. Roth, W. and Bauer, W. H., J. Phys Chem, 60, 639-41, 1956

33. Goldstein, M. S., PhD Thesis, Rensselaer Poly Inst., 1960

34. Bauer, W.H., and Wiberley, S.E., "Explosive Oxidation of Boranes, "Advances in Chemistry Series," (32), 115-126, 1961

35. Fehlner, T. P. and Koski, W.S., JACS 86, 1012, March 1964

36. Porter, R. F. and Grimm, F. A., "Mass Spectrometric Study of Intermediates In the Photochemical Oxidation of Diborane," in Advances In Chemistry Series, Number 72, A. C. S., 1968

37. Gobbett, E. and Sinnett, J. W., J. Chem Soc., 2893-2907, 1962

38. Jolly, W. L. and Schmitt, T., JACS/88:18/ 4282-84, 1966

39. Fehlner, T. P. and Koski, W. S., JACS, 86, 2733, 1964

40. Berl, W. G., "A Brief Review on the Combustion of Boron Hydrides," presented at AIAA Heterogeneous Combustion Conf., held at Palm Beach, Florida, Dec 11-13, 1963

41. Vincenti, W. G. and Kruger, C. H., Jr., "Introduction to Physical Gas Dynamics," J. Wiley & Sons, Inc., 1965

42. Bauer, S. H., et al, Reference 1 give absorption coefficient = 2.3×10^6 cm^2/mole at T = 2830°K.

43. Wolfherd, H. G., Clark, A. H. and Vanpee, M. "Characteristics of Diborane Flames," loc. cit.

44. Bauer, S. H., et al, Ibid, Absorption Measurements of OH Below 3200°K

45. Scholt, G. L., and Kinsey, J. L., Ibid, Absorption Measurements of OH to 1100°K.

46. Asaba, T., Gardiner, W. C., Jr., and Stubbeman, R. F., "Shock Tube Study of the Hydrogen-Oxygen Reaction," give OH Measurement Sensitivities to 3 x 10^{-7} moles/liter in Tenth Symposium (Int'l) on Combustion, 295-302, The Combustion Institute, Pittsburgh, Penn., 1965

47. Oppenheim, A. K., "The No-Mans' Land of Gas Dynamics of Explosions," JAIAA

48. Soloukhin, R. I., Shock Waves and Detonations in Gases, Mono Book Corporation, 1966

49. Behrens, H., and Roessler, F., "Supersonic Diffusion Flames," pp 159-169; Gross, R. A. and Nicholls, J. A., "Stationary Detonation Waves," 4th AGARD Colloquim on Combustion and Propulsion, pp 169-176, Milan 1960, Jaumotte, A. L., Lefebvre, A. H., and Rothcock, A. M., Pergamon Press, 1961

50. Da Riva, I., "Diffusion Flames and Supersonic Combustion," Final Report AF-EOAR, AD 622-581, Grant 1963-64

51. Duff, R. E., J. Chem Phys 28, 1193, 1958

52. Nicholls, J. A., Dabora, E. K., and Gealer, R. L., "Studies in Connection with Stabilized Detonation Waves," 7th International Symposium on Combustion, London, Butterworths Scientific Publication, pp 766-772, (1959)

53. Gross, R. A., "Exploratory Studies of Combustion in Supersonic Flow," AFOSR TN59-587 AD 216-769, June 1959

Vol I, "Plain Detonation Waves"
Vol II, "Oblique Detonation Waves"

54. Oppenheim, A. K. and Rosciszewski, J., "Determination of the Detonation Wave Structure," p 424, 9th International Symposium on Combustion, A. P., 1963

55. Nichols, J. A., Adamson, T. C., Jr. and Morrison, R. B., "Ignition Time Delay of Hydrogen-Oxygen-Diluent Mixtures at High Temperatures," Vol 1 (10) AIAA Journ, p 2253, October 1963

56. Gordon, W. E., Mooradian, A. J., and Harper, S. A., "Limit and Spin Effects in Hydrogen-Oxygen Detonations," p 752, 7th International Symposium on Combustion, London, Butterworths Scientific Publication," 1959

57. White, D. R., "Discussion on Detonations," pp 415, 416, 474, 9th International Combustion Symposium, A. P. 1963

58. Oppenheim, A. K., "The No Mans' Land of Gas Dynamics of Explosions," AIAA, to be published

59. Soloukin, R. I., "Transition From Combustion to Detonation in Gases," PMTF No. 4 pp 128-135, July-August 1961

60. Urtiew, P. A. and Oppenheim, A. K., "Detonative Ignition Induced by Shock Merging," 11th International Combustion Symposium, U. C. Berkeley, August 1966

61. Predvoditelev, A. S., "Concerning Spin Detonation," p 760, 7th International Symposium on Combustion, London, Butterworths Scientific Publication, 1959

62. Duff, R. E., and Davidson, N., J. Chem Phys 31, 1018, 1959

63. Matthews, D. L., J. Phys of Fluids 2, 170, 1959

64. Carrington, T., and Davidson, N., J. Chem Phys 19, 1313, 1951

65. Britton, D., Davidson, N., and Schott, G. L., J. Chem Phys 25, 804 1956

66. Marrone, P. V., "Inviscid, Nonequilibrium Flow Behind Bow and Normal Shock Waves," Part I. General Analysis and Numerical Examples, Cornell Aeronautical Laboratory (CAL) Report No. QM-1626-A-12(I), May 1963. (Also see Parts II and III for Computer Codes and Revisions)

67. Hirschfelder, J. O. and Curtiss, C. F., J. Chem Phys, 28, 1130-47, 1958 1958

68. Linder, B., Curtiss, C. F., and Hirschfelder, J. O., J. of Chem Physics, 28, 1147-51, 1958

69. Adamson, T. C., Jr., J. Physics of Fluids 3, 706, 1960

70. Petrone, F. J., J. Phys. Fluids, 11, 1473-78, 1968

71. Scala, S. M. and Gordon, P., "Solution of the Time-Dependent Novier-Stokes Equations for the Flow of Dissociating Gas Over a Circular Cylinder," presented at AGARD Fluid Dynamics Panel Specialists Meeting on "Fluid Plysics of Hypersonic Wakes," held at Colorado State University, Fort Collins, Colo., May 10-12, 1967

72. Williams, F. A., Combustion Theory, Addison-Wesley, 1965

73. Bethe, H. A., and Teller, E., "Deviations from Thermal Equilibrium in Shock Waves," BRL, 1945, also University of Michigan, E. R. I., 1951

74. Vincenti, W. G., and Kruger, C. H., Jr., Ibid

75. Herzberg, H., "Molecular Spectra and Molecular Structure," D. Van Norstrand Company, Inc., 1950

76. Landau, L., and Teller, E., Phys Z. Soviet, 10, 34 (1935)

77. Treanor, C. E., and Marrone, P. V., "Effect of Dissociation on The Rate of Vibrational Relaxation," Cornell Aeronautical Laboratory, Inc., 1962; also Physics of Fluids, 5, (9) September, 1962

78. Sherman, M. P., "Radiation-Coupled Chemical Non-Equilibrium Normal Shock Waves," General Electric TIS Report R66 SD 17, March 1966

79. Henrici, H. and Bauer, S. H., J. Chem Phys, 50, 1333-42, 1969

80. Hersh, S., Frey, H. M., and Gerstein, M., "Combustion Chemistry and Mixing in Supersonic Flow," Dynamic Sciences Rept. D. S. TR-A-69-101 (Also Air Force Rept. AFOSR 69-0104 TR, 1969

81. Schott, G. L., Private Communication

82. Skinner, G. B., and Ringrose, G. H., J. Chem Phys 42, 2190-92, 1965

83. Hirschfelder, J. O., Curtiss, C. F. and Bird, R. B., "Molecular Theory of Gases and Liquids," John Wiley and Sons, 1964

84. Specialist Conference on Molecular Radiation and its Application to Diagnostic Techniques, NASA TMX-53711, October 1967

85. e.g., Reference 5, pp 1194-7

86. Mason, E. A., and Monchick, L., J. Chem Phys 36, 1622-39, March 1962

87. Hirschfelder, J. O., "Heat Conductivity in Polyatomic, Electronically Excited, or Chemically Relaxing Mixtures, III," pp 351-366, The 6th Symp (Int'l) on Combustion, The Combustion Institute, 1957

88. Hirschfelder, J. O., J. Chem Phys 26, pp 274-85, February 1957

89. Brokaw, R. S., J. Chem Phys 32, 1005, 1960

90. Butler, J. N., and Brokaw, J. Chem Phys 26, pp 1636-43, June 1957

91. Secrest, D., and Hirschfelder, J. O., J. of Phys of Fluids, 4 (1) 61-73, January 1961

92. Brokaw, R. S., J. Chem Phys 35, 1569, 1961

93. Treanor, C. E. and Marrone, P. V., J. of Phys of Fluids, 5 (9) 1022-26, September 1962

94. Treanor, C. E., J. Math of Comp XX (93) 39-45, January 1966

95. Rush, D. G., and Pritchard, H. O., "Vibrational Disequilibrium in Chemical Reactions," and:

96. Bray, K. N. C., and Pratt, N. H., "Conditions for Significant Gasdynamically Induced Vibration-Recombination Coupling," pgs 13-22 and 23-36, respectively, in the 11th Symp (Int'l) on Combustion, The Combustion Institute, 1967

97. Svehla, R. A., "Estimated Viscosities and Thermal Conductivities of Gases at High Temperatures," NASA TR R-132, 1962

98. Vincenti, W. G. and Kruger, C. H., Jr., Ibid

99. Sherman, M. P., "Radiation-Coupled Chemical Nonequilibrium Normal Shock Waves," General Electric Space Sciences Laboratory, Technical Information Series Report R66SD17, March 1966

100. Herzberg, G., "Spectra of Diatomic Molecules," 2nd Edition Van Nostrand, New York, 1950

101. Chandrasekhar, S., Radiative Transfer, Oxford at the Clarendon Press, 1950

102. Herzberg, G., Ibid

103. Penner, S. S., Quantitative Molecular Spectroscopy and Gas Emissivities, Chapter 14, "The Emissivity of Heated Air," Addison-Wesley, 1959

104. Herzberg, G., op cit, page 381-383

105. Bethe, H. A. and Salpeter, E. E., Quantum Mechanics of One and Two Electron Atoms, page 251, Academic Press, Inc., N. Y. 1957

106. Penner, S. S., op cit, page 398

107. Kivel, B., Mayer, H., and Bethe, H., "Radiation from Hot Air, Part I Theory of Nitric Oxide Absorption," Anals of Physics 2, 57-80, 1957

108. Keck, J. C., Camm, J. C., Kivel, B., and Wentink, T., Jr., "Radiation from Hot Air, Part II Shock Tube Study of Absolute Intensities," Anals of Physics 7, 1-38, 1959

109. Herzberg, G., op cit, pp 169-192

110. Klein, M. M. and Brueckner, K. A., "Interaction of Slow Electrons With Atomic Oxygen and Atomic Nitrogen," Phys Rev III, 4, page 1115-1120, 1958

111. Cooper, J. W. and Martin, J. B., "Electron Photodetachment from Ions and Elastic Collision Cross-Sections for O, C, Cl and F," N. B. S., Washington D. C., 1962

UNCLASSIFIED
Security Classification

DOCUMENT CONTROL DATA - R & D

(Security classification of title, body of abstract and indexing annotation must be entered when the overall report is classified)

ORIGINATING ACTIVITY (Corporate author) Martin Marietta Corporation Research Division Orlando, Florida 32801	2a. REPORT SECURITY CLASSIFICATION UNCLASSIFIED 2b. GROUP

REPORT TITLE

COMBUSTION CHEMISTRY OF HIGH ENERGY PYROPHORIC FUELS

DESCRIPTIVE NOTES (Type of report and inclusive dates)

Scientific Final

AUTHOR(S) (First name, middle initial, last name)

Charles A. Andrade

REPORT DATE 26 May 1969	7a. TOTAL NO. OF PAGES 120	7b. NO. OF REFS 11
8a. CONTRACT OR GRANT NO. AF-49-(638)-1566 b. PROJECT NO. 9711-01 c. 61102F d. 681308	9a. ORIGINATOR'S REPORT NUMBER(S) OR 10119 9b. OTHER REPORT NO(S) (Any other numbers that may be assigned this report) AFOSR 69-2197 TR	

10. DISTRIBUTION STATEMENT

1. This document has been approved for public release and sale; its distribution is unlimited.

11. SUPPLEMENTARY NOTES TECH, OTHER	12. SPONSORING MILITARY ACTIVITY AF Office of Scientific Research (SREP) 1400 Wilson Boulevard Arlington, Virginia 22209

13. ABSTRACT

Research reported herein is directed toward further understanding of the fundamental processes in supersonic combustion. Part One describes a branching chain mechanism constructed for oxy-diborane mixtures diluted in argon. Included in this postulated mechanism is the production of hydroxyl as an ignition intermediate. A spectrograph was used to view the oxy diborane system through the end plate of a single pulse shock tube. Hydroxyl and several boron intermediates were identified, qualitatively verifying both mechanism and equilibrium calculations. Ignition induction measurements were performed up to 950°K behind the reflected shock wave. These measurements extend previously known data by two orders of magnitude in the induction time. Part Two of this report describes the CAL Nonequilibrium Normal Shock Wave Program which was extended for use with highly exothermic branching chain reactions, checked out with known hydrogen oxygen kinetics, and reformulated to include transport and radiative energy transfer mechanisms.

DD FORM 1473

UNCLASSIFIED

14 KEY WORDS	LINK A ROLE	LINK A WT	LINK B ROLE	LINK B WT	LINK C ROLE	LINK C WT
Pyrophoric fuels						
Supersonic combustion						
Shock wave						
Oxy-diborane						
Boron compounds						